Production of Hydrogen by Reforming of Crude Ethanol

A Thesis Submitted to the College of Graduate Studies and Research
in partial fulfilment of the requirements for the degree of
Master of Science
in the Department of Chemical Engineering
University of Saskatchewan
Saskatoon, Saskatchewan

By

Abayomi John Akande

Copyright Abayomi John Akande February 2005

All Rights Reserved

COPYRIGHT

The author has agreed that the Libraries of the University of Saskatchewan may make this thesis freely available for inspection. Moreover, the author has agreed that permission for extensive copying of this thesis for scholarly purposes may be granted by the professor(s) who supervised this thesis work recorded herein or, in their absence, by the Head of the Department of Chemical Engineering or the Dean of the College of Graduate Studies. Copying or publication or any other use of the thesis or parts thereof for financial gain without written approval by the University of Saskatchewan is prohibited. It is also understood that due recognition will be given to the author of this thesis and to the University of Saskatchewan in any use of the material of the thesis.

Request for permission to copy or to make other use of material in this thesis in whole or parts should be addressed to:

Head

Department of Chemical Engineering

University of Saskatchewan

105 Maintenance Road

Saskatoon, Saskatchewan

S7N 5C5

Canada

ABSTRACT

The purpose of this work was to design and to develop a high performance catalyst for the production of hydrogen from reforming of crude ethanol and also, to develop the kinetics and reactor model of crude ethanol reforming process. Crude ethanol reforming is an endothermic reaction of ethanol and other oxygenated hydrocarbons such as (lactic acid, glycerol and maltose) with water present in fermentation broth to produce hydrogen (H_2) and carbon dioxide (CO_2). Ni/Al_2O_3 catalysts were prepared using different preparation methods such as coprecipitation, precipitation and impregnation methods with different Ni loadings of 10 – 25 wt.%, 10-20 wt.%, and 10-20 wt.% respectively.

All catalysts were characterised by thermogravimetric/differential scanning calorimetry (TG/DSC), X-ray diffraction (XRD), (including X-ray line broadening), temperature programmed reduction, BET surface area measurements, pore volume and pore size distribution analysis. TG/DSC analyses for the uncalcined catalysts showed the catalyst were stable up from 600^{o}C. XRD analyses showed the presence of NiO, $NiAl_2O_4$ and Al_2O_3 species on the calcined catalysts whereas Ni, $NiAl_2O_4$, and Al_2O_3 were present on reduced catalysts. BET surface area decreased and average pore diameter reached a maximum and then decreased as the Ni loading increased. The temperature programmed reduction profiles showed peaks corresponding to the reduction of NiO between 400-600^{o}C and reduction of $NiAl_2O_4$ between 700-800^{o}C.

Catalyst screening was performed in a micro reactor with calcination temperature, reaction temperature and the ratio of catalyst weight to crude ethanol flow rate (W/F_{crude-}

$_{C2H5OH}$) of 600 ^{o}C, 400^{o}C and 0.59 h respectively. Maximum crude-ethanol conversion of 85 mol% was observed for catalyst with 15wt% Ni loading prepared by precipitation method (PT15), while maximum hydrogen yield (= 4.33 moles H_2 / mol crude-ethanol feed) was observed for catalyst with 15wt% Ni loading prepared by coprecipitation (CP15).

Performance tests were carried out on (CP15) in which variables such as space velocity (WHSV) 1.68h^{-1}to 4.68h^{-1}, reduction temperature 400 to 600^{o}C and reaction temperature 320 to 520 ^{o}C, were changed for optimum performance evaluation of the selected catalyst. The catalyst deactivated over first three hours of 11 hours time-on-stream (TOS) before it stabilized, the reaction conditions resulted in a drop of ethanol conversion from 80 to 70mol%.

The compounds identified in the liqiud products in all cases were ethanoic acid, butanoic acid, butanal, propanone, propanoic acid, propylene glycol and butanedioic acid. The kinetic analysis was carried out for the rate data obtained for the reforming of crude ethanol reaction that produced only hydrogen and carbon dioxide. These data were fitted to the power law model and Eldey Rideal models for the entire temperature range of 320-520 ^{o}C. The activation energy found were 4.405×10^3 and 4.428×10^3 kJ/kmol respectively. Also the simulation of reactor model showed that irrespective of the operating temperature, the benefit of an increase in reactor length is limited. It also showed that by neglecting the axial dispersion term in the model the crude ethanol conversion is under predicted. In addition the beneficial effects of W/F_{AO} start to diminish as its value increases (i.e. at lower flow rates).

ACKNOWLEDGMENT

I wish to express my appreciation to Drs. A. K. Dalai and R. O. Idem for their guidance throughout my graduate program. I also wish to express my gratitude to other members of the advisory committee, Drs. G. Hill. and N. N. Bakhshi for their helpful discussions and suggestions.

I appreciate the effort of Mr. Keith Rueve, plant manager Pound maker Agventure Lanigan for supplying the fermentation broth used for this research. I deeply appreciate the contributions of Dr. Ahmed Aboudheir in reactor modeling tasks, I also appreciate the efforts of all members of Process System Engineering Laboratory, University of Regina especially Hussam Ibrahim, Abiodun Fatokun, Nnaemeka Okochi, Itoro Uyanga, Olanike Lawal, Adeola Bello, Lauren Ericson and Robyn Fahlma. I also thank Mr Harald & Alan Berwald and other members of engineering design workshop, Faculty of Engineering University of Regina for their technical assistance at various stages of this work. My sincere appreciation also goes to all the members of the Catalysis and Chemical Reaction Laboratories, University of Saskatchewan especially Adenike Adebanjo, Nikhil Das, Thiru Vallyapan, and Abena Owusu-Boakye.

Last but not the least, thanks to my beloved wife (Ifeoluwa) and our newborn baby (Adefikayo) for their enthusiastic support at all times.

The financial assistance from Canada Research Chair program to Dr. A. K. Dalai was gratefully acknowledged.

DEDICATION

This work is dedicated to

My beloved wife, Ifeoluwa

And

Baby, Adefikayo

Table of Contents

LIST OF TABLES

LIST OF FIGURES

NOMENCLATURE

AAD	Average absolute deviation
C_i	concentration of specie i in the reactor, kmol m^{-3}
C_p	Heat capacity, kJ/kg K
$C_{(a)}$	Concentration of unoccupied active sites
$C_{i(a)}$	site occupied by species *i*
C_e	equilibrium reaction coefficient
Dp	diameter of catalyst pellet, mm
D	Internal diameter of the reactor, mm
D_z	Effective diffusivity in axial direction, m^2/s
D_r	Effective diffusivity in radial direction, m^2/s
E	activation energy, kJ/kmol
F_{AO}	flow rate of crude ethanol at the reactor inlet, kg-crude s^{-1}
ΔG	Gibbs' energy of formation, kJ/k mol
ΔH	heat of reaction, kJ/kmol
Kp	overall equilibrium constant for ethanol steam reforming reaction
K_i	equilibrium constant of reaction step i
k_o	pre-exponential constant $(kg\text{-}cat.s)^{-1}$
L	catalyst bed height, mm
n	order of reaction with respect to crude ethanol
N_i	number of moles of species i, kmol/s
P^o	Standard-state pressure, 1 atm
P_r	reduced pressure

P_c	critical pressure, atm
$-r_A$	rate of disappearance of crude ethanol, kmol s^{-1} $kg.cat^{-1}$
R	ideal gas constant, kJ/ kmol K
S_{H2}	H_2 selectivity
T_o	feed inlet temperature, K
T_r	reduced temperature
T_c	critical temperature, K
T	absolute temperature, K
U_{TW}	heat transfer coefficient (tube wall), kJ/m^2 s K
ν	stoichiometry number
v_z	flow velocity in axial direction, m/s
W	catalyst loading weight, kg
W/F_{AO}	Space time kg-cat. s/kg-crude ethanol
X	fractional conversion of crude ethanol
Y_{H2}	H_2 yield, mol H_2/mol crude ethanol fed
y_{CO2}	mole fraction of CO_2 in the gas mixture
y_{C2H5OH}	mole fraction of C_2H_5OH in the gas mixture
y_{H2}	mole fraction of H_2 in the gas mixture
y_{H2O}	mole fraction of H_2O in the gas mixture

Greek Letter

λ_z	Effective thermal conductivity in axial direction, kJ/m s K
λ_r	Effective thermal conductivity in radial direction, kJ/m s K

ρ_B	Catalyst bulk density, kg/m^3
ρ_g	gas density, kg/m^3
φ_i	Activity coefficient of species i

Subscripts

(a)	active catalyst site
A	C_2H_6O
A*	CH_4O*
S*	CH_2
C	CO_2
D	H_2
AO	crude ethanol in the feed
i	species i
TW	tube wall
z	axial direction
r	radial direction

1.0 INTRODUCTION

The majority of current energy needs are supplied by combustion of non-renewable energy sources such as fossil fuels, which is associated with release of large quantities of greenhouse gases (GHG), especially carbon dioxide (CO_2) and other harmful emissions to the atmosphere. The gradual depletion of these fossil fuels reserves and efforts to combat pollution and greenhousegas emissions have generated a considerable interest in using alternative sources of energy (Cortright et al., 2002; Haga et al., 1998)

On the other hand, strong efforts are being made to commercialize the use of fuel cells such as the proton exchange membrane (PEM) fuel cell for the generation of electric power for both electric vehicles and distributed electric power plants (Creveling, 1992; Dunison and Wilson, 1994). The major reason for the interest is the high energy efficiency of the fuel cell with an overall energy efficiency of about 85%, in some cases (Whitaker, 1994). Also, with an equally strong interest in the use of hydrogen (H_2) as the fuel, PEM fuel cells are the most certain to meet future ultra low NO_x, SO_x, CO, CH_4 and CO_2 emissions targets (Creveling, 1992). Thus, H_2 has a significant future potential as an alternative fuel that can solve the problems of CO_2 emissions as well as the emissions of other air contaminants. It is well known that H_2 production can be accomplished by gasification or reforming of fossil fuels (Gary and Handwerk, 1994; Simanzhenkov and Idem, 2003) or biomass (Garcia et al., 2000). However, if a global cycle of clean and sustainable production of energy is envisaged, a

new eco-friendly reservoir of hydrogen is needed. In this context, ethanol (a form of biomass) satisfies most of these requirements since it is easy to produce, and is also safe to handle, transport and store (Anthanasio et al., 2004; Cavallaro et al., 1996). It is to be noted that about 352 liters of ethanol can be produced from approximately 1 tonne or 1 acre of wheat. As such, ethanol provides an environmentally responsible energy source that can significantly reduce GHG emissions (Haga et al., 1998). It is also known that the application of ethanol for the production and use of H_2 energy is CO_2 neutral (Anthanasio, 2002).

Furthermore, since ethanol does not contain heteroatoms and metals, its use as source of energy does not result in emissions of NOx, SOx, particulates and other toxics. In addition, ethanol is mostly an oxygenated hydrocarbon, which leads to complete combustion during its application to produce power. As such, little or no CO is produced. These attributes have made H_2 obtained from ethanol reforming a very good energy vector, especially in fuel cells applications. H_2 production from ethanol has advantages when compared with other H_2 production techniques, including steam reforming of methanol and hydrocarbons. Unlike hydrocarbons, ethanol is easier to reform and is also free of sulfur, which is a catalyst poison in the reforming of hydrocarbons (Cavallaro et al., 1996). Also, unlike methanol, which is sourced from hydrocarbons (Klouz et al., 2002) and has a relatively high toxicity, ethanol is completely biomass based and has low toxicity.

1.1 Knowledge Gaps and Problem Identification

Extensive studies on hydrogen production from ethanol have been reported in the literature, [Anthanasio et al. (2002, 2004), Breen et al. (2002), Cavallaro et al.

(2003), Freni, (2002), Galvita et al. (2001), Haga et al. (1998), Jose et al. (2003), Leclerc et al. (1998), Marino et al. (1998) and Velu et al. (2002)]. These authors have used catalysts such as Ni/MgO, Cu/ZnO, Cu/SiO_2, Cu/ZnO_2, Cu/Al_2O_3, Cu/MgO, $Cu/NiO/Cr_2O_3$, Ni/Al_2O_3, $CuO/ZnO/Al_2O_3$, $Pt/\alpha\text{-}Al_2O_3$, Rh/Al_2O_3, and Co/Al_2O_3. It, however, appears from the literature that there is very little or no research activity in the area of crude ethanol reforming, and also, no work has been done on the kinetic modeling and reactor design.

A wide literature review on ethanol steam reforming has been done. This is to identify a catalyst that promotes hydrogen production from ethanol steam reforming. The past experience of ethanol steam reforming will be used to design an efficient catalyst for crude ethanol reforming.

1.2 Justification

The production of hydrogen by steam reforming of pure ethanol has been widely investigated. Jordi et al. (2002) performed their investigation on Co/ZnO catalyst using a water to ethanol molar ratio of 13:1 (20% v/v ethanol), whereas Leclerc et al. (1998) reported that water to ethanol ratios in the range of 20:1 (14%v/v ethanol) to 30:1 (10%v/v ethanol) enhanced hydrogen selectivity and inhibited the production of undesirable product such as methane (CH_4), carbon monoxide (CO), acetaldehyde, ethylene and carbon. Gavita et al. (2001) used water to ethanol molar ratios of 3:1 and 8.1:1, and obtained the highest ethanol conversion on Ni/MgO catalyst at water to ethanol molar ratio of 8.1:1 (28%v/v ethanol). Das, (2003) used water to ethanol molar ratio of 6:1 (35% v/v ethanol) on Mn promoted Cu based catalyst to obtain optimum ethanol conversion, hydrogen yield and selectivity.

In all these cases, water was needed as a co-feed to the process, consequently there is no need to reduce the water and organic contents of fermentation product (fermentation broth produced from a fermentation process) since this contains approximately 12%v/v ethanol, which is within the range of water to ethanol molar ratio used for literature cited ethanol reforming processes. Besides, by using crude ethanol, the other organic compounds present in the fermentation broth could equally be reformed to produce additional H_2. Also, this process would eliminate the large amount of energy wasted during distillation to remove water from fermentation broth in order to produce dry or pure ethanol. Haga et al., 1998 suggested that in order to obtain a widespread use of ethanol for hydrogen production, the economics and energetics of the ethanol production process have to be greatly improved. Thus, by circumventing the distillation and drying step, this process of reforming crude ethanol (i.e. fermentation broth) provides an ability to produce H_2 from crude ethanol solution in a cost-effective manner.

1.3 Research Objectives

The main objectives of this research were (1) to design and develop a high performance catalyst that is capable of efficiently catalyzing the production of hydrogen from crude ethanol, (2) to kinetically model the reforming reaction in order to obtain a rate expression and (3) to carry out comprehensive reactor modeling in order to simulate the reactor responses to changes in process parameters.

The aim would be to maximize crude ethanol conversion and hydrogen selectivity for the best performing Ni/Al_2O_3 catalysts. The performance of the screened catalyst would be tested for different process variables such as, reaction temperature,

weight of catalyst and flow rate ratio ($W/F_{crude\text{-}C2H5OH}$) and catalyst reduction temperatures. The stability of the catalyst would be tested by time-on-stream runs. Characterization studies by different techniques would be carried out for the fresh and spent catalysts to correlate their activities with different physical and chemical properties. Within these objectives various phases of research were mapped out with each phase having set of objectives. These phases are outlined below.

1.3.1 Phase I Preparation and Characterization of Catalysts

Ten different Ni-based catalysts were prepared and characterised in this phase. Three preparation methods were used; coprecipitation, precipitation and impregnation. Catalysts characterisation was performed in order to obtain the relationship between the catalyst characteristic and its performance.

The techniques used for catalyst characterisation were (1) Thermo gravimetric analysis/ differential thermal analysis, (2) Powder X-ray diffraction, (3) BET surface area, pore volume and pore size distribution analysis. and (4) Temperature programmed reduction (TPR).

1.3.2 Phase II Evaluation of Catalyst Performance for Crude Ethanol Reforming in a Packed Bed Tubular Reactor

The experimental phase was carried out in a fixed bed reactor in order to screen the catalysts and to identify the best one among the ten Ni-based catalysts. The screening tests were conducted at fixed temperature of 400^{o}C and W/F_{AO} of 0.59 kg-cat-h/kg crude ethanol. Variables such as space velocity (WHSV) 1.68 to 4.62h^{-1}, reaction temperature 320 to 520 ^{o}C, and reduction temperature 400 to 600 ^{o}C were changed for optimum performance evaluation of the selected catalyst.

1.3.3 Phase III Kinetic and Reactor Modeling

This phase involved the following tasks:

(a) Proposition of reaction mechanism

(b) Development of rate equation using Eley-Rideal approach and estimation of the kinetic parameters

(c) Development of power law rate model and estimation of kinetic parameters

(d) Development of reactor model and simulation

The performance evaluation data for the best catalyst will be chosen to study the kinetics of the crude ethanol reforming reaction. The differential method of kinetic analysis will be used to find the reaction rates from the performance evaluation experiments. The rate parameters will be estimated by fitting the experimental data to the different catalytic reaction model, by non-linear regression method. Also, a rigorous reactor model will be developed by coupling of partial differential equations involving mass and energy balance in order to simulate the reactor responses to changes in different process parameters.

2.0 LITERATURE REVIEW

2.1 Introduction

Review of production of hydrogen by the steam reforming of ethanol will be presented in this chapter. The review will focus on catalysts currently available for the production of hydrogen from ethanol with emphasis on the performance for H_2 production. Crude ethanol reforming is primarily targeted to supply hydrogen as an energy vector in fuel cells; therefore, review of different types of fuel cells, fuels used in fuel cells and their applications have been carried out as part of literature review for this work.

2.2 The Fuel Cell

Austin, (1959), defined fuel cell as an electrochemical device that transforms chemical energy stored in fuels directly into electrical energy. Fuel cells have no moving parts and have no useful energy loss due to friction. Therefore fuel cells are highly energy efficient, and an overall energy efficiency of 85% has been reported for a particular (PEM) type of fuel cell (Whitaker, 1994).

In a typical fuel cell such as solid oxide fuel cell (SOFC), reactions that take place are as follows, a catalyst (such as lanthanum strontium manganite (LSM)) embedded in the cathode converts oxygen (supplied by air) into oxygen ion. When fuel gas containing hydrogen is passed over the anode, a flow of negatively charged oxygen ions moves across the electrolyte (yittra stabilized zirconia) to oxidize the

fuel. Electrons generated at the anode travel through an external load to the cathode, completing the circuit and supplying electric power along the way.

Cathode: $O_2 + 4e^- = 2O^{2-}$

Anode: $2H_2 + 2O^{2-} = 2H_2O + 4e^-$

2.2.1 Types of Fuel Cells

Fuel cells are classified according to the electrolyte they employ (Creveling 1992). This determines the kind of chemical reactions that take place in the cell, the kind of catalysts required, the temperature range in which the cell operates, and the fuel required. There are several types of fuel cells, each with different advantages, limitations and potential applications. These are: alkaline fuel cell (AFC), used in space vehicle power systems; the phosphoric acid fuel cell (PAFC) used in both road transportation and stationary engines; the solid polymer fuel cell (SPFC) also used in both road transportation and stationary engines; the molten carbonate fuel cell (MCFC) used in stationary engines, and the solid oxide fuel cell (SOFC) used only in stationary engines.

2.2.1.1 Alkaline Fuel Cell

The alkaline fuel cell uses alkalis such as aqueous potassium hydroxide or sodium hydroxide as the electrolyte, and hydrogen as the fuel. It operates at low temperature of 20 –90^{o}C (Gulzow, 1996) and is, therefore, sensitive to hydrogen fuel impurities. Alkaline fuel cells can be used in artificial space satellite (Austin, 1959) and also in automobiles and locomotives (Ahuja and Green, 1998).

2.2.1.2 Molten Carbonate Fuel Cell (MCFC)

The molten carbonate fuel cell (MCFC) uses a molten carbonate electrolyte that usually consists of potassium or sodium carbonate (K_2CO_3 or Na_2CO_3), which is mixed with lithium carbonate (Li_2CO_3) to lower the melting point (Austin, 1995). It operates at high temperatures usually > 500 ^oC. This high temperature enables the MCFC to use fuels such as natural gas, coal-derived gases, refinery gases, methanol, and process gas directly in the fuel cell section (Austin, 1995). The MCFC is capable of tolerating high level of impurities in the fuel at the operating temperature.

2.2.1.3 Solid Oxide Fuel Cell (SOFC)

The SOFC uses a solid oxide such as zirconia as the electrolyte (Hsu et al, 1994). Zirconia has refractory property which enables the operation of the SOFC at temperatures as high as 1000 ^oC. At this high temperature, zirconia has the unique property of conducting oxygen ions instead of electrons. This property is essential for the operation of the fuel cell. Because of the extremely high temperature, SOFC can also use liquid fuels such as gasoline, diesel and kerosene directly (Hsu et al., 1994). SOFC can also tolerate high levels of impurities in the fuel.

2.2.1.4 Phosphoric Acid Fuel Cell (PAFC)

PAFC uses phosphoric acid as the electrolyte (Whitaker, 1994). At the operating temperature of 120^oC only hydrogen can be used directly as the fuel. Natural gas, refinery gas, methanol or coal derived gases are types of fuels usually supplied to the fuel cell power plant. These gases are usually processed in the gas processing section to produce hydrogen, which then enters the fuel cell section. PAFC has low tolerance to impurity due to low operating temperature.

2.2.1.5 Proton Exchange Membrane Fuel Cell (PEMFC)

The proton exchange membrane (PEM) or the solid polymer fuel cell (SPFC) uses a solid proton exchange membrane (PEM), such as polyper-fluorosulfonic acid, as the electrolyte. The operating temperature is about 80^{o}C. This permits rapid start-up. The fuel used in the PEMFC is usually hydrogen. If other types of fuels such as natural gas or methanol are used, they are usually reformed in the fuel processing section into a hydrogen rich gas before being allowed to enter the fuel cell section. Because the operating temperature is lower than that of PAFC, the level of tolerance of this type of fuel cell to fuel impurity is relatively lower.

2.3 Fuel for Fuel Cell

Hydrogen, natural gas, methanol, gases obtained from the gasification of coal, gasoline vapour, refinery gases, process gas, kerosene and diesel are the common fuels for fuel cells. The choice of fuel depends on factors such as cost of the fuel, availability, as well as ease of transportation and storage of the fuel. The type of fuel has a great impact on the fuel cell operating temperature and, consequently, on the type of electrolyte and other components used in the fuel cell stack or system (Idem 1995).

2.4 Methods of Production of Hydrogen

Hydrogen can be produced by electrolysis of water using Hoffman's apparatus, steam reforming of natural gas and other fossil fuels, as off-gases from petroleum refinery operations, and by steam reforming of methanol or ethanol. Ethanol is the only renewable source of hydrogen since it can be produced from biomass by fermentation process.

2.5 Thermodynamic and Catalytic Research

Although there is no published literature report on the reforming of crude ethanol, past experience of the steam reforming of "pure" ethanol will be used in order to understand the reforming potentials of crude ethanol. This section will present reports of catalysts that have been previously used for hydrogen production by steam reforming of "pure" ethanol.

In the thermodynamic studies carried out by Vasudeva et al. (1996), they reported that in all ranges of conditions considered, there was nearly complete conversion of ethanol and only traces of acetaldehyde and ethylene were present in the reaction equilibrium mixture. For a water- to-ethanol molar ratio in the feed of 20:1, the ratio of moles of hydrogen produced to moles of ethanol consumed was 5.56 compared to the stoichiometric maximum achievable of 6.0. Methane and carbon monoxide also decreased substantially when the water-to-ethanol ratio in the feed was increased from 10 to 20. They also reported that for a water-to-ethanol molar ratio of 20:1, an increase in the temperature from 525 to 925^{o}C decreased the equilibrium amounts of methane and carbon dioxide, but increased the amount of carbon monoxide. The yields of acetaldehyde, ethylene and carbon, which were only in trace quantities were not affected. For an increase in temperature from 525 to 625 ^{o}C the yield of hydrogen initially increased from 5.56 to 5.72 moles per mole of ethanol consumed, and thereafter decreased to 5.17 at 925 ^{o}C. Also, they showed that at lower water content (e.g. less than 10 moles of water / mole ethanol) and constant temperature of 725 ^{o}C, the yields of methane and carbon monoxide increased with pressure while yield of hydrogen decreased substantially.

Freni et al. (1996), investigated thermodynamic analysis of ethanol steam reforming reaction at temperature range of 600 to 700^{o}C, pressure 1 atm and water to ethanol molar ratio of 2:1. They observed that thermodynamically favored products were hydrogen, carbon monoxide, methane, acetaldehyde, ethylene and carbon. They also observed that the amount of hydrogen produced by the ethanol reforming was influenced by the temperature. At 600 ^{o}C the amount of hydrogen produced was 46.8%, and increased to 58.95% at 700 ^{o}C. Hydrogen yield was enhanced at low pressure and a value as high as 95% of theoretical value was reported. Also high water to ethanol molar ratio in the feed reduced the yield of undesirable products like carbon monoxide, methane and carbon.

Garcia and Laborde (1991) reported that it was possible to obtain hydrogen by the steam reforming of ethanol at temperatures greater than 280 ^{o}C and atmospheric pressure with methane being an unwanted product. Hydrogen production is however favored by high temperature, low pressure and high water-to-ethanol feed ratio. These conditions also reduce the level of by-products significantly. The effects of pressure (1-9atm) on the production of hydrogen and methane were also studied. The study showed that hydrogen production increased at all pressures as temperature increased but it increased at a much higher rate at atmospheric pressure and temperature above 327 ^{o}C. The study also showed that concentration of methane in the product stream decreased with the decrease in pressure. At a temperature of 527 ^{o}C and a water-to-ethanol feed ratio of 1:1, the methane content was 32% for atmospheric pressure and 40% for operating pressure of 3 atm. The production ratio of hydrogen to methane increased for a water-to-ethanol molar ratio of 10:1, an operating pressure of 1atm and temperatures

above 427 ^{o}C. At atmospheric pressure and temperatures above 327 ^{o}C, production of hydrogen reached a maximum with minimum CO production for a water-to-ethanol molar ratio of 10:1.

The thermodynamic analysis of Thoephilus, (2001) on steam reforming of ethanol in a solid polymer fuel cell at 1 atm, temperature range of 527 to 1027 ^{o}C, and water-to-ethanol feed ratios of 3:1 to 6:1 showed that the ethanol-steam reforming reaction needs to be carried out in two steps: (i) a high-temperature endothermic step (steam reforming), in which ethanol is converted to a gaseous mixtures of H_2, CO, CO_2, CH_4 and unreacted H_2O, (ii) a subsequent, low temperature step (water-gas shift reaction) in which CO is reacted with water to form H_2 and CO_2. Since the shift reaction is equilibrium-limited, CO conversion is not complete and an additional step of CO removal is necessary (e.g. by selective CO oxidation). He concluded that hydrogen yield of nearly 100% was obtained at optimum condition of water-to-ethanol ratio 5:1 and temperature 727 ^{o}C.

Cavallaro and Freni, (1996) investigated the ethanol steam reforming reaction over $CuO/ZnO/Al_2O_3$ catalyst, and others such as $NiO/CuO/SiO_2$, $Cu/Zn/Cr/Al_2O_x$, Pt/Al_2O_3, $Pt/La_2O_3/Al_2O_3$, Pt/TiO_2, $Pt/MgO/Al_2O_3$, Rh/SiO_2, Rh/Al_2O_3, and $Rh/MgO/Al_2O_3$**.** The experiments were carried out in a packed-bed reactor at temperature range of 357 to 477^{o}C; pressure of 1 atm, water-to-ethanol molar ratio of 6:1and 10:1. At low temperature of 377^{o}C, no traces of intermediate products such as acetic acid, acetaldehyde and ethyl acetate were produced. These compounds were produced at temperatures below 325^{o}C when the hydrogen and carbon dioxide

selectivity was very low. Hydrogen, carbon dioxide and carbon monoxide selectivity increased with increase in temperature.

Haga et al. (1998) investigated the effects of crystallite sizes on different alumina-supported cobalt catalysts on steam reforming of ethanol over the reaction conditions: temperature range of 223 to 452 ^{o}C; pressure of 1 atm; and water-to-ethanol feed ratio of 4.2:1. They reported that methane, acetaldehyde, ethene, diethyl ether and carbon dioxide were observed as product. The steam reforming of ethanol over cobalt catalysts however preceded via the formation of acetaldehyde at the temperature below 400^{o}C. The ethanol conversion reached a maximum value of 100% at 400^{o}C. Also, the results obtained using Co from different initial materials showed that the activity for ethanol conversion was independent of the starting materials such as cobalt acetate, cobalt carbonyl and cobalt chloride that produced cobalt catalyst.

The production of acetaldehyde steadily increased at lower temperatures and reached a maximum at around 330 ^{o}C. Above this temperature, acetaldehyde was converted to carbon dioxide and hydrogen. The carbon monoxide selectivity increased and reached its maximum (53%) at about 380 ^{o}C after which it decreased sharply to 23% at 400 ^{o}C. Methane selectivity reached a maximum of 20% at 400 ^{o}C after which it decreased gradually to 10% at 450 ^{o}C.

Marino et al. (1998) studied the activity of γ-alumina supported copper-nickel catalysts for hydrogen production from steam reforming of ethanol at 1 atmospheric pressure and water to ethanol molar ratio of 2.5:1. The effects of the copper loading and calcination temperature on the structure and performance of Cu/Ni/K/γ-Al_2O_3 catalysts were examined. The copper loading was varied from 0.00 wt.% to 6.36 wt.%, the

catalysts were calcined at 550 and 800^{o}C for 5h before examination. The effluent gas stream after the reaction contains H_2, CO, CO_2, CH_4, C_2H_4O, $(C_2H_5)_2O$, C_2H_5OH and H_2O. The catalysts exhibited acceptable activity, stability and hydrogen selectivity when the reaction was carried out at 300 ^{o}C. They concluded that doping of catalysts with potassium hydroxide neutralizes the acidic sites of the support and in this way minimizes diethyl ether and ethene production. In the catalyst, copper was the active agent; nickel promotes C-C bond rupture and increases hydrogen selectivity and potassium neutralizes the acidic sites of the γ-alumina and improves the general performance of the catalyst. The results of catalyst activity and selectivity measurements together with those on catalyst structure indicated that catalyst must have a high dispersion of the active agent in order to maximize ethanol conversion per copper mass unit; the higher copper dispersion was therefore achieved when catalyst was calcined at the lower temperature (550^{o}C).

Anthanasio et al. (2002) investigated ethanol steam reforming reaction at 750^{o}C and water to ethanol molar ratio 3:1 over Ni-based catalyst supported on yittra-stabilized-Ziconia (YSZ), La_2O_3, MgO and Al_2O_3. It was reported that Ni/La_2O_3 catalyst exhibited high activity and selectivity towards hydrogen production and also has long term stability of about 100h on stream for steam reforming of ethanol. The long term stability of Ni/La_2O_3 was attributed to the scavenging of coke deposition on the Ni surface area by lanthanum oxycarbonate species. Results obtained from time-on-stream over Ni/Al_2O_3 catalyst are comparable to those of Ni/ La_2O_3, but the selectivities toward reaction products decreased. In case of Ni/YSZ catalyst, selectivity towards hydrogen was constant; however selectivity towards CO_2 and CO decreased with time,

which became stable only after 20h on stream. Ni/MgO catalyst was very stable under the prevailing conditions, but poorly selective compared to other catalyst mentioned earlier.

Luengo et al. (1992) examined ethanol steam reforming reaction using Ni, Cu and Cr based catalysts on γ-Al_2O_3 and α-Al_2O_3 supports. The experiments were carried out at temperature range of 300 to 550 ^oC; pressure of 1 atm; water-to-ethanol feed ratio of 0.4:1 to 2:1; and ethanol space velocity of 2.5 to 15 h^{-1}. The metallic concentration was chosen to maximize the total conversion and increase selectivity to CO and H_2. α-Al_2O_3 supported catalyst gave maximum ethanol conversion of 100% and high selectivity to H_2 and CO, unlike γ-Al_2O_3 supported catalyst in which the ethanol conversion and selectivity to desired product was lower.

Velu et al. (2002) studied the steam reforming of ethanol over Cu-Ni-Zn-Al mixed oxide catalyst in the presence or absence of air. The reaction products were H_2, CO, CH_3COOH, CH_3CHO, CH_4 and CO_2. The ethanol conversion increased with increase in O_2/ethanol ratio and reached 100% at the O_2/ethanol ratio of 0.6. Also, the selectivity of both CO and CO_2 increased until an O_2/ethanol ratio of 0.4 was reached, CO selectivity however dropped at O_2/ethanol ratio of 0.6. Hydrogen yield decreased from 3 mols/mol of ethanol reacted to 2 mol/mole of ethanol reacted in the absence of oxygen. They concluded that addition of oxygen improved the ethanol conversion and also oxidation of CH_3CHO to CH_4 and CO_2. It was also reported that Cu–rich catalyst favored the dehydrogenation of ethanol to acetaldehyde, while the addition of nickel to Cu/Al_2O_3 system ruptured the C-C bond, enhanced the ethanol gasification and reduced the selectivity of acetaldehyde and acetic acid.

Cavallaro et al. (2003) reported that rhodium impregnated on γ-alumina is highly suitable for steam-reforming of ethanol. The performance evaluation of Rh/γ-Al_2O_3 as reforming catalyst at 650^oC showed that the main reaction products were CO_2, CO, CH_4 and CH_3CHO. Also high conversion of ethanol was obtained at gas hourly space velocity (GHSV) between 5000 and 80, 000h^{-1}, which decreased as the GHSV increased to 300,000h^{-1}. Maximum hydrogen selectivity was obtained at much lower GHSV of 10h^{-1}, which also decreased as the GHSV increased. The catalyst stability was investigated with and without oxygen. It was observed that catalyst deactivates very fast without oxygen, the presence of oxygen positively enhanced the catalyst stability and only 10% of activity was lost after 95h of reaction.

Breen et al. (2002) investigated steam reforming of ethanol at 400 to 750 ^oC over a range of oxide-supported metal catalysts at water to ethanol molar ratio of 3:1. They concluded that the support plays an important role in the steam reforming of ethanol. They observed that alumina-supported catalyst are very active at lower temperatures for dehydration of ethanol to ethene which at higher temperatures (550^oC) is converted into H_2, CO and CO_2 as major product and CH_4 as minor product. The activity of the metal was in the order of Rh>Pd>Ni=Pt. Ceria/zirconia supported catalysts were most active and exhibited 100% conversion of ethanol at high space velocity and high temperature of ~650^oC. The order of activity at higher temperatures was Pt ≥ Rh>Pd. By using combination of a ceria/zironia-supported metal catalyst with the alumina support, it was observed that the formation of ethene does not inhibit the steam reforming reaction at higher temperatures.

Freni, (2001) examined the ethanol steam reforming reactions over Rh/Al_2O_3 catalyst. The reaction was carried out at temperature range of 392 to 650 ^oC; pressure of 1.4 atm; and water-to- ethanol feed ratio of 4.2:1 to 8.4:1. The results indicated the catalytic activity of alumina (Al_2O_3) was not negligible; there was production of ethene and water at 347 ^oC, the production increased and reached equilibrium at 600 ^oC. It was observed that water content did not influence the ethene formation. When 5% Rh was added to alumina, the product analyses below 460^oC showed the presence of carbon dioxide, methane and acetaldehyde. The main steam reforming reaction occurred above 460^oC and the products included hydrogen, carbon dioxide, carbon monoxide and methane.

Freni et al. (2002) also examined the steam reforming ethanol for hydrogen production for molten carbonate fuel cell on Ni/MgO. They reported that the catalyst exhibited very high selectivity to hydrogen and carbon dioxide. The CO methanation and ethanol decomposition were considerably reduced. In addition, coke formation was strongly depressed because of the benefits induced by the use of the basic carrier, which positively modified the electronic properties of Ni.

Galvita et al. (2001) investigated the steam reforming of ethanol for syn-gas production in a two-layer fixed bed catalytic reactor. The reaction conditions were as follows, temperature range of 210 to 380 ^oC; pressure of 1 atm; and water-to-ethanol feed ratio of 8.1:1 and 1.04:1. In the first bed, the ethanol was converted to a mixture of methane, carbon oxides, and hydrogen on Pd/C (Pd supported on Sibunit, a special porous carbonaceous material) catalyst and then this mixture was converted to syn-gas over a Ni-based catalyst for methane steam reforming. It was observed that ethanol

conversion increased with increasing temperature, which attained 100% at 330 and 360 ^{o}C for water-to-ethanol ratios of 8.1 and 1.04, respectively. They concluded that the use of two-layer fixed-bed reactor prevented the coke formation and provided the yield close to equilibrium.

Jordi et al, (2002) examined the hydrogen production process by steam reforming of ethanol over several cobalt supported catalyst. The reaction temperature was varied from 300 to 450^{o}C and water to ethanol molar ratio of 13:1 was used. It was observed that negligible steam reforming of ethanol occurred over Co/Al_2O_3 catalyst. The dehydration of ethanol to ethene took place to a large extent. This was attributed to the acidic behaviour of Al_2O_3 under similar conditions. Co/MgO catalyst showed low conversion of ethanol of only 30%, and the main reaction was dehydrogenation of ethanol to acetaldehyde. Co/SiO_2 also showed dehydrogenation of ethanol to acetaldehyde as the main reaction. At low temperature, 100% ethanol conversion was obtained on Co/V_2O_5, about 84% of ethanol converted was through dehydrogenation to acetaldehyde, while the rest was the actual ethanol steam reforming. Co/ZnO exhibited the highest catalytic performance of all catalysts studied. 100% ethanol conversion was achieved and the highest selectivity of hydrogen, and carbon dioxide per mole ethanol reacted were obtained without catalyst deactivation.

Aupretre et al. (2002) also studied the effects of different metals (Rh, Pt, Ni, Cu, Zn and Fe) and role of the supports (γ-Al_2O_3, 12%CeO_2-Al_2O_3, CeO_2 and $Ce_{0.63}Z_{0.37}O_2$) on steam reforming of ethanol. The experiments were carried at water to ethanol ratio of 3:1 and constant temperature between 500 and 800^{o}C and 1 atm pressure.

At 700°C, γ-Al_2O_3 supported Rh and Ni catalysts appeared to be the most active and selective catalysts in ethanol reforming reaction. Ni/Al_2O_3 gave a higher yield but lower selectivity to CO_2 compared with Rh/Al_2O_3. While concentrating on Rh and Ni catalysts the role of other oxides supports were investigated. The results obtained at 600°C showed the catalyst activity in following descending order for Rh; Rh/ $Ce_{0.63}Z_{0.37}O_2$>Rh/ CeO_2-Al_2O_3 > Rh/ CeO_2 > Rh/ γ-Al_2O_3. A similar trend was obtained for Ni; Ni/ $Ce_{0.63}Z_{0.37}O_2$ > Ni/ CeO_2 > Ni/ CeO_2-Al_2O_3 > Ni/ γ-Al_2O_3.

Jose et al. (2003) examined the steam reforming reaction over Ni/Al_2O_3 catalyst. They concluded that high temperature above 773K, higher water to ethanol molar ratio (6:1) increased the high hydrogen yield (5.2) and selectivity (91%). The excess water in the feed enhanced methane steam reforming and depressed carbon deposition.

In the comprehensive study carried out by Jordi et.al (2001), various metallic oxides such as MgO, γ-Al_2O_3, TiO_2, V_2O_5, CeO_2, ZnO, Sm_2O_3, La_2O_3, and SiO_2 were used as catalysts for steam reforming of ethanol at temperature between 300°C and 450°C. The ethanol conversion increased with increase in temperature in all cases. However, significant differences were observed in terms of activity, stability and selectivity of the catalysts. It was observed that γ-Al_2O_3 and V_2O_5 although showed high conversion of ethanol, at lower temperature (350°C), they were not suitable for H_2 production as both were highly selective for ethylene production by dehydration of ethanol (being acidic in nature). The results also showed that MgO and SiO_2 gave total conversion less than 10% and were also selective for dehydrogenation of ethanol to form acetaldehyde, La_2O_3 and CeO_2 gave total conversion of approximately 20%. Other oxides such as TiO_2 and Sm_2O_3 showed high deactivation process with conversions

decreasing from 100% to 3.9% and from 67.2% to 37.2% respectively. After reaction these catalysts appeared black. This was attributed to the carbon deposition during the reaction, which could have been responsible for the drop in activity of the catalyst.

ZnO reportedly enhanced the steam reforming of ethanol, and showed high selectivity for H_2 and CO_2. They concluded that ethanol is capable of forming wide range of products. The product selectivity obtained with different catalysts can be explained with following reactions:

- Ethanol-steam reforming

$$C_2H_5OH + 3H_2O \longrightarrow 2CO_2 + 6H_2 \quad (1.1)$$

- Ethanol decomposition to methane

$$C_2H_5OH \longrightarrow CO + CH_4 + H_2 \quad (1.2)$$

- Ethanol dehydration

$$C_2H_5OH \longrightarrow C_2H_4 + H_2O \quad (1.3)$$

- Ethanol dehydrogenation

$$C_2H_5OH \longrightarrow CH_3CHO + H_2 \quad (1.4)$$

- Ethanol decomposition to acetone

$$2\ C_2H_5OH \longrightarrow CH_3COCH_3 + CO + 3H_2 \quad (1.5)$$

- Water-gas shift reaction

$$CO + H_2O \longrightarrow CO_2 + H_2 \quad (1.6)$$

Methane, acetaldehyde, acetone, ethene, are all undesirable products because they compete with H_2 for the hydrogen atoms.

2.6 Rational for Selecting Catalyst Components

Ni/Al_2O_3 catalyst was selected based on well documented fact that Ni enhances steam-reforming reaction (Gavita et al., 2001; Idem et al., 2003). Also, Ni ensures C-C bond rupture of ethanol or other oxygenated hydrocarbon components of crude ethanol (Luengo et al., 1992; Marino et al., 1998), in addition, it enhances ethanol gasification, reduces selectivity of acetaldehyde and acetic acid (Velu, 2002). On the other hand, γ-Al_2O_3 was chosen as support because it is cheaply available; it has high surface area and high thermal stability (Richardson, 1989).

2.7 Catalyst Characterization

The main reasons for characterizing catalysts are (i) to elucidate the processes taking place during each step of catalyst preparation, (ii) to determine the catalyst characteristics responsible for catalyst performance, and (iii) to use these characterizations as feedback during subsequent stages of design of catalyst for improved performance (Idem 1995). No information is available in the literature about any previous work or catalyst used for the reforming of crude ethanol. However, previous characterization studies for nickel-based catalysts will be examined.

The characterization of Ni/Al_2O_3 catalysts was done by Jianjun et al. (2004), the characterization techniques used were temperature-programmed reduction (TPR), thermogravimetric analysis (TG/DTA) and powder X-ray diffraction (XRD). Juan-Juan et al. (2004) used temperature-programmed reduction (TPR) and X-ray photoelectron spectroscopy (XPS) techniques to characterize the alumina supported nickel catalyst with potassium doping. Also Jae-Hee et al. (2004) used techniques such as temperature-programmed reduction (TPR), temperature programmed oxidation (TPO), powder X-

ray diffraction (XRD) and transmission electron microscopy (TEM). It may be noted that extensive characterization studies were done on Ni based catalysts used mostly for CO_2 reforming of methane. The brief description of the characterization techniques for Ni based catalysts is presented below.

2.7.1 X-Ray Diffraction (XRD) Studies

Jianjun et al. (2004) carried out XRD studies on Ni/Al_2O_3 catalysts prepared by impregnation of alumina with nickel nitrate solution. NiO and Al_2O_3 phases were detected on the calcined samples by these authors. Jae-Hee et al. (2004) also carried out XRD studies on Ni/Al_2O_3 and $Cu/Ni/Al_2O_3$ catalysts. Phases such as $NiAl_2O_4$, NiO were identified on Ni/Al_2O_3 catalyst at angle 2θ between 37.0 to 66.2^oC, when Cu was added, a new peak appeared corresponding to $(Cu_{0.2}\ Ni_{0.8})O$, other phases like CuO and $CuAl_2O_4$ were also identified. The XRD pattern of both catalysts after reduction in 5% H_2/Ar at 750^oC for 3 hours revealed the presence of Ni metal at 44.5^oC.

2.7.2 Temperature Programmed Reduction

Jianjun et al. (2004) carried out TPR experiments on Ni/Al_2O_3 and $Ni/MgO/Al_2O_3$ catalysts calcined at 550^oC as well as pure NiO samples calcined at 800^oC. Two reduction peaks were observed for Ni/Al_2O_3 and $Ni/MgO/Al_2O_3$ catalysts between 500-600^oC and 600-900^oC. Pure NiO prepared by decomposition of $Ni(NO_3)_2$ and calcined at 800^oC for 5 hours showed one peak at 397.9^oC. The authors concluded that the reducibility may depend on the degree of aggregation of nickel oxide. Also fine distribution of nickel oxide on the support resulted to stronger interaction between NiO and support (which led to formation of $NiAl_2O_4$) which was at higher reduction temperature. A TPR peak assigned to nickel oxides that were not completely integrated

in the spinel structure, but however had certain degree of interaction with support was observed at approximately 505^{o}C. They also reported that high temperature around 800^{o}C was required to reduce nickel aluminate spinel ($NiAl_2O_4$).

2.7.3 Temperature Programmed Oxidation

Jae-Hee et al. (2004) reported that the deactivation of Ni-based catalysts can be due to the carbon formation on the catalyst during the reaction. Therefore, the TPO experiments were conducted to investigate the type of carbon deposited on the catalyst after 16 h of run. The TPO spectral of Ni/Al_2O_3 catalyst showed two major peaks at 400^{o}C and 660^{o}C.The peak at 400^{o}C was assigned to the reversible carbonaceous species, which was supposed to be reversibly converted to CO_2 by CO oxidation, while the peak at 660^{o}C was assigned to an inactive graphitic carbon. They also noted that graphitic carbon was mainly produced on $Cu/Ni/Al_2O_3$ and hence carbon deposition from CH_4 decomposition could be prevented on Cu-Ni alloy. The TEM images of the used catalysts were taken to examine the morphology of the carbon. A number of carbon tubes with different sizes of 10-100nm were observed on the used Ni/Al_2O_3 catalyst, while carbon tubes of uniform sizes were formed on $Cu/Ni/Al_2O_3$. The Ni particles of 10-20nm were mainly observed on Ni/Al_2O_3 catalyst by TEM images.

2.7.4 Thermogravimetric Analysis (TG/DTA) of Spent Catalyst

Jianjun et al. (2004) reported the TG/DTA results of spent $5\%NiMgAl_2O_3$ catalyst in an oxidative atmosphere. In their analyses they observed that initial step of weight loss occurred at the temperature above 100^{o}C. This was ascribed to thermal desorption of H_2O and adsorbed CO_2 and removal of easily oxidizeable carbonaceous species. The oxidation of coke to CO and CO_2 was observed mainly at 450-650^{o}C.The

DTA profiles of the same catalyst under oxidative environment revealed two distinctive exothermic peaks at 470^{o}C and 600^{o}C. It was concluded that the main part of the coke deposited on the catalyst was oxidatively removed at around 600^{o}C.

3.0 EXPERIMENTAL

The preparation and characterization procedures of the Ni/Al_2O_3 catalysts prepared by coprecipitation, precipitation and impregnation methods shall be described in this chapter. The experimental set-up and procedures for catalytic reforming of crude ethanol and kinetic studies are also discussed.

3.1 Catalyst Preparation

Three different catalyst preparation techniques such as co-precipitation, precipitation and impregnation methods were used for the preparation of catalysts. Ten different catalysts were prepared by varying the concentration of nickel.

3.1.1 Chemicals

The sources of nickel was nickel (ii) nitrate hexahydrate, 99.999% pure [$Ni(NO_3)_2$. $6H_2O$; obtained from Sigma-Aldrich, Inc., St Louis, Mo, USA] while that for aluminum was aluminum nitrate nonahydrate [$Al(NO_3)_3$. $9H_2O$; 98.0-99.99% pure; obtained from EM Science, Gibbstown, NJ, USA]. Sodium carbonate [Na_2CO_3, 99.5% pure] and commercial alumina [Al_2O_3] were obtained from EM Science, Gibbstown, NJ, USA].

3.1.2 Coprecipitation Procedure

The solution mixture of nickel nitrate hexahydrate and aluminum nitrate nonahydrate of appropriate concentrations (depending on nickel loading) were prepared. Precipitation was brought about by adding this solution in a drop-wise manner with

constant stirring to sodium carbonate solution (pH =11.5) maintained at 40°C in a 3-liter flask. The quantity of sodium carbonate solution taken was 1.1 times the stoichiometric requirement. The resulting slurry (pH ≅ 8.0) was vigorously stirred for another 60 min. The precipitate was filtered and dried at 80°C overnight. The dried precipitate was then washed several times with warm water and finally with cold water and then dried at 110°C overnight in air. The dried sample was then calcined, characterized and used for performance evaluation for the reforming of crude ethanol.

3.1.3 Precipitation Procedure

The precipitation method involved the preparation of solutions of predetermined amounts of nickel nitrate hexahydrate (depending on the Ni loading). This solution was added to another solution containing an appropriate quantity of sodium carbonate (to induce complete precipitation of the former), and commercial alumina. The resulting slurry was vigorously stirred for 24 h to enhance precipitation of nickel on the γ-alumina. The precipitate was filtered and dried at 80°C overnight. The dried precipitate was then washed several times with warm water and finally with cold water and then dried at 110°C overnight in air. The dried sample was then calcined, characterized and used for performance evaluation for the reforming of crude ethanol.

3.1.4 Impregnation Procedure

The impregnation method involved preparation of nickel solutions of different concentrations dissolved in a solution of a fixed amount of the same type of commercial alumina (γ-alumina obtained from EM Science, Gibbstown NJ, USA) as used in the precipitation method. The resulting slurry was stirred vigorously for 24 h and then filtered; the filtered sample was dried at 110°C overnight in air. The dried sample was

analyzed for elemental composition by inductively coupled plasma–mass spectroscopy (ICP-MS). The information was used to prepare a calibration curve that was used for subsequent preparation of catalysts with the desired Ni loading.

3.1.5 Calcination

Calcination was carried out in a muffle furnace by placing the catalyst samples in a crucible. The temperature of the furnace was slowly raised to 600^{o}C and maintained at this temperature for 3 hours. After calcination, the catalyst was allowed to remain inside the switched off furnace to cool down slowly to room temperature. Due to the loss of material during calcination such as moisture, nitrates and carbonates, the catalyst reduced in size appreciably.

3.1.6 Activation

The catalysts were activated in-situ prior to performance evaluation by reducing in a stream of 5 % H_2 in N_2 (obtained from Praxair, Regina, SK, Canada) at 600 ^{o}C for 2 hours.

3.1.7 Composition of Catalysts

The designations and elemental compositions of the calcined catalysts are given in Table 3.1. CP, PT and IM indicate coprecipitation, precipitation and impregnation techniques, respectively. The numbers in these designations represent the loadings while the symbols represent the methods. For example, CP10 indicates a catalyst with 10% Ni loading prepared by coprecipitation method.

Table 3.1: Name and Chemical Compositions of Catalysts Prepared

Preparation method	Catalyst Name	Ni Composition (wt.%)	Al Compisition (wt.%)	O Composition (wt.%)
Coprecipitation	CP10	10	47.63	42.37
	CP15	15	44.98	40.02
	CP20	20	42.34	37.66
	CP25	25	39.69	35.31
Precipitation	PT10	10	47.63	42.37
	PT15	15	44.98	40.02
	PT20	20	42.34	37.66
Impregnation	IM10	10	47.63	42.37
	IM15	15	44.98	40.02
	IM20	20	42.34	37.66

3.2 Catalyst Characterization

Catalyst characterization was carried out to identify the properties of the catalyst that are responsible for the catalyst activity. These were performed for dried, calcined and reduced catalysts. The different techniques used for the catalysts characterization include: Thermogravimetric/differential scanning calorimetry (TG/DSC), Powder X-ray diffraction (XRD), temperature programmed reduction (TPR), and BET surface area, pore volume and pore size distribution (see Table 3.2 for key information). The different characterization techniques are briefly described in the following sections.

3.2.1 Thermo-Gravimetric / Differential Scanning Calorimetry

The objective of the Thermo gravimetry / differential scanning alorimetry (TG / DSC) analyses was to determine the weight loss, rate of weight loss as well as heat effects due to drying or decomposition of the catalyst sample with the change of temperature. From the generated profiles, it can be predicted if the weight loss of the

sample was caused by drying or decomposition of complexes. Catalyst samples were analyzed by the TG-DSC in order to determine the maximum temperature after which the catalyst weight loss was negligible. TG-DSC analyses were performed with TG-DSC-1100 supplied by Setaram Scientific and Industrial Equipment, NJ, USA. 20 to 50 mg of catalyst sample was placed in a balance inside the analyzer. The analyzer read the weight of the sample automatically. The sample was heated in flowing argon from 40 to 800 ^{o}C with a heating rate of 10 ^{o}C / min. This helped to determine the approximate temperature of decomposition of constituent carbonates, hydroxide and other compounds.

3.2.2 Powder X-Ray Diffraction Analyses

At different stages of preparation, all the catalysts were examined by X-ray diffraction (XRD) using D8 diffractometer with GADDS with a Cu-Kα radiation at 40 kV and 40 mA, both manufactured by Bruker AXS, U.S.A, in order to identify the component phases present as a function of preparation method. This was applied to dried, calcined and reduced catalyst samples. The powdered samples were smeared on metal holder at room temperature. The X-ray diffractograms were recorded from 20^{o} to 100^{o} at a speed of 5^{o} (2θ) per min. The crystallite sizes of the samples were also obtained by X-ray line broadening using the same equipment.

3.2.3 Temperature Programmed Reduction (TPR)

The objective of temperature programmed reduction (TPR-H_2) was to determine the reducibility as well as the optimum reduction temperatures for the catalysts before the reforming reaction. It was also useful in determining the type of species present in the calcined samples when combined with XRD analyses. The TPR analysis was performed

Table 3.2: Summary of catalyst characterization studies

No.	Characterization	Place Carried Out	Key Information
1	X-Ray Diffraction	Process Systems Engineering Laboratories, U of R	To obtain information on various phases of the catalysts
2	Temperature Programmed Reduction	Catalysis and Chemical Reaction Engineering Laboratories, U of S	To measure the extent of reduction (intensity and reduction temperature) for various phases of the catalysts
3	Thermo Gravimetric/ Differential Scanning Calorimetry	Process Systems Engineering Laboratories, U of R	To determine the thermal stability and weight loss of the catalysts
4	Temperature Programmed Oxidation	Catalysis and Chemical Reaction Engineering Laboratories, U of S	To determine the carbon deposition on catalyst surface
5	BET Surface area, Pore Volume and Pore Size Distribution	Process Systems Engineering Laboratories, U of R	To measure physical surface area, pore volume and pore size distribution of the catalysts

for the calcined catalysts using Quantachrome equipment (Model ChemBET 3000, manufactured by Quantachrome Corporation, FL, USA). About 0.1 g of the catalyst sample was placed in a U shaped glass tube. The sample tube was placed in an electric furnace with precise temperature control. The sample tube was heated from 35 to 900 ^{o}C at a linearly programmed rate of 10 ^{o}C/min at atmospheric pressure in a reducing gas stream of 3 mol% H_2 with balanced N_2 (obtained from Praxair, Mississauga, ON,

Canada) with a flow rate of 35 ml/min. The TPR plot was logged using an on-line data acquisition system.

3.2.4 BET Surface Area, Pore Volume and Pore Size Distribution

The BET surface area, pore size, pore volume and pore size distribution measurements of the catalysts were determined by using a Micromeritics adsorption equipment (Model ASAP 2010, manufactured by Micromeritics Instruments Inc., Norcross, GA, USA) using N_2 gas (99.995 % pure; obtained from Praxair, Regina, SK, Canada). BET surface area includes the surface area of the pores as well as that of the outside of the catalyst. The BET analyses were performed for the calcined catalysts. Each analysis required about 0.50g of catalyst sample. Prior to analysis, each catalyst sample was evacuated at 200 ^{o}C to ensure that there was no adsorbed moisture on the catalyst surface. The adsorption and desorption isotherms used in the evaluation of BET surface area were obtained at the boiling temperature of liquid nitrogen which is -195 ^{o}C. These values are characteristic for a given catalyst sample and are reproducible.

3.3 Reaction Feed Stock

The feed for this process was fermentation broth and was obtained from Pound Maker Agventures, Lanigan, Saskatchewan, Canada. This was used as received except for the removal of particulate matter by filtration. However, for the purpose of evaluating the performance of the catalysts, crude ethanol was defined as the combination of all the oxygenated hydrocarbon components present in fermentation broth; namely, ethanol, lactic acid, glycerol and maltose. Analysis of the fermentation broth was carried out to identify and quantify these components of fermentation broth using a high performance liquid chromatograph (HPLC), Agilent 1100 series supplied

by Agilent Technologies, Wilmington, Delaware, USA. The HPLC was equipped with a 250 by 4.1 mm HC-75 column and a refractive index detector, while 0.05 mM succinic acid was used as the mobile phase.

3.4 Experimental Set-up and Procedure

3.4.1 Catalyst Performance Evaluation

Experiments were carried out in a packed bed tubular reactor (PBTR) setup. The reactor assembly is shown in Figure 3.1. The reactor used was BTRS model number 02250192-1 supplied by Autoclave Engineers, Erie, PA, USA. It was made of a stainless steel tube of 8 mm internal diameter (D) placed in an electric furnace. Crude ethanol was delivered to the reactor chamber by means of a HPLC pump regulated at desired flow rates. The reaction temperature was measured with a sliding thermocouple placed inside the bed. The error on temperature measurement was within $\pm 1^{o}C$.

A typical run for the reforming of crude ethanol was performed as follows: approximately 1 g of the catalyst was mixed with 2 g of Pyrex glass (i.e. inert material) of the same average particle size and then loaded into the reactor. The feed consisting of crude ethanol (comprising of ethanol plus other organics and water) was then pumped at the desired flow rate (i.e. space velocity) to the vaporizer maintained at $250^{o}C$ before entering the reactor. Prior to reaction the catalyst was reduced in-situ by treatment with 5% H_2 in N_2 gas (supplied by Praxair, Regina, SK, Canada) flowing at 100 mL/min for 2 h. The reactions were carried out at atmospheric pressure and reaction temperature of $400^{o}C$. The product mixture during reaction was passed through a condenser and gas-liquid separator to separate the gaseous and liquid products for analysis.

3.4.2 Kinetic Studies

The same reactor was used to generate kinetic data for modeling the crude ethanol reforming process over catalyst CP15 which was identified as the best catalyst in this work.

The experiments to collect kinetic data were performed at reaction temperatures of 593, 693 and 793K, and ratios of weight of catalyst to mass flow rate of crude ethanol (W/F_{A0}) of 2143, 1382, 1071, 952 and 779 kg-cat-s/kg-crude ethanol using catalyst of 0.6 mm average particle size. According to Rase, (1987), Geankoplis, (2000) and Froment et al. (1990), there are requirements for packed-bed reactors to ensure that flow conditions in the reactor are close to plug flow in order to obtain isothermal reactor operation, eliminate backmixing and minimize channeling. These are: (a) ratio of catalyst bed height to catalyst particle size (L/D_p) > 50, and (b) ratio of internal diameter of the reactor to the catalyst particle size (D/D_p) > 10. In this work, L/D_p and D/D_p of 88.33 and 13.33 were respectively used in all kinetic experiments in order to ensure plug flow behavior in the reactor.

3.5 Analysis of Products

The liquid product was analyzed using the HPLC described in section 3.3 above as well as GC-MS. GC-MS analysis was performed using GC-MS model HP 6890/5073 supplied by Hewlett-Packard Quebec, Canada. A HP–Innowax column (length = 30m, internal diameter = 250 μm, thickness = 0.25 μm) packed with cross - linked – poly – ethylene glycol was used in the GC for the separation of components. The composition of the output gas stream was analyzed on-line by gas chromatography (Model HP 6890)

using molecular sieve and hysep columns, a thermal conductivity detector (TCD) and helium as carrier gas.

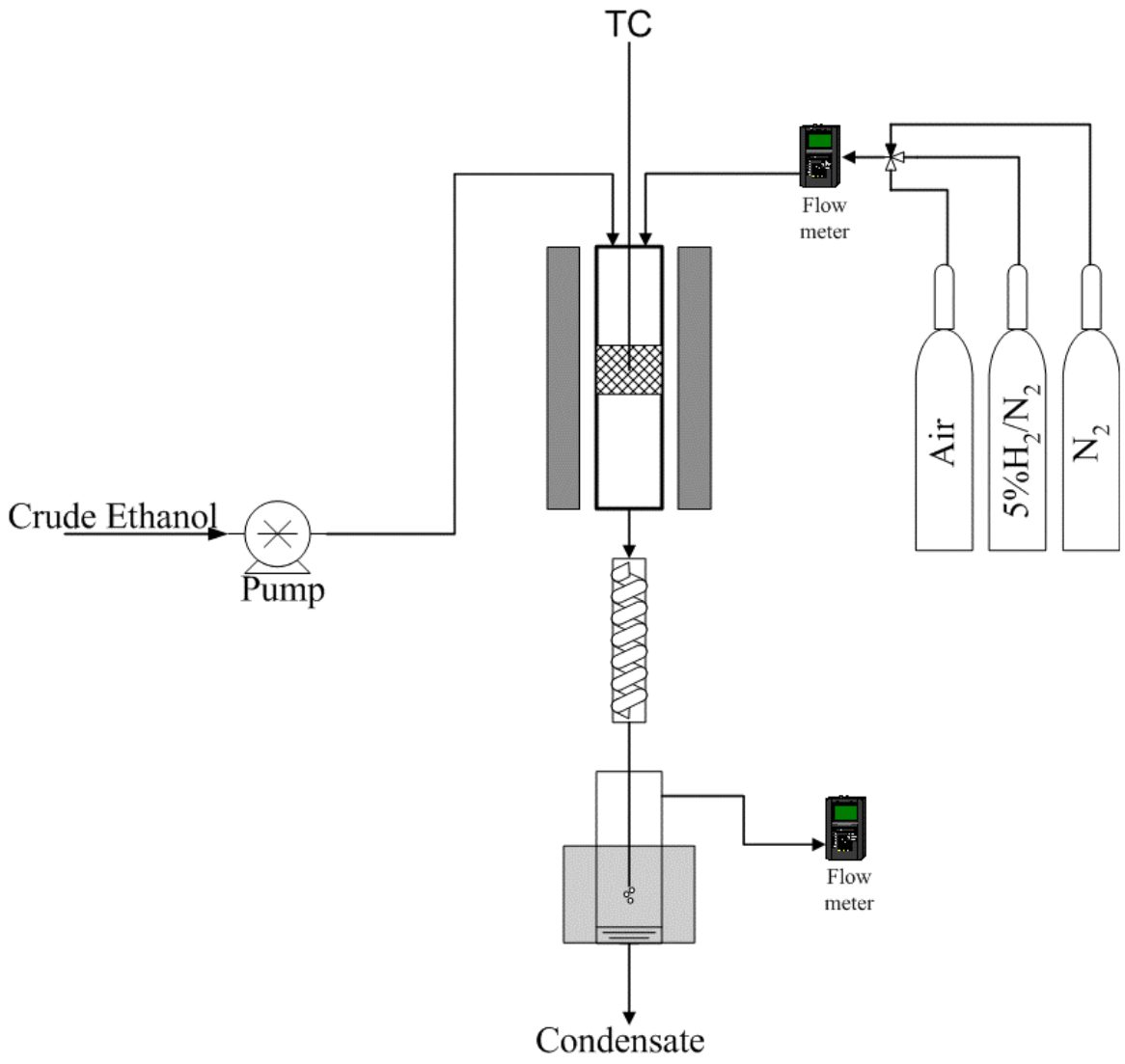

Figure 3.1: Schematic diagram of the experimental rig for the production of hydrogen from crude ethanol

4.0 RESULTS AND DISCUSSION

The results of catalyst characterization studies, catalyst performance evaluation, kinetic and reactor modeling are presented and discussed in this section.

4.1 Catalyst Characterization

4.1.1 BET surface area, Pore size and Pore volume

BET surface area, pore volume and pore size studies were performed on the calcined catalysts. The results are given in Table 4.1 for pore volume and average pore size and in Figure 4.1 for BET surface area.

Table 4.1: Summary of Pore volume and Pore sizes of catalysts

Catalyst Name	Pore Volume (cm^3/g)	Pore Size (nm)
CP10	0.26	12.6
CP15	0.29	14.5
CP20	0.22	12.8
CP25	0.19	12
PT10	0.23	5.4
PT15	0.22	5.6
PT20	0.12	5.4
IM10	0.18	4.3
IM15	0.18	4.6
IM20	0.17	4.5

In the coprecipitation method, the BET surface area (Figure 4.1) decreased in a monotonic fashion from 83 to 65 m^2/g as the Ni loading increased. In contrast, the pore size and pore volume initially increased with Ni loading and reached a maximum of 14.5 nm and 0.29 cm^3/g, respectively and then decreased with further increase in the Ni loading. The pore volume of catalysts which were prepared by precipitation and impregnation methods showed a somewhat different trend as compared to the trend for coprecipitation. It was observed in the PT and IM catalysts that 10 and 15% Ni loading catalysts gave identical values in each case.

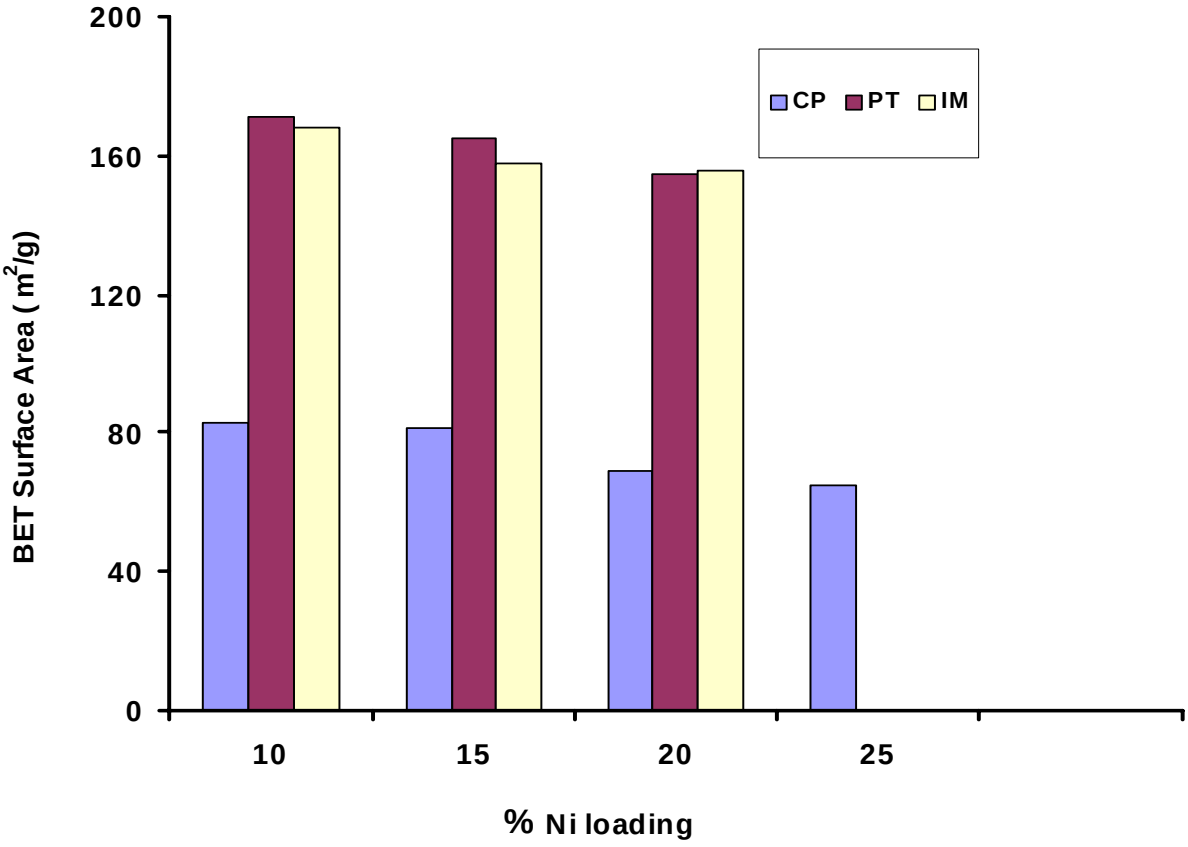

Figure 4.1: BET surface areas as function of Ni loading for catalysts calcined at 600°C

Calcined catalysts prepared by precipitation and impregnation methods exhibited high surface area and low pore sizes compare to those prepared by the coprecipitation method. However their trends with nickel loading were similar.

4.1.2 Powder X-ray Diffraction (XRD)

Powder XRD analyses were performed on the dried, calcined and reduced catalysts to identify the species present in the catalysts at various stages of preparation. Figure 4.2 shows the XRD spectra obtained for dried (Figure 4.2a), calcined (Figures 4.2b-d) and reduced (Figure 4.2e) catalysts. Typical spectra of dried catalysts (15% Ni loading) exhibited common XRD peaks corresponding to nickel hydroxide ($Ni(OH)_2.4H_2O$) and nickel oxide hydroxide (NiOOH). Only the catalyst prepared by the impregnation method gave XRD peaks corresponding to hydrated alumina ($Al_2O_3.3H_2O$) whereas the catalyst prepared by coprecipitation had XRD peaks corresponding to nickel aluminium carbonate hydroxide ($Ni_2Al(CO_3)_2(OH)_3$ and $NiAl(CO_3)(OH)_3$) and nickel carbonate hydroxide hydrate ($Ni_2(CO_3)(OH)_2.4H_2O$). The catalysts prepared by the coprecipitation and precipitation methods exhibited XRD peaks corresponding to aluminium carbonate hydroxide ($Al(CO_3)_2(OH)_4.3H_2O$ and $Al(CO_3)(OH)$). The formation of nickel aluminium carbonate hydroxide, nickel carbonate hydroxide hydrate and aluminium carbonate hydroxide were attributed to using Na_2CO_3 for precipitation (Idem, 1995).

Catalysts prepared by all the three different methods were compared at different Ni loadings in the case of calcined catalysts. For the catalysts with 10% Ni loading, the XRD spectra (Figure4.2b) showed common peaks corresponding to nickel oxide (NiO), alumina (Al_2O_3) and nickel aluminate ($NiAl_2O_4$) even though the latter was only

pronounced for IM10 whereas for the catalysts with 15% Ni loading, only nickel oxide and alumina were the common species. Nickel aluminate was observed only on coprecipitated (CP15) and impregnated (IM15) samples. The same scenario was observed for the catalyst samples with 20% Ni loading. The formation of nickel aluminate was attributed to the close interaction between NiO and Al_2O_3 at a high temperature as shown in Equation 4.1 mainly for impregnated catalyst samples or the decomposition of nickel aluminium carbonate hydroxide followed by Equation 4.1 for coprecipitated catalyst samples. This was similar to the results of Idem and Bakhshi, (1996a).

$$NiO + Al_2O_3 = NiAl_2O_4 \quad (4.1)$$

The formation of nickel aluminate is an indication of strong metal-support interaction. Also, the appearance of peaks corresponding to nickel species is an indication of strong crystallinity of the species and that monolayer coverage of Al_2O_3 by the applicable Ni species was exceeded. On the other hand, the absence of some of the Ni species (such as $NiAl_2O_4$) in some of the calcined catalyst samples (e.g. the PT catalysts) is an indication that Ni species is still within monolayer coverage (i.e. the amount present is too small and thus cannot be detected by XRD) or is completely absent.

In the case of the reduced catalysts, typical XRD spectra for catalysts with 15% Ni loading (Figure 4.2e) show common peaks corresponding to nickel metal (Ni) and aluminum oxide. The spinel, nickel aluminate, was observed only for catalysts prepared by coprecipitation and impregnation methods. This shows that the reduction temperature of 600^{o}C used for catalyst reduction with H_2 was not sufficient to reduce all the nickel aluminate species to Ni metal and alumina for these two types of catalysts.

Table 4.2 shows the results of crystallite size measurements for NiO species obtained by X-ray line broadening as a function of preparation method and Ni loading. At 10% Ni loading all catalysts have relatively small crystallite sizes with that prepared by impregnation having the smallest crystallite size. However, with Ni loadings of 15 and 20%, the catalysts prepared by the impregnation method produced a dramatic increase in crystallite size (105.8 and 160.2 nm, respectively). These were much larger than the crystallite sizes of the corresponding Ni loadings for catalysts prepared by coprecipitation and precipitation methods. The overall large crystallite sizes (especially for Ni loading $\geq$ 15%) shows the existence of agglomeration of Ni species and that monolayer coverage was exceeded.

Table 4.2: Crystallite size of catalysts

Catalysts Name	Crystallite size(nm)
CP10	26.5
CP15	29.8
CP20	38.5
PT10	21.5
PT15	20.8
PT20	39.6
IM10	15.3
IM15	105.8
IM20	160.2

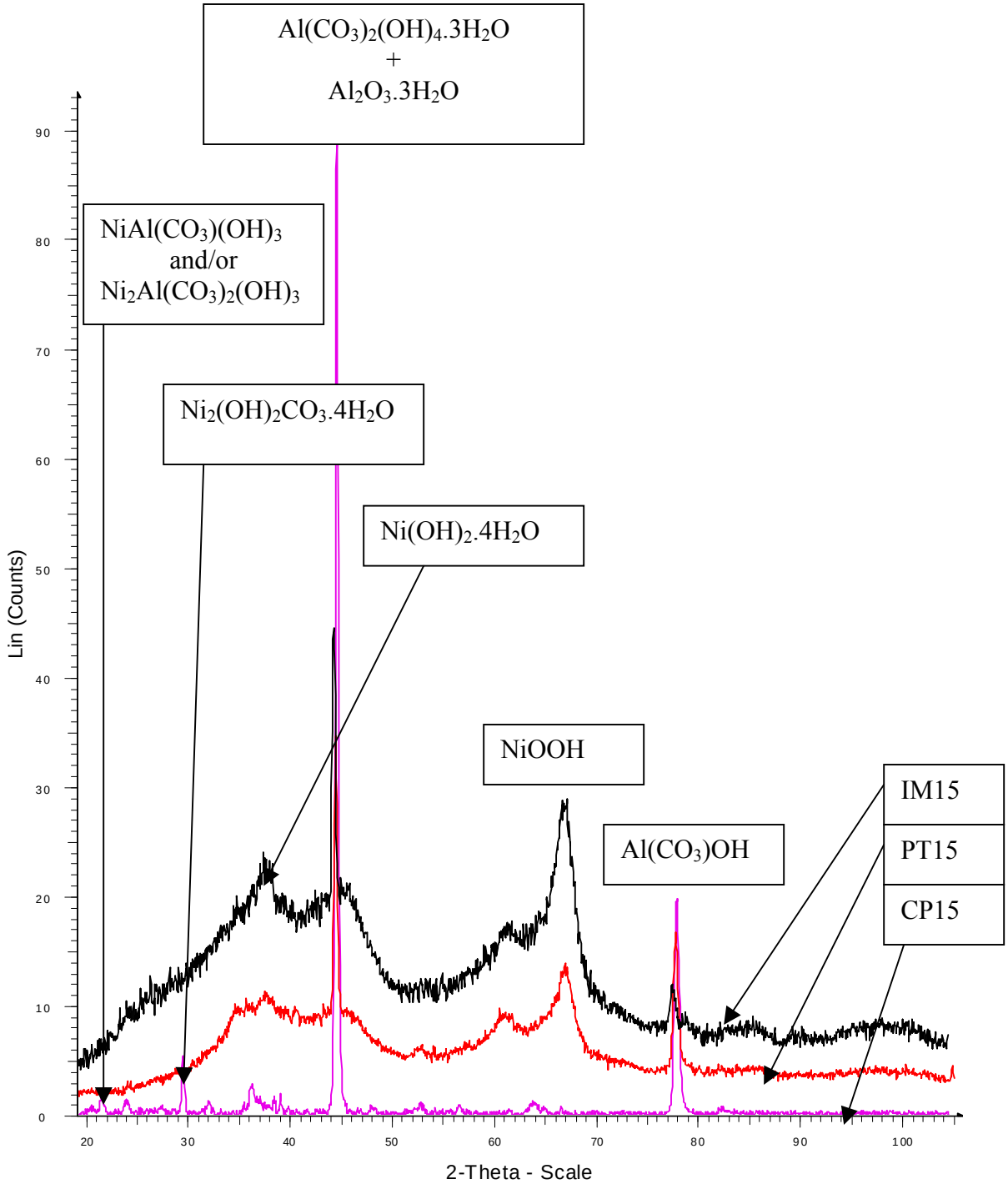

Figure 4.2a: XRD pattern of dried catalysts (15% Ni loading)

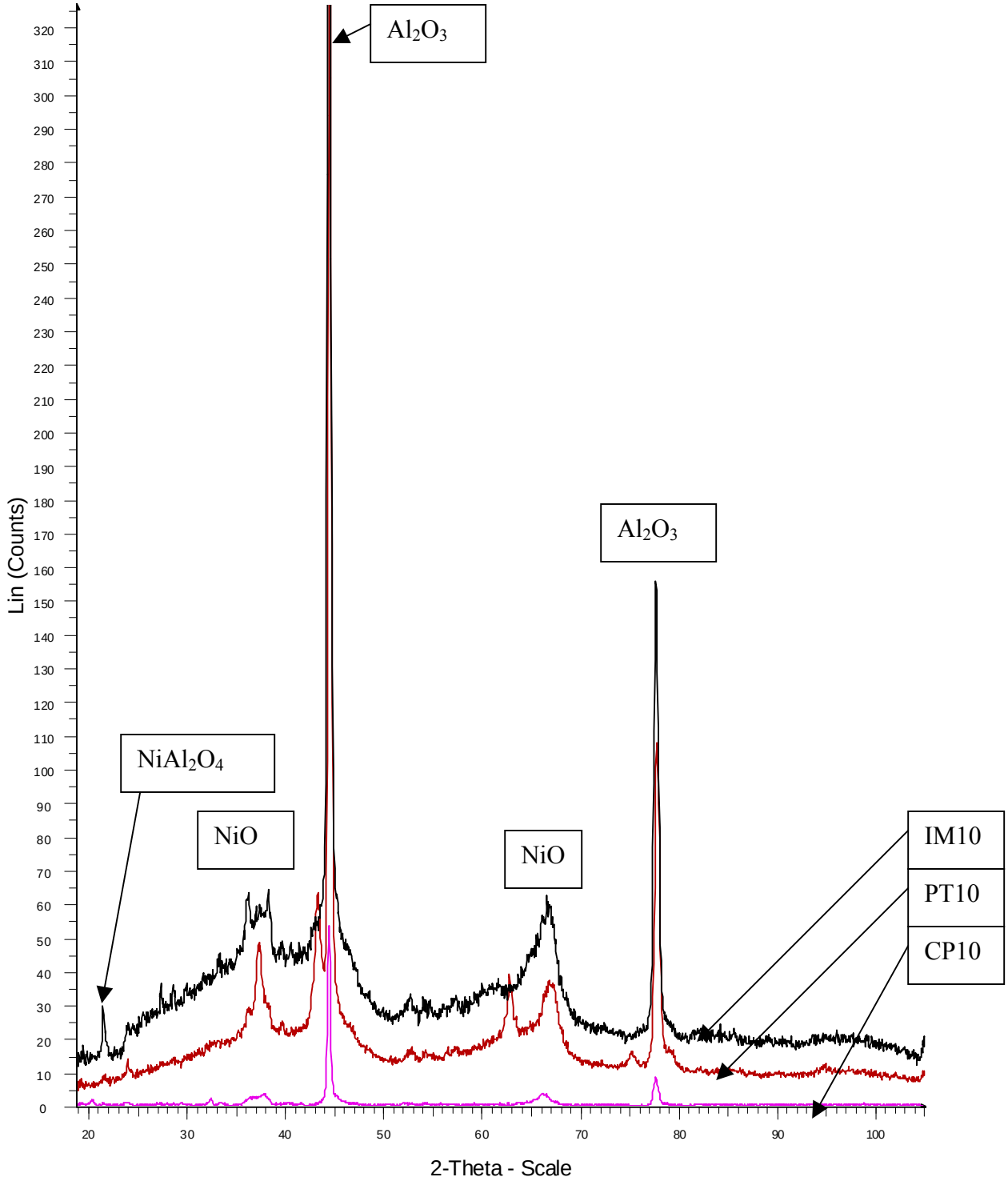

Figure 4.2b: XRD pattern of calcined catalysts (10% Ni loading)

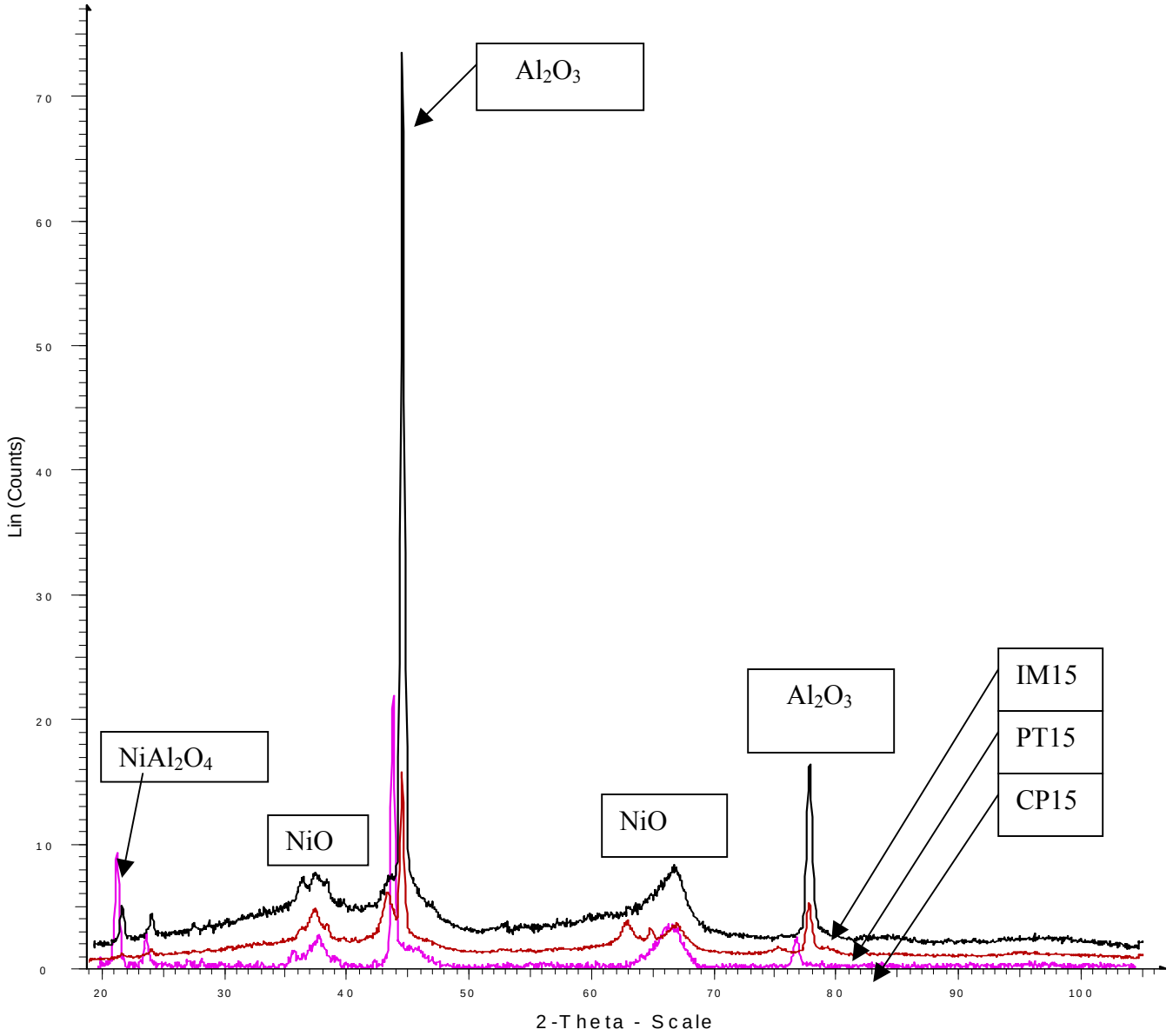

Figure 4.2c: XRD pattern of calcined catalysts (15% Ni loading)

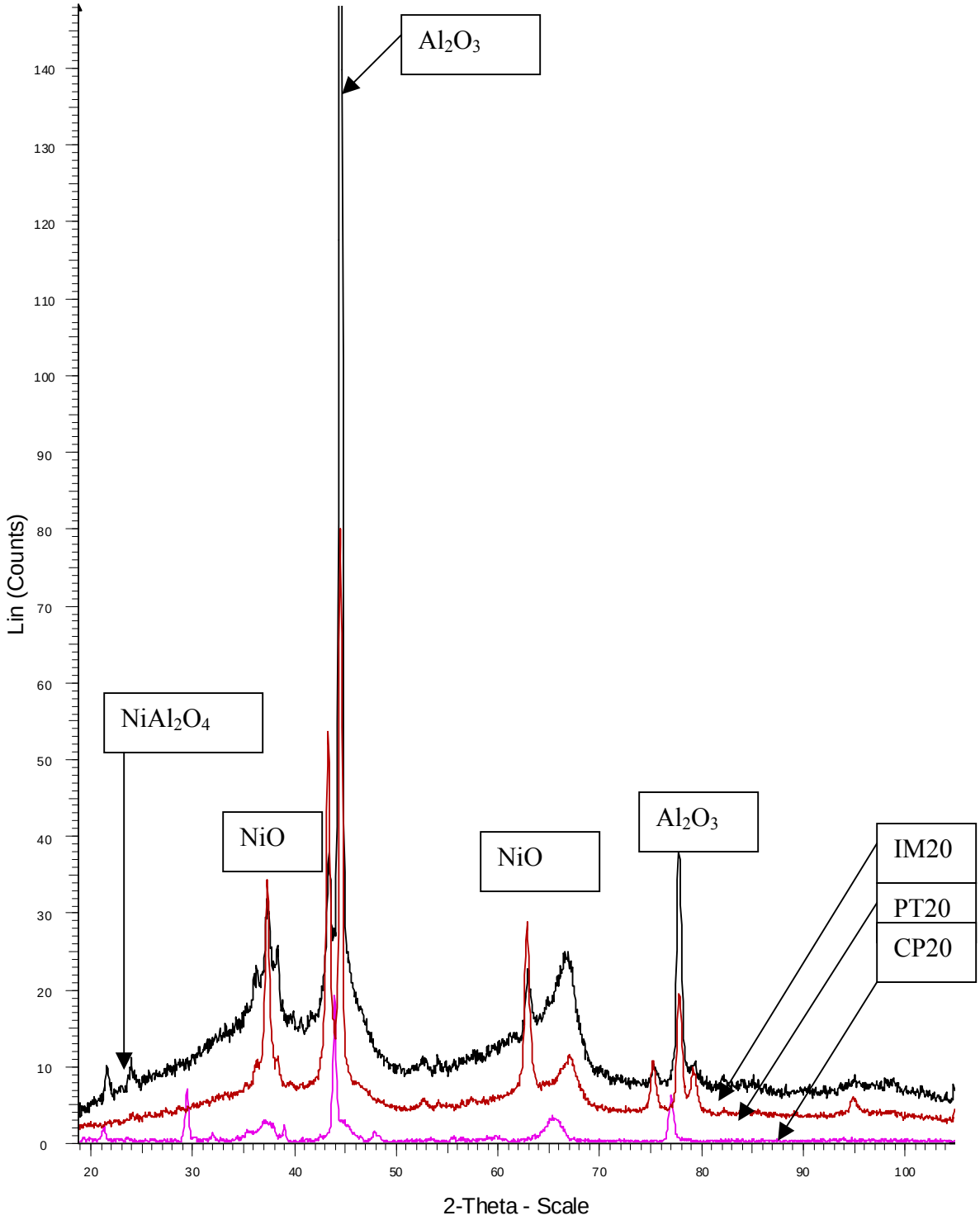

Figure 4.2d: XRD pattern of calcined catalysts (20 % Ni loading)

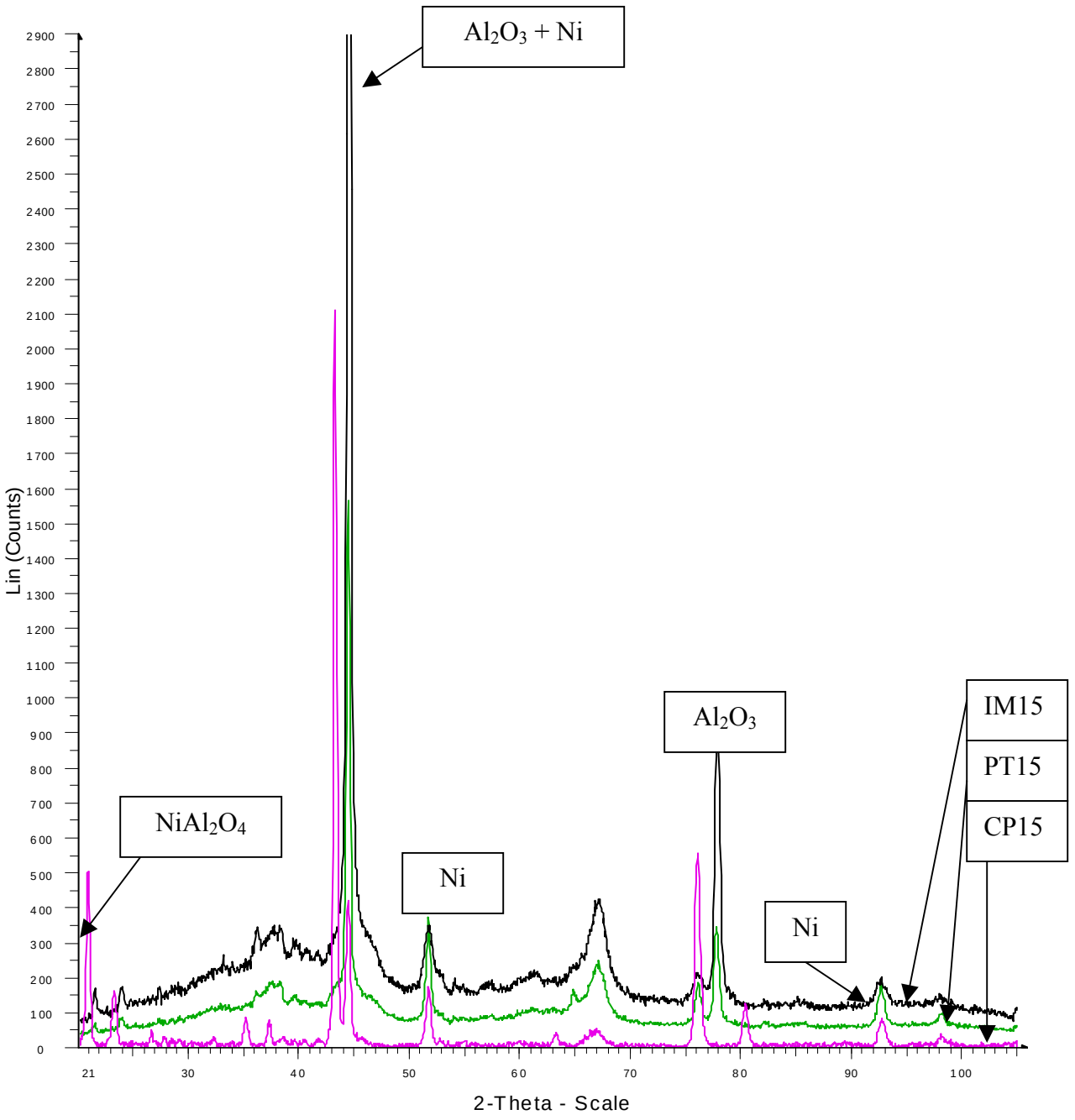

Figure 4.2e: XRD pattern of reduced catalysts (15% Ni loading)

4.1.3 Thermo-Gravimetric / Differential Scanning Calorimetry

The evaluation of weight loss as well as the rate of weight loss associated with drying or decomposition of dried catalysts as a function of temperature is important because it helps to determine the maximum temperature after which the catalyst weight loss is negligible (i.e. complete decomposition). This, in turn, helps to establish the minimum temperature at which catalyst becomes thermally stable, and as such, the minimum temperature for catalyst calcination. The TGA profiles for dried catalysts samples are shown in Figures 4.3(a-i).

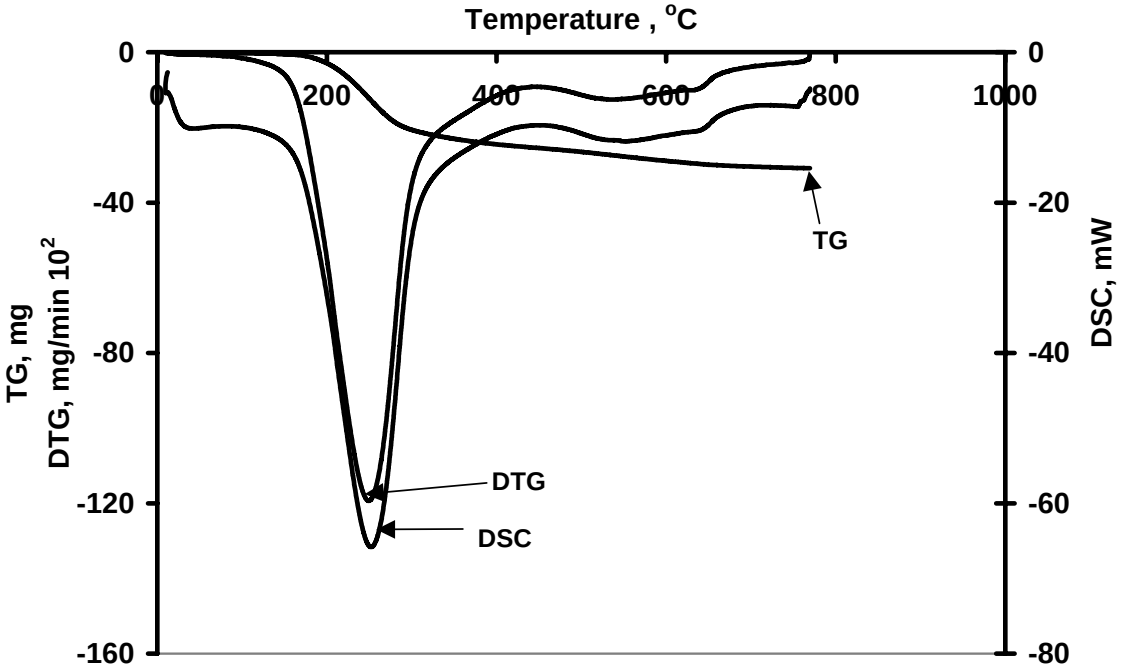

Figure 4.3a: TG-DSC profile of dried CP10 catalyst

The profiles of these dried catalysts, in general, show an endothermic peak between 100-150°C corresponding to thermal desorption of H_2O and adsorbed CO_2 as reported by Jianjun et al. (2004). The peak at about 250-350°C corresponds to the abstraction of chemically bound water from nickel hydroxide hydrate ($Ni(OH)_2.4H_2O$)

and aluminum hydroxide. It could also correspond to the thermal decomposition of nickel aluminum carbonate hydroxide ($Ni_2Al(CO_3)_2(OH)_3$) by removal of CO_2. The endothermic peak at about 500-600^oC corresponds to the thermal decomposition of nickel hydroxide into NiO and H_2O as reported by Parthasarathi et al. (2000) and the thermal decomposition of nickel aluminum hydroxide into $NiAl_2O_4$ and H_2O. The nickel hydroxide described in the former case results from the elimination of H_2O and CO_2 from $Ni_2(OH)_2CO_3.4H_2O$ and by abstraction of H_2O from $Ni(OH)_2.4H_2O$. Since the peak that was observed specifically at 600^oC was obtained only in the CP catalysts and was absent in the PT and IM catalysts, it can be concluded that the $Ni(OH)_2$ in this case originated from $Ni_2(OH)_2CO_3.4H_2O$, whereas the one at about 500^oC originated from $Ni(OH)_2.4H_2O$. Also, since the peak at 600^oC is specific to the CP catalysts, the results imply that the decomposition of nickel aluminum hydroxide to yield $NiAl_2O_4$ occurs at this temperature. The TG profiles for these dried catalyst samples suggest that the calcination temperature of 600^oC was adequate and was able to stabilize all the catalysts except in CP20 where a higher calcinations temperature would be required for stabilizing the catalyst.

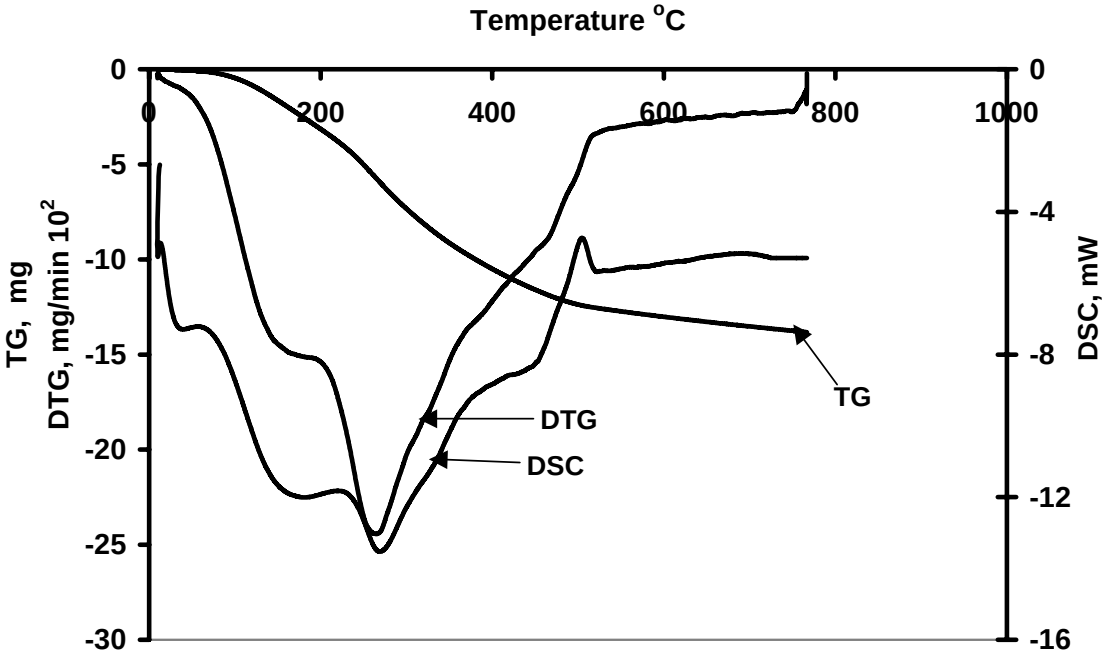

Figure 4.3b: TG-DSC profile of dried PT10 catalyst

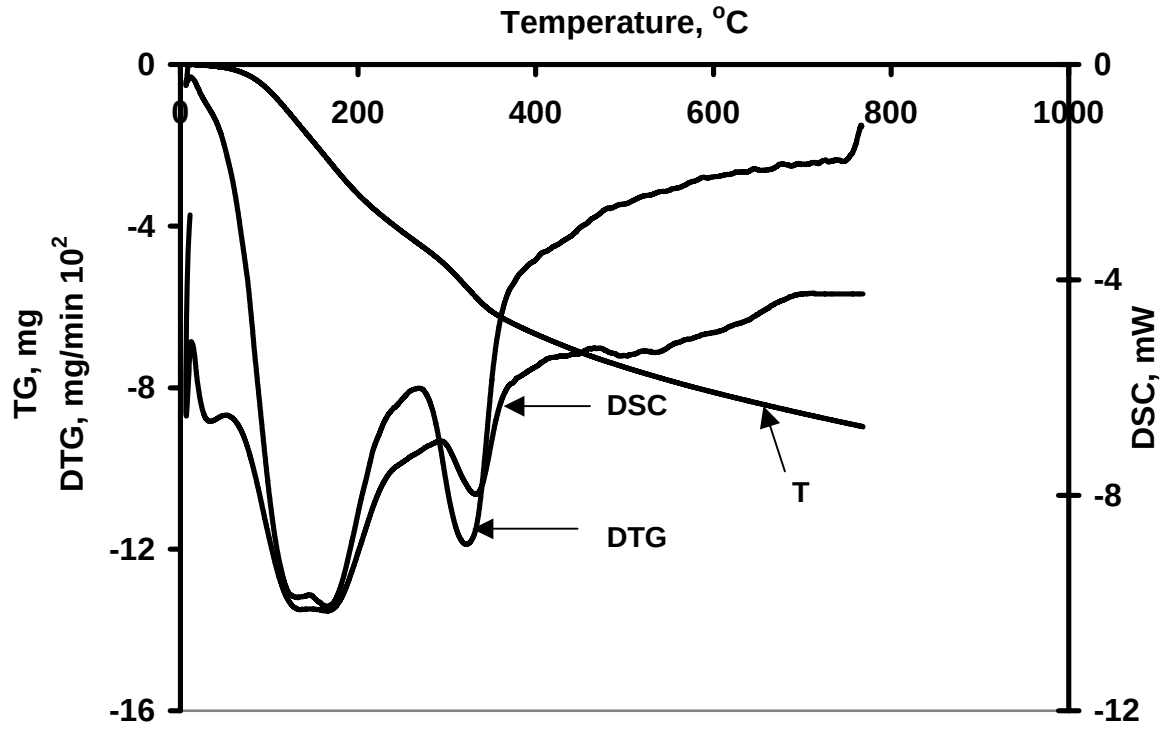

Figure 4.3c TG-DSC profile of dried IM10 catalyst

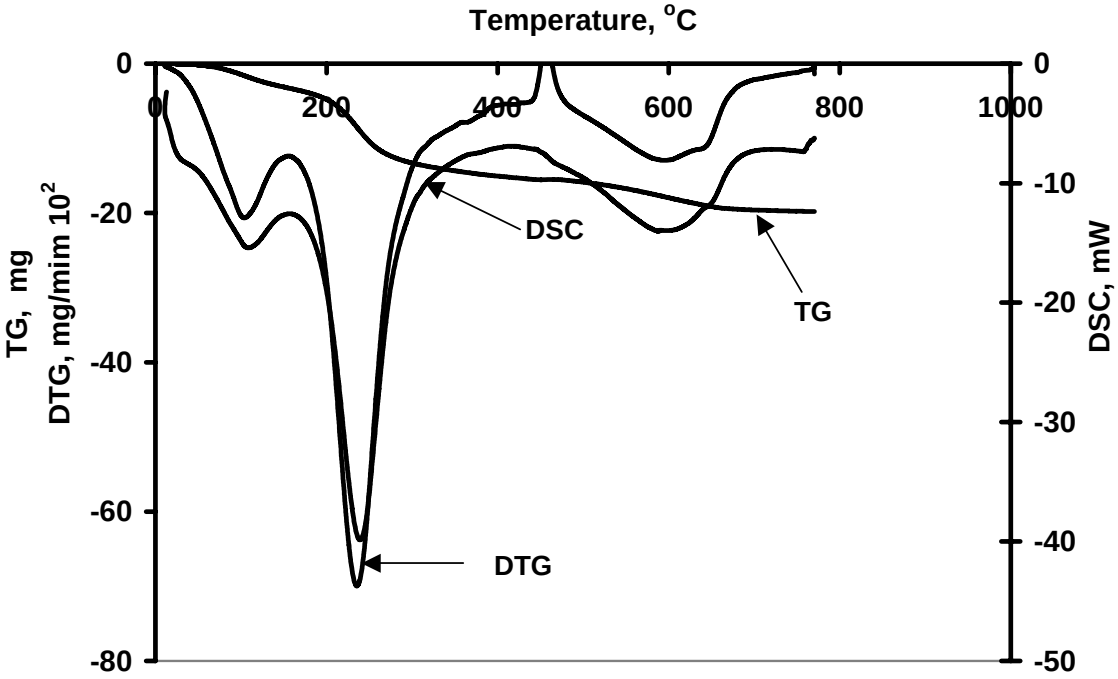

Figure 4.3d: TG-DSC profile of dried CP15 catalyst

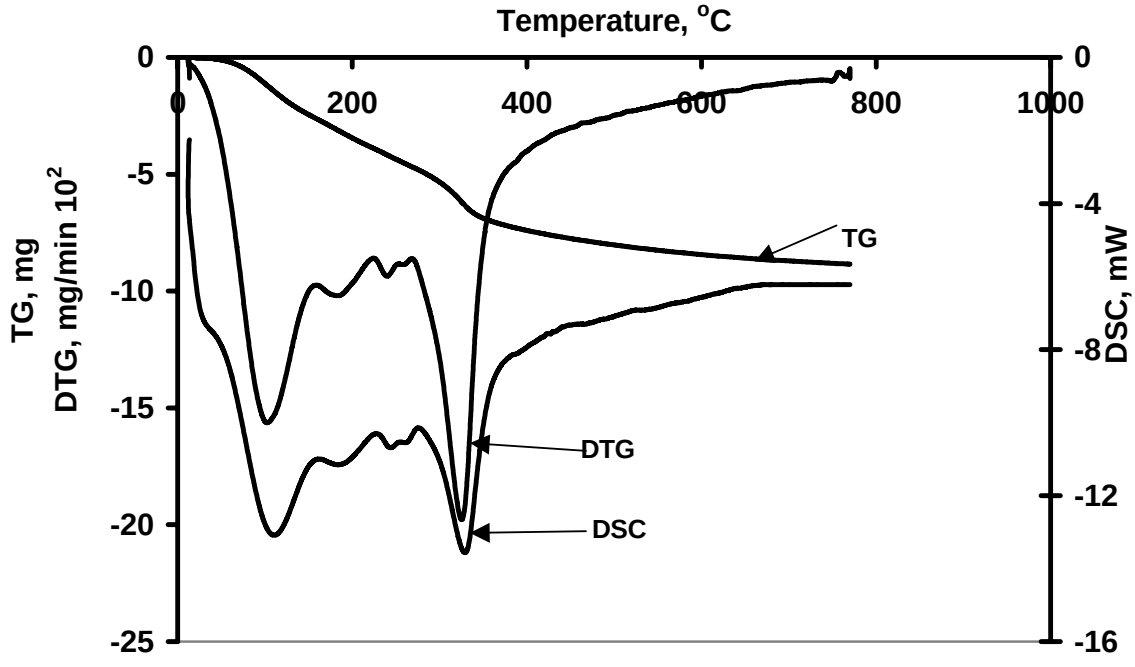

Figure 4.3e: TG-DSC profile of dried PT15 catalyst

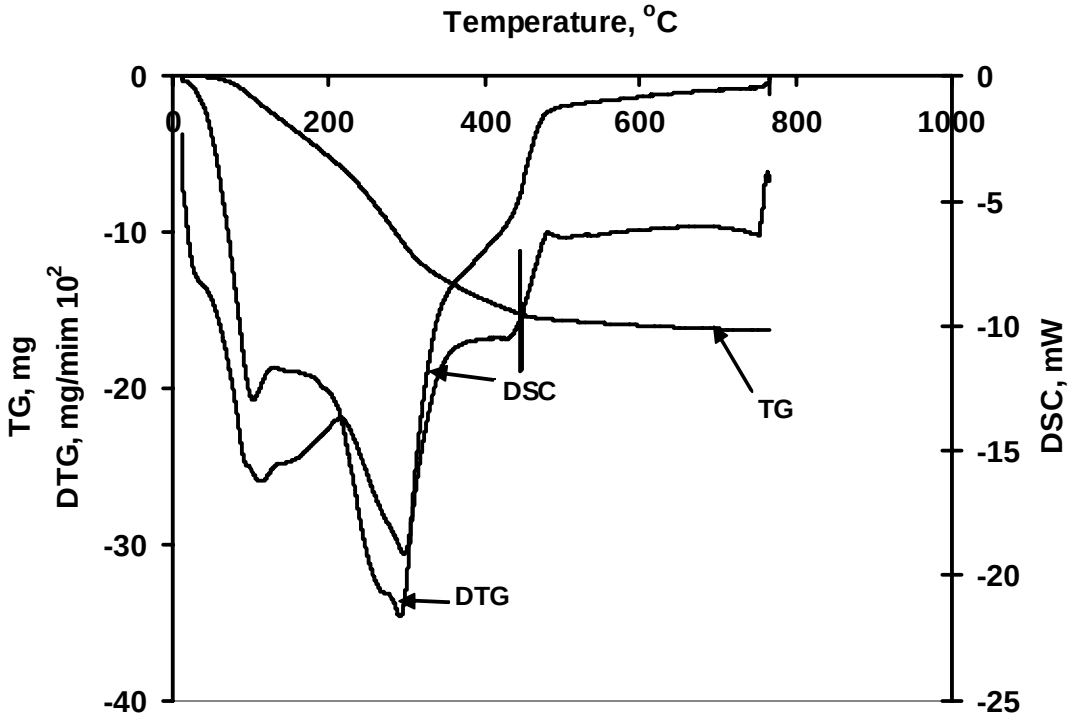

Figure 4.3f: TG-DSC profile of dried IM15 catalyst

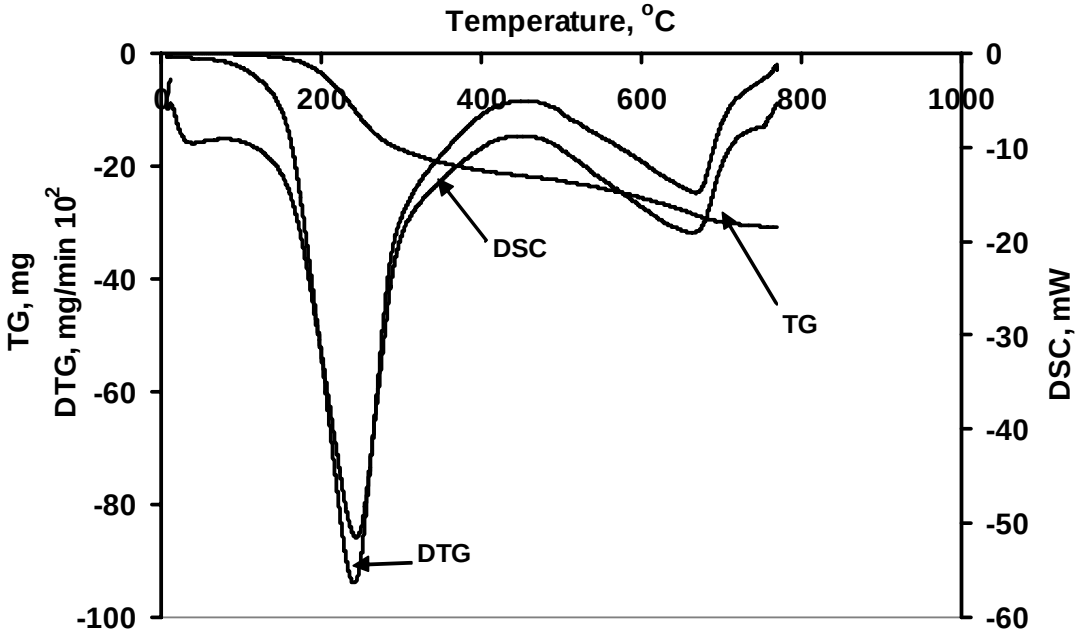

Figure 4.3g: TG-DSC profile of dried CP20 catalyst

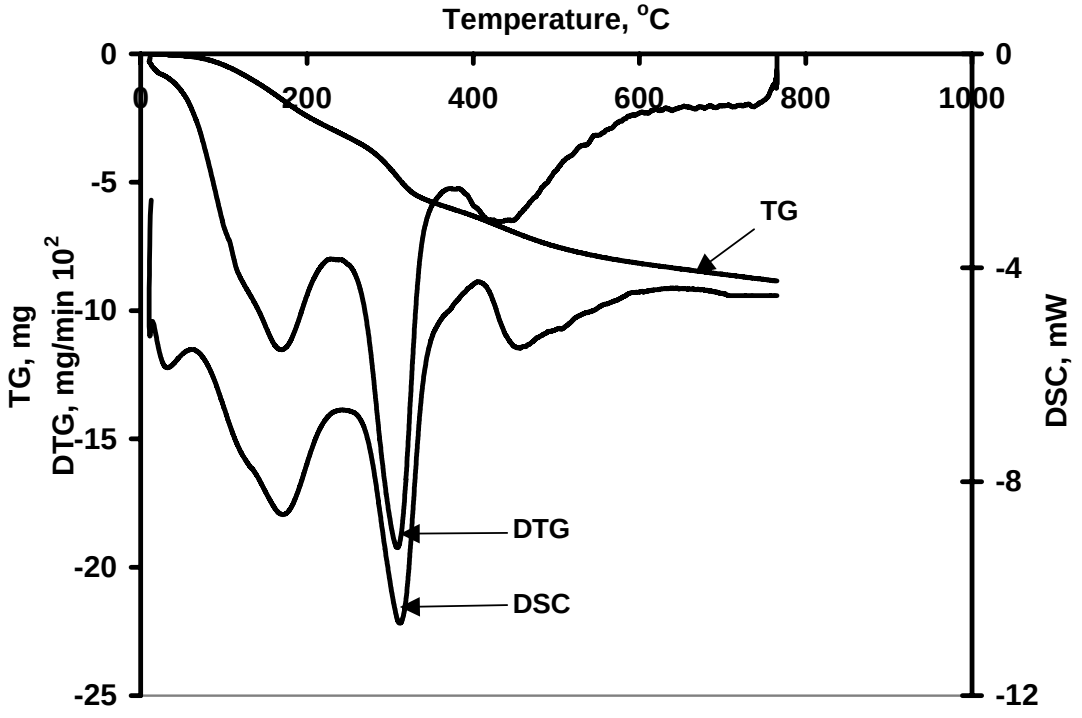

Figure 4.3h: TG-DSC profile of catalyst PT20 catalyst

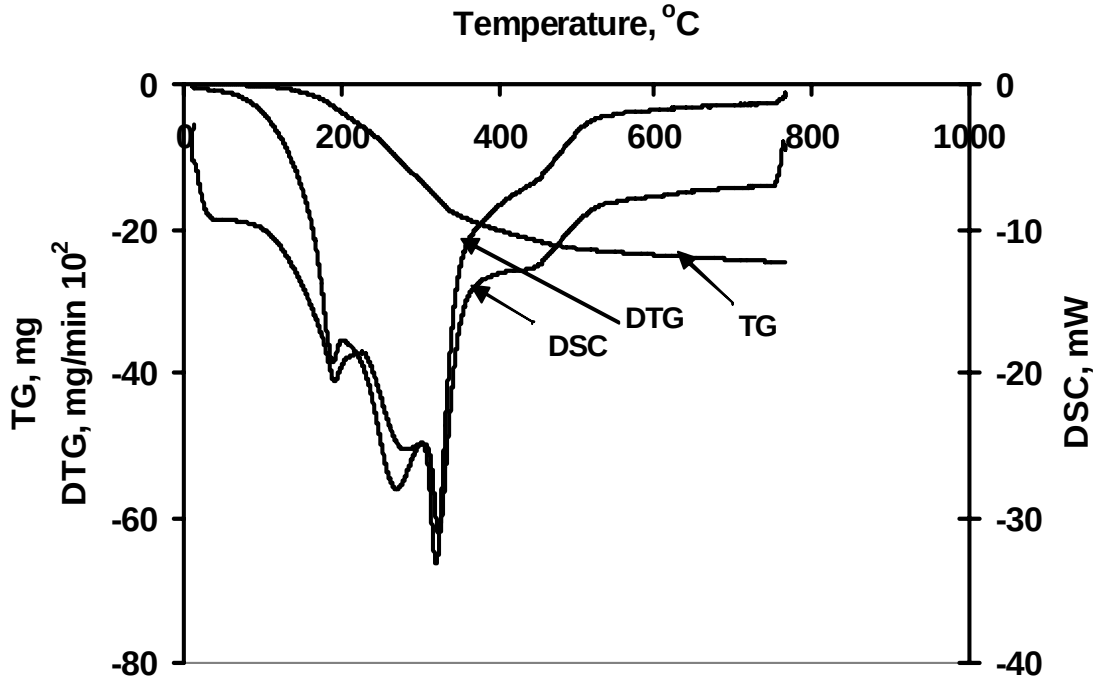

Figure 4.3i: TG-DSC profile of fresh IM20

4.1.4 Temperature Programmed Reduction (TPR-H_2)

The objective of TPR-H_2 experiments was to determine the reducibility as well as the optimum reduction temperature for the catalysts for the reforming of crude ethanol. In conjunction with XRD data, it was also useful in determining the type of species present in the calcined catalysts. The TPR-H_2 profiles of all the catalysts calcined at 600^oC are given in Figure 4.4a-c for catalysts prepared by coprecipitation, precipitation and impregnation, respectively. The peak temperatures and the corresponding species are summarized in Table 4.3

All the reduction peaks between 400 and 612^oC represent the reduction of NiO. The oxide of nickel was produced by the thermal decomposition of various non-aluminum containing nickel species at appropriate temperatures, as evidenced from XRD and TGA studies. The presence of these peaks has been reported by Idem et al. (2000) for Co-Ni-ZrO_2/sulphated-ZrO_2 hybrid catalysts and by Jae-Hee et al. (2004) for Ni/Al_2O_3 catalyst. The peaks observed in the temperature range of 750-812^oC represent the reduction of $NiAl_2O_4$ species. The presence of this peak has been reported by Marino et al. (1998), Jae-Hee et al. (2004) and Juan-Juan et al. (2004) for Ni/Al_2O_3 and Cu-Ni/Al_2O_3 catalysts. The reduction temperature and the peak width are indications of the ease of reduction and the degree of interaction between different species, respectively. High reduction temperature indicates difficulty in reduction whereas wide peaks indicate a great degree of interaction between the species and the support. It is seen from TPR-H_2 profile that the PT catalysts are almost completely reduced at 600^oC whereas the CP and IM catalysts require a higher reduction temperature (approximately 800^oC) due to the presence of the $NiAl_2O_4$ species.

Table 4.3 Summary of TPR Analyses for Calcined Ni/Al_2O_3 Catalysts

Catalysts name	Number of peaks	Peak temperature ^oC	Major reducible species
CP10	3	471, 534, 700	NiO, $NiAl_2O_4$
CP15	3	501, 569, 731	NiO, $NiAl_2O_4$
CP20	3	514, 572, 738	NiO, $NiAl_2O_4$
PT10	2	438, 633	NiO
PT15	3	434, 602, 769	NiO
PT20	2	446, 529	NiO
IM10	3	444,594, 794	NiO, $NiAl_2O_4$
IM15	3	472, 602, 812	NiO, $NiAl_2O_4$
IM20	3	488, 612, 830	NiO, $NiAl_2O_4$

This implies that PT catalysts have higher reducibility than the CP and IM catalysts. It is important to note that the respective major higher TPR-H_2 peak temperatures (about 800^oC) for the IM and CP catalysts increased with the Ni loading, implying that reducibility decreased with the Ni loading. In contrast, the major higher TPR-H_2 peak temperature (600^oC) in the case of PT catalysts shifted to lower temperatures as the Ni loading increased implying that reducibility increased with Ni loading. Also, the TPR-H_2 peaks for the PT catalysts were narrower than those for the CP and IM catalysts implying a higher degree of interaction of Ni species with Al_2O_3 for CP and IM catalysts, as evidenced by the presence of $NiAl_2O_4$.

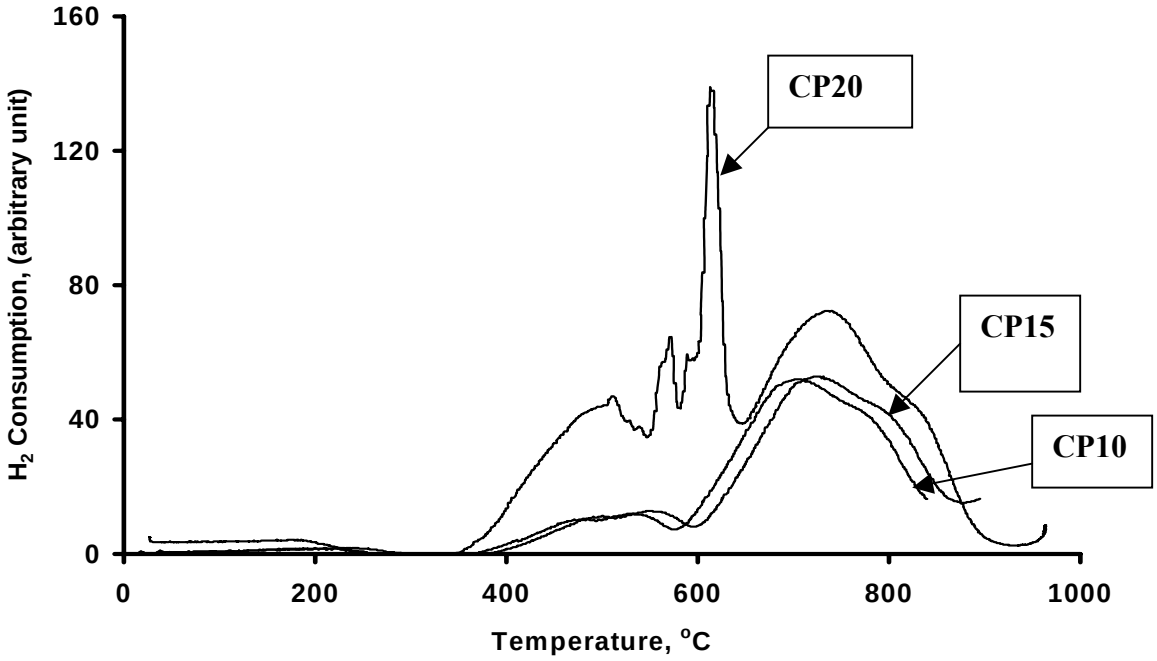

Figure 4.4a: TPR-H_2 profiles of calcined catalysts prepared by the coprecipitation method

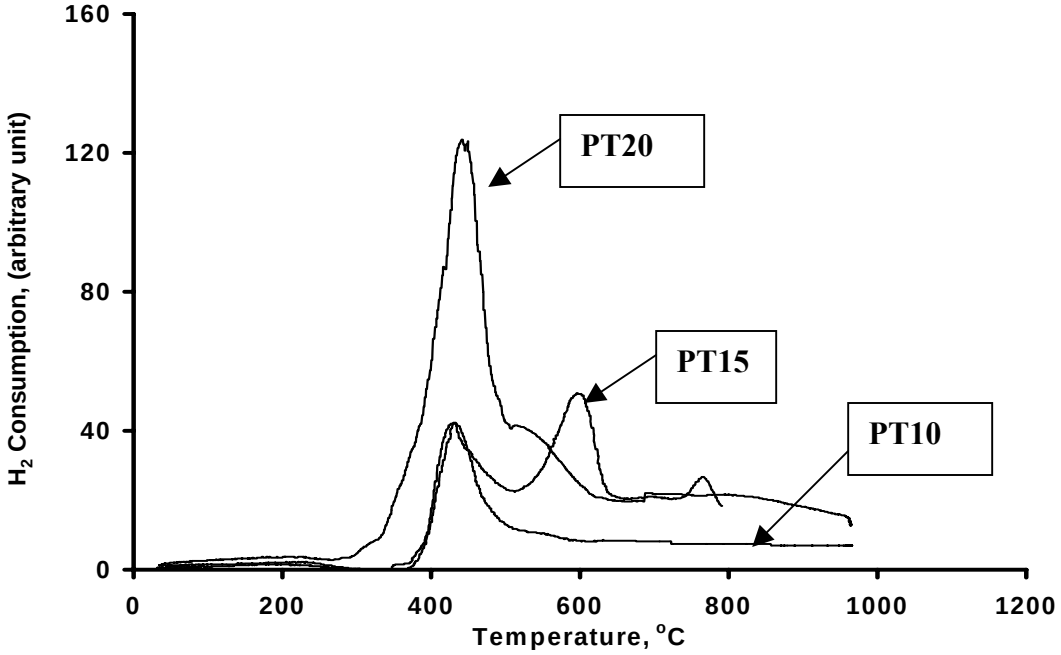

Figure 4.4b: TPR-H_2 profiles of calcined catalysts prepared by the precipitation method

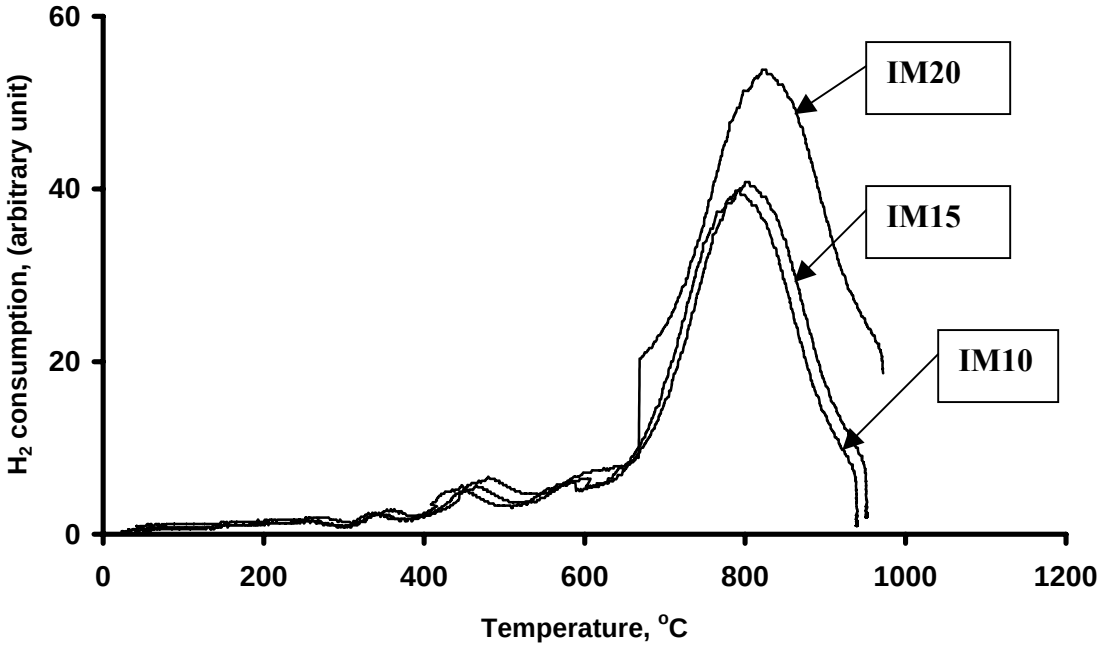

Figure 4.4c: TPR-H_2 profiles of calcined catalysts prepared by the impregnation method

4.2 Experimental Studies

4.2.1 Crude Ethanol Composition

As mention earlier in section 3.3, the feed stock for this process was fermentation broth obtained from Pound maker Agventures Lanigan Saskatchewan, Canada. It was analyzed using a high performance liquid chromatograph (HPLC). The result of the analysis is shown in Table 4.4. Consequently, the overall molecular formula of crude ethanol based on the weighted average of these components is $C_{2.12}H_{6.12}O_{1.23}$. Based on this composition, the general equation representing the reforming of crude-ethanol can be represented as in Equation (4.2).

$$C_{2.12}H_{6.12}O_{1.23} + 3.01H_2O \longrightarrow 2.12CO_2 + 6.07H_2 \qquad \Delta H = 129kJ/mol \qquad (4.2)$$

Table 4.4: Crude-ethanol composition

Crude ethanol components	Volume %	Mole % (on a water free basis)
Ethanol	12.005	88.417
Lactic acid	0.998	5.713
Glycerol	0.994	5.868
Maltose	0.001	0.001
Water	86.002	Not applicable

4.2.2 Reaction Involved in Crude Ethanol Reforming

There are several reactions involved in the reforming of crude-ethanol. The components found from the product analyses were: hydrogen, carbon dioxide, carbon monoxide, methane, 2-propanone, butanedioic acid, propanoic acid, 2,3-butanediol, propylene glycol (1,2 propane diol), 2-butanol and acetic acid. Two sets of reactions were considered to be taking place, first is the basic steam reforming reaction that involved the crude ethanol and water to produce the desired products, hydrogen and carbon dioxide, and second is the possibility of crude components reacting together to form undesired products.

4.2.3 Catalyst Performance Evaluation

The catalysts were evaluated for their performance in the reforming of crude ethanol. Some of the test runs were repeated to check the reproducibility of results. The error was within 4.0 %. The evaluation criteria used were crude ethanol conversion, H_2 selectivity and H_2 yield. Crude ethanol conversion was defined according to Equation

4.3 while H_2 yield and selectivity were defined according to Equations 4.4 and 4.5, respectively. An overall mass balance was done for every run, which varied within 1 to 5% uncertainty range. The mass balance error was attributed to carbon deposition which was not quantified.

$$\text{Crude ethanol conversion (X)} = \frac{\text{gmol (organics)in} - \text{gmol (organics)out}}{\text{gmol (organics)in}} \quad (4.3)$$

where organics = ethanol + lactic acid + glycerol + maltose

$$\text{Hydrogen yield } (Y_{H2}) = \frac{\text{gmol } (H_2)\text{out}}{6.07 * \text{gmol (organics)in}} \quad (4.4)$$

$$\text{Hydrogen selectivity } (S_{H2}) = \frac{\text{gmol } (H_2)\text{out}}{6.07 * \text{gmol (organics)in} * \text{Conversion(X)}} \times 100 \quad (4.5)$$

4.2.3.1 Crude Ethanol Conversion

This evaluation was carried out on all prepared catalysts at a calcination temperature of 600^{o}C, weight hourly space velocity (WHSV) of 1.68h^{-1}, reaction temperature of 400^{o}C, and catalyst reduction temperature of 600^{o}C. Figure 4.5 shows the crude ethanol conversion behavior for catalysts prepared by the coprecipitation method. It is seen in the figure that each catalyst showed an initial high activity with a high initial crude ethanol conversion. This was attributed to the initial high activity of the catalysts. The conversion decreased with time and then stabilized at about 180 min time on stream (TOS). CP15 gave the highest stable conversion of crude-ethanol (79 mol%), followed by CP25 (59 mol%) while CP10 gave the lowest conversion (32 mol%) under the same experimental conditions.

Figure 4.6 gives crude ethanol conversions for the catalysts prepared by the precipitation method. The figure shows trends similar to those exhibited by catalysts prepared by the coprecipitated method.

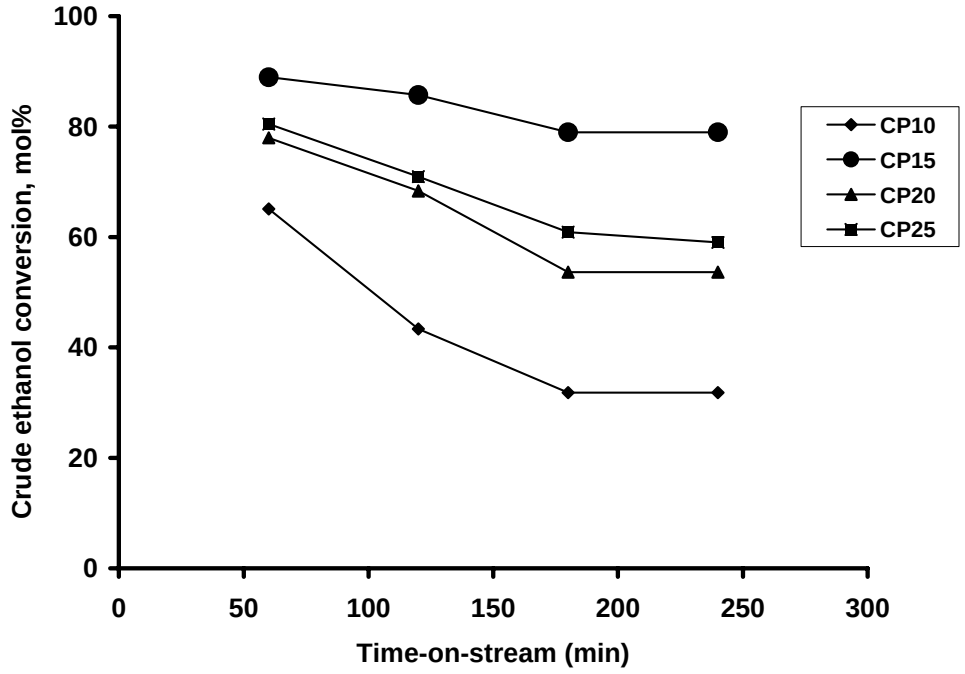

Figure 4.5: Conversion of crude ethanol as a function of time-on-stream (TOS) on catalyst prepared by coprecipitation method

Similar reasons as for the trend in the coprecipitated method could also be used to explain the behavior. Also, the highest stable conversion of crude ethanol was obtained on PT15 (85 mol%). This was followed by PT20 (83 mol%) while the lowest conversion was obtained on PT10 (44.0 mol%).

Figure 4.7 shows that the trend for crude ethanol conversion as a function of time-on-stream (TOS) obtained on catalysts prepared by the impregnation method were similar to those for the CP and PT catalysts. It was observed that the IM15 and IM20 did not show any difference in their crude ethanol conversion activities as stable crude

ethanol conversions of 47.0 and 47.0 mol% were respectively obtained on these catalysts. On the other hand, IM10 gave a lower stable conversion of 44.0 mol%.

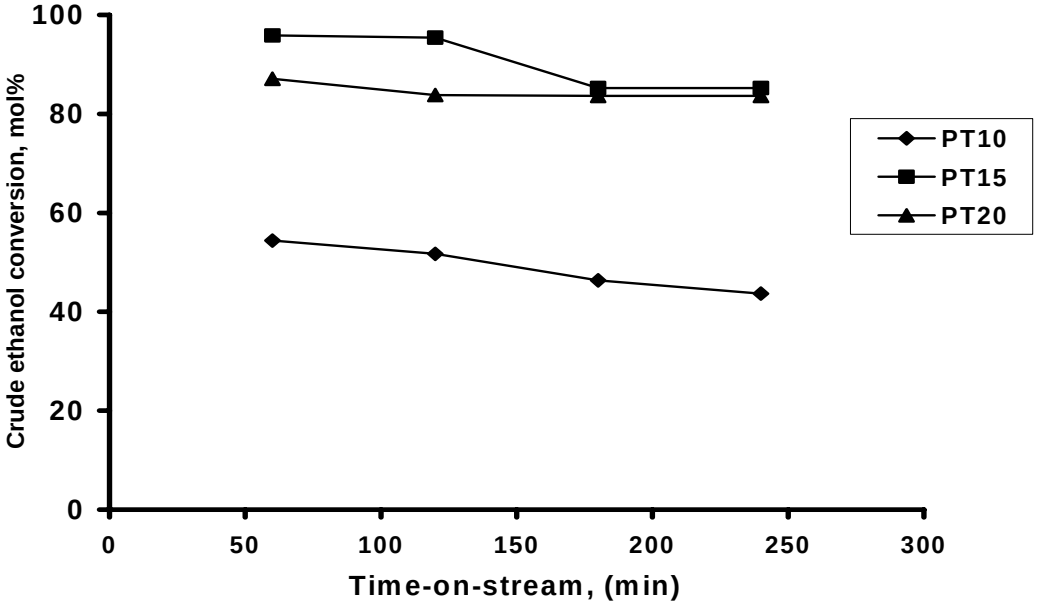

Figure 4.6: Conversion of crude-ethanol as a function of time-on-stream (TOS) on catalyst prepared by precipitation method

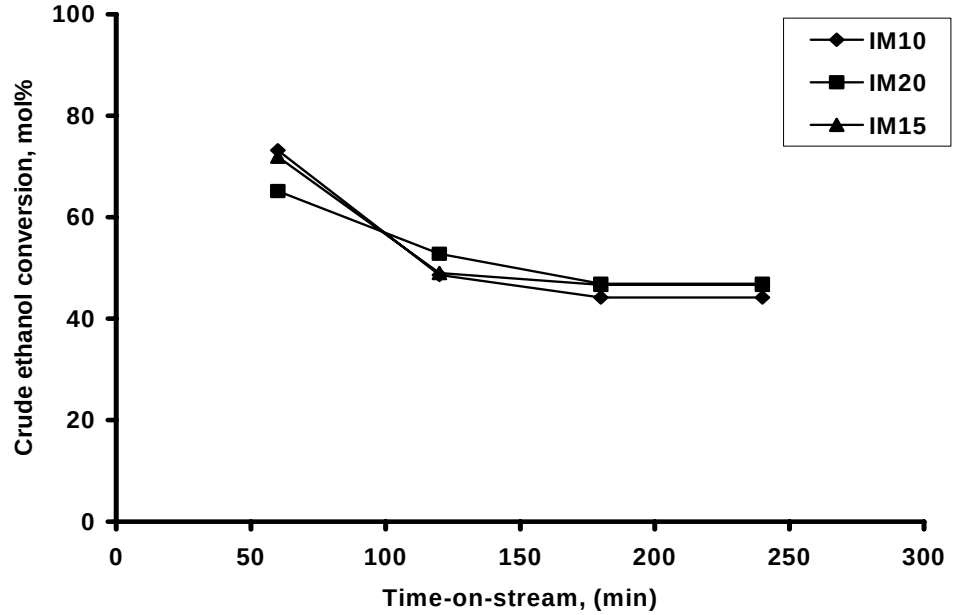

Figure 4.7: Conversion of crude ethanol as a function of time-on-stream (TOS) on catalyst prepared by impregnation method

In order to evaluate the effect of Ni loading, the stable crude ethanol conversions obtained on catalysts prepared by the three methods as a function of Ni loading were compared. The results are given in Figure 4.8. For catalysts prepared by coprecipitation, the stable conversion increased with Ni loading and reached a maximum value of 79 mol% at a Ni loading of 15 wt%. Beyond this loading, the conversion of crude ethanol decreased. A similar trend was observed in the case of catalysts prepared by the precipitation method for which the lowest stable conversion was 44 mol % by PT10 and the maximum stable conversion was 85 mol % by PT15.

Catalysts prepared by impregnation method exhibited a slightly different trend in which crude ethanol conversion reached a maximum value of 46.7 mol% on IM15

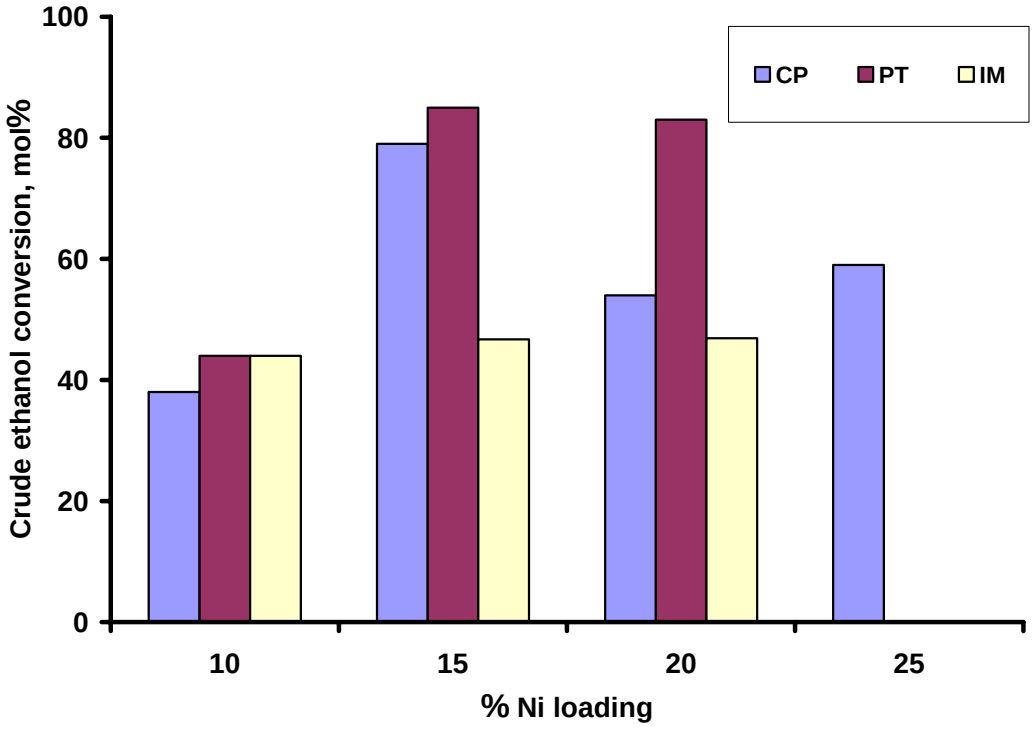

Figure 4.8: Comparison of stable conversion of crude ethanol on various catalysts (T = 400^{o}C, WHSV = 1.68h^{-1})

from 44 mol% on IM10. A further increase from 15% to 20% Ni loading did not result in any appreciable change in crude ethanol conversion.

4.2.3.2 Hydrogen Yield

The activities of all the catalysts were also evaluated in terms of H_2 yield as defined in Equation 4.4. Figure 4.9 illustrates the variation of H_2 yield as a function of Ni loading. CP10 gave a H_2 yield of 2.12 mol H_2/mol crude ethanol fed, the yield increased as Ni loading increased and reached maximum of 4.33 mol H_2/mol crude-ethanol fed on CP15, and then decreased as the Ni loading increased beyond 15%.

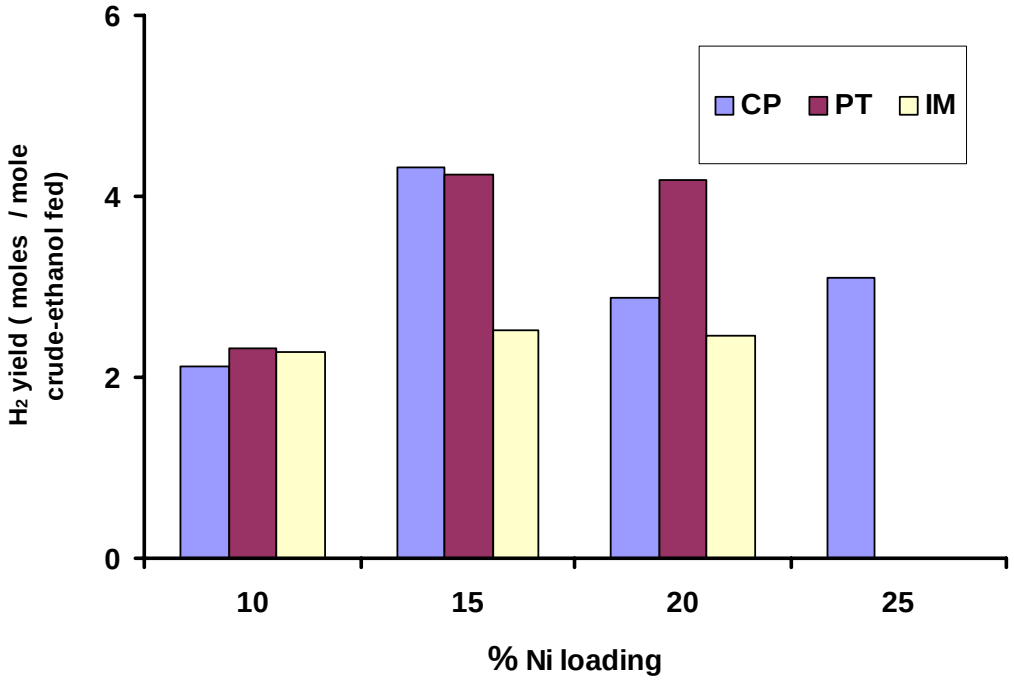

Figure 4.9: Variation of hydrogen yield with Ni loading (T = 400^{o}C and WHSV=1.68^{-1})

Similar trends were obtained in both the catalysts prepared by precipitation and impregnation methods with maximum H_2 yields of 4.24 and 2.52 mol H_2/mol crude-ethanol fed obtained on PT15 and IM15, respectively. Since the production of

hydrogen was a major objective in this work, catalyst CP15 was considered the optimum catalyst. This is because it gave the highest hydrogen yield of 4.33 moles H_2/mole crude-ethanol fed, and also had a high stable crude-ethanol conversion of 79 mol% even though slightly lower than that for PT15 (85 mol%).

4.2.3.3 Hydrogen Selectivity

The higher H_2 yield for CP15 as compared with PT15 (that gave a higher crude ethanol conversion) was attributed to the higher H_2 selectivity of CP15. This was confirmed in Figure 4.10, which shows the variation of H_2 selectivity with Ni loading for all catalysts.

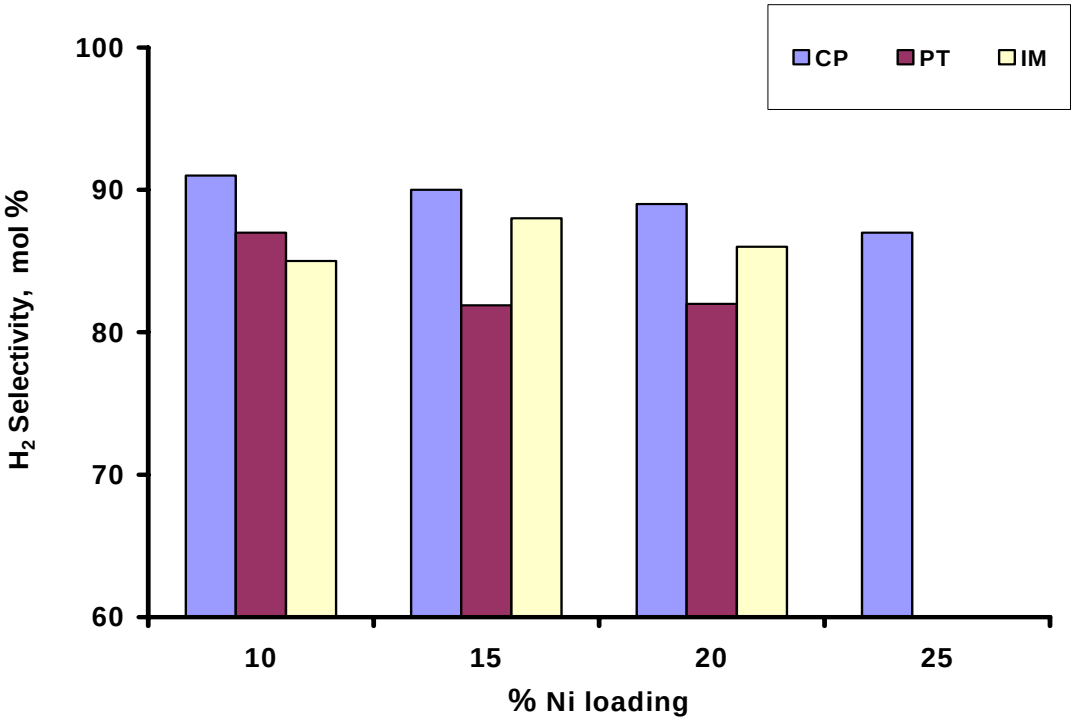

Figure 4.10: Hydrogen selectivity as a function of Ni loading at T = 400°C WHSV=1.68^{-1}

Catalysts prepared by coprecipitation method were the most selective to hydrogen production with CP10 giving the highest H_2 selectivity of 91 mol%, followed by CP15, 90 mol%. CP25 gave the lowest selectivity of 87 mol%. The catalysts prepared by the precipitation method gave a trend similar to that for the coprecipitation method. PT10 gave the highest selectivity of 87 mol% followed by PT15 and PT20 with equal selectivity of 82 mol%. In contrast, catalyst prepared by the impregnation method showed a somewhat different trend, in which IM10 gave the lowest selectivity of 85 mol%. The selectivity reached a maximum of 88 mol% for IM15 and reduced to 86 mol% as the Ni loading increased to 20% in IM20. In order to evaluate circumstances that led to a better performance of the PT and CP catalysts over the IM catalysts, an attempt was made to correlate the catalyst synthesis method to catalyst characteristics and to performance. Two catalyst characteristics, resulting from the three synthesis methods that exhibited a definite correlation with catalyst performance (in terms of crude ethanol conversion) were catalyst reducibility and crystallite size of Ni species.

4.2.3.4 Effect of Catalyst Reducibility on Crude Ethanol Conversion

Table 4.3 shows that the three preparation methods had a strong effect on catalyst reducibility. In this section the extent of these differences in reducibility and how they affected catalyst performance measured in terms of crude ethanol conversion were evaluated. Reducibility was measured in terms of the minimum temperature required for complete reduction of the catalysts as provided by TPR-H_2 results (Figure 4.11 and Table 4.3).

Figure 4.11 shows the typical effect of the reducibility of catalyst on conversion. PT15 was the most reducible catalyst because the dominant NiO species were

completely reduced at 600°C thereby making a larger amount of the active metal available for the reforming reaction.

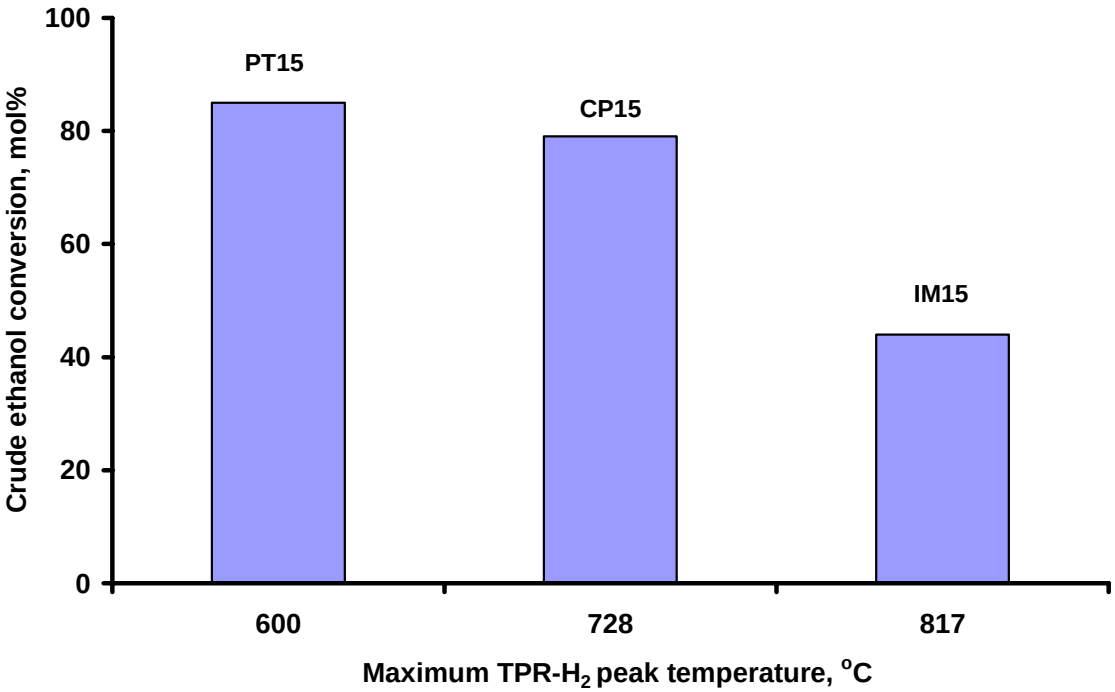

Figure 4.11: Effect of reducibility on crude ethanol conversion on various catalysts

In contrast, the presence of $NiAl_2O_4$ formed as a result of a strong-metal-support-interaction (see Equation 4.1) in both CP15 and IM15 made them less reducible as compared to PT15. The consequence is that a larger fraction of the Ni species were very tightly bound to the support, and therefore, not reduced at the reduction temperature used. Consequently, a small fraction of reduced active Ni metal species was available for the reforming reaction in both the CP and IM catalysts. Thus, while PT15 gave a crude ethanol conversion of 85% at the operating reduction temperature of 600°C, CP15 and IM15 gave crude ethanol conversion of 79 and 46.7 mol%, respectively. This is in good agreement with the results of Idem and Bakhshi, (1994b).

Based on the latter two results, it would appear that the low crude ethanol conversion of 46.7 mol% for IM15 may not be solely due to reducibility factors as this alone should not produce such a drastic change.

4.2.3.5 Effect of Reduction Temperature on Crude Ethanol Conversion and Hydrogen Yield

In order to further investigate the effect of reducibility on catalyst performance, experiments were also performed to determine the effect of reduction temperature on ethanol conversion and hydrogen yield. All the experiments were conducted on CP15 using a $W/F_{crude\text{-}ethanol}$ ratio of 0.59 h (i.e. WHSV = $1.68h^{-1}$). The results are shown in Figure 4.12. Crude ethanol conversion increased from 50 to 77 mol % and the hydrogen yield also increased from. 2.8 to 4.2 mol/mole crude ethanol fed as the reduction temperature was increased from 400 to 600°C.

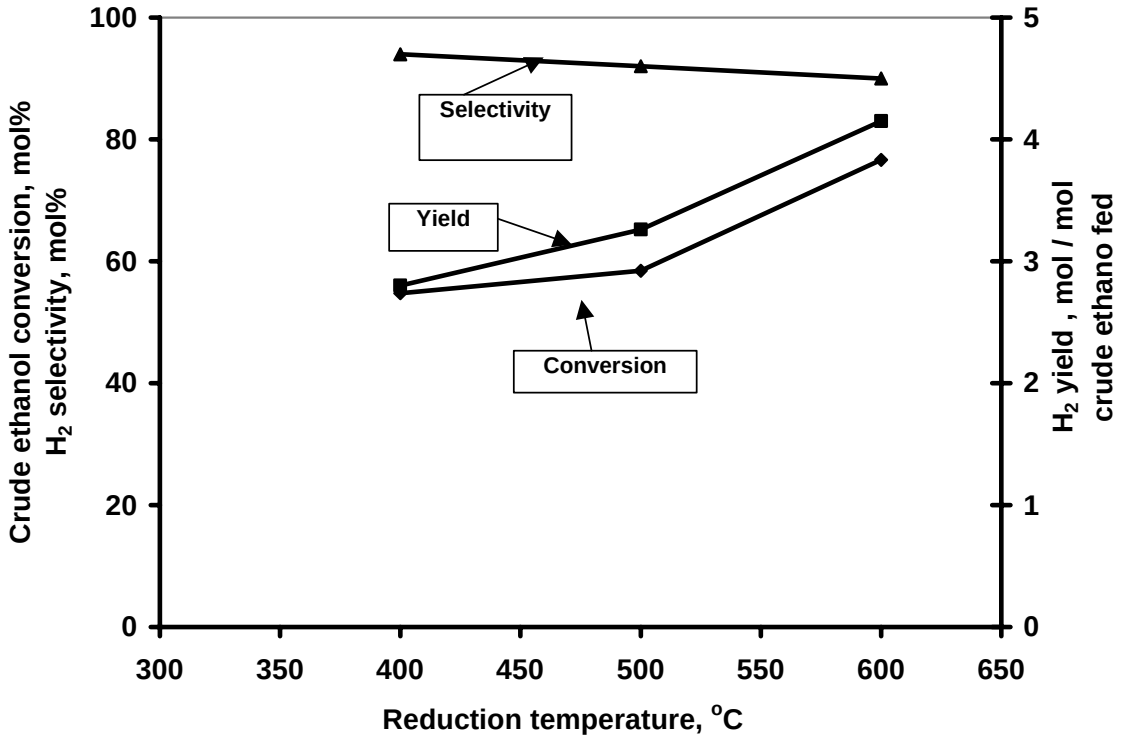

Figure 4.12: Crude ethanol conversion, H_2 selectivity and H_2 yield as functions of reduction temperature for CP15 at WHSV = $1.68h^{-1}$

This result could be attributed to the small amount of the active Ni sites made available for the reforming reaction by reduction at the lower reduction temperature as compared with the amount available at higher temperatures. This can be confirmed from the TPR-H_2 profiles for catalyst CP15 (Figure 4.4a) in which this catalyst was more reduced at 600^{o}C.The figure further shows that the amount of Ni metal generated at 600^{o}C was definitely larger than those at 500 and 400^{o}C.

4.2.3.6 Effect of Crystallite Sizes on Crude Ethanol Conversion

The major differences in performance of the catalysts prepared by the three methods had earlier been attributed to factors other than reducibility alone. One of these other factors was the crystallite size of the NiO species. Table 4.2 shows that preparation methods affect the crystallite sizes of the active Ni species as observed in the X-ray line broadening results.

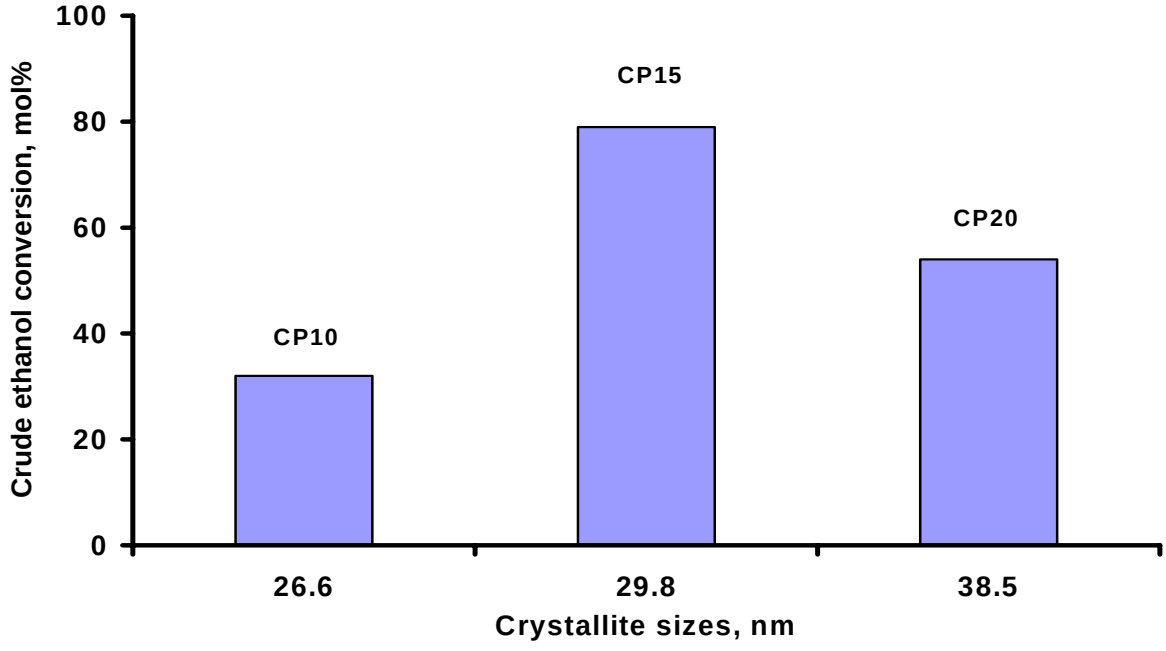

Figure 4.13: Crude ethanol conversion as a function of crystallite size for catalysts prepared by the coprecipitation method

The effects of the preparation method and Ni loading on the crystallite sizes and their ultimate effect on crude ethanol conversion are illustrated in Figures 4.13-4.15. Figure 4.13 shows the activities of catalysts prepared by coprecipitation method as a function of crystallite sizes and Ni loading. It is observed that an increase in Ni loading from 10 to 15 % produces only a slight difference in crystallite size of the catalyst, but a large increase in crude ethanol conversion from 32 to 79 mol%. This large increase is attributed to a larger amount of Ni being available because of the higher Ni loading of CP15 as compared to CP10. On the other hand, a further increase in Ni loading as in CP20 increased the crystallite size appreciably. This lowered the Ni dispersion on the catalyst such that the activity in CP20 dropped to 54 mol% even though its Ni loading was higher than CP15.

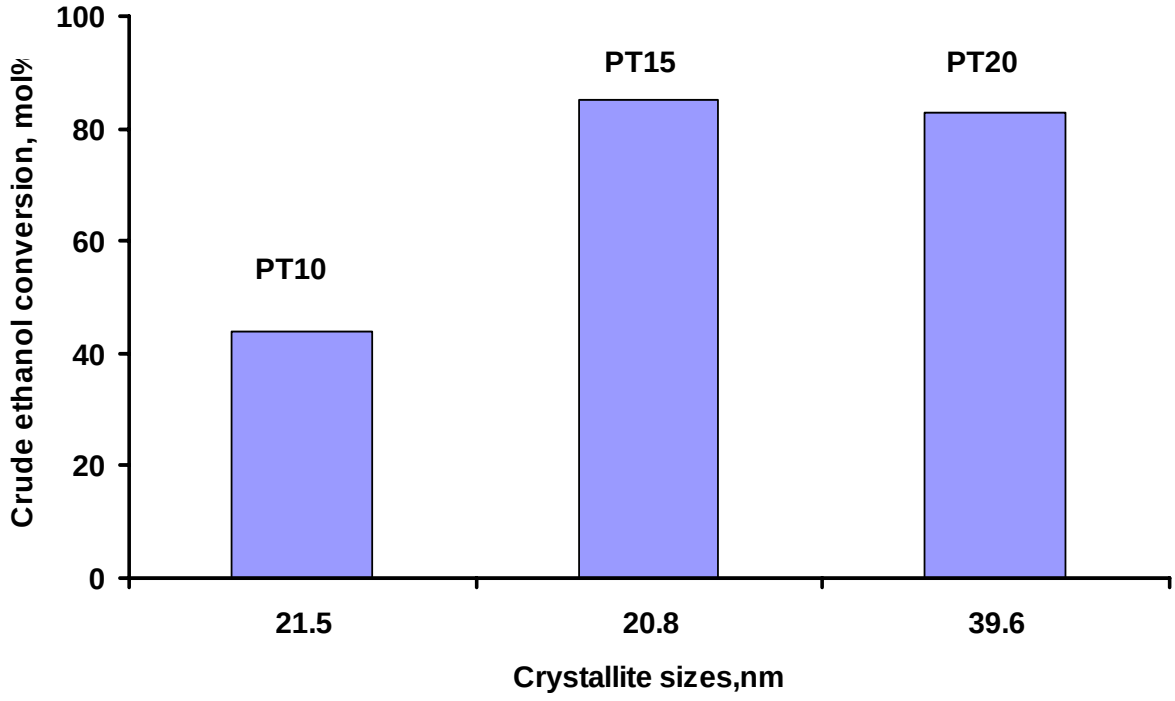

Figure 4.14: Crude ethanol conversion as a function of crystallite size for catalysts prepared by the precipitation method

In this case, the adverse effect of a larger crystallite size (lower Ni dispersion) outweighed the beneficial effect of Ni loading of CP20. Similar results were obtained when catalysts prepared by the precipitation method was used as shown in Figure 4.14.

The conversion dropped slightly when loading increased from 15 to 20%, the magnitude of change in this case is a reflection of the magnitudes of the detrimental effect of larger crystallite size as opposed to the beneficial effect of higher reducibility. In the case of the catalysts prepared by the impregnation method, a completely different behavior was observed (Figure 4.15). The crystallite size of IM10 was the smallest and there was a rapid increase in crystallite size as the Ni loading increased from 10 to 15% and a corresponding but slight increase in the activity of the catalysts with respect to crude ethanol conversion.

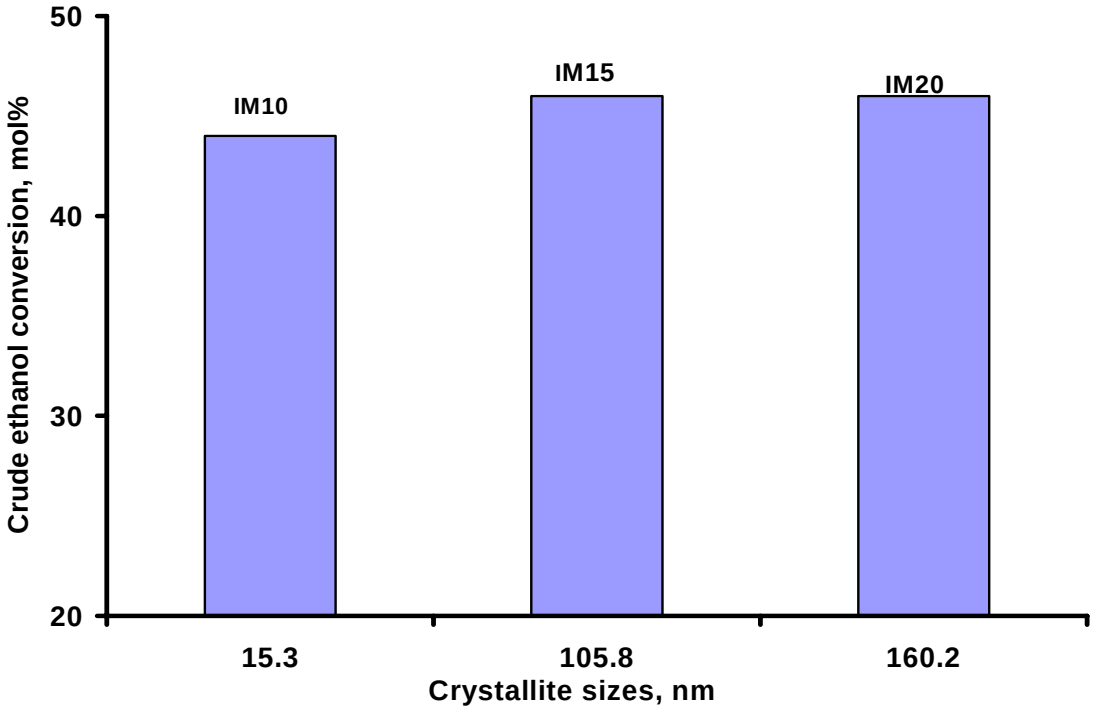

Figure 4.15: Crude ethanol conversion as a function of crystallite size for catalysts prepared by the impregnation method

For this preparation method, the beneficial effect of Ni loading of the catalysts appeared to have overcome the adverse effect of a larger crystallite size.

In all cases it was observed that the crystallite size increased with Ni loading. Also, except for the IM series of catalysts, high Ni loading beyond 15% did not increase the activity with respect to crude ethanol conversion. This is in agreement with the results of Ming-Tseh et al. (2002) on supported Ni catalyst, in which the author observed that at low nickel loading the dispersion was higher than that at high nickel loading and decreased gradually with loading. This was attributed to the fact that at low nickel content, the small nickel crystallites exhibit no agglomeration, while at high nickel loading, there was the existence of agglomeration due to the presence of significant nickel density. These results on the effect of the crystallite size on catalyst performance explain the major difference between CP15 and IM15, which exhibited similar reducibility but widely different crude ethanol conversions. The results confirm that the major contributing factor in this case is the crystallite size of NiO species which is larger in IM15 (105.8 nm) as compared with CP15 (29.8 nm).

4.2.4 Effect of Operating Conditions

4.2.4.1 Effect of Temperature on Crude Ethanol Conversion and Hydrogen Selectivity

Experiments were performed to study the effect of the reaction temperature on the overall crude-ethanol conversion using CP15, as shown in Figure 4.16. The reaction temperatures used were 320, 400, 420 and 520^{o}C for a fixed weight hourly space velocity of 1.68h^{-1}. As expected, crude-ethanol conversion was lowest (64 mol%) at 320^{o}C and as the temperature was increased, the conversion increased and reached a maximum of 80.1 mol% at 520^{o}C. In contrast, the H_2 selectivity decreased with an

increase in temperature, also as expected, due to the increased methanation activity as well as the formation of carbon monoxide on this catalyst at higher temperatures.

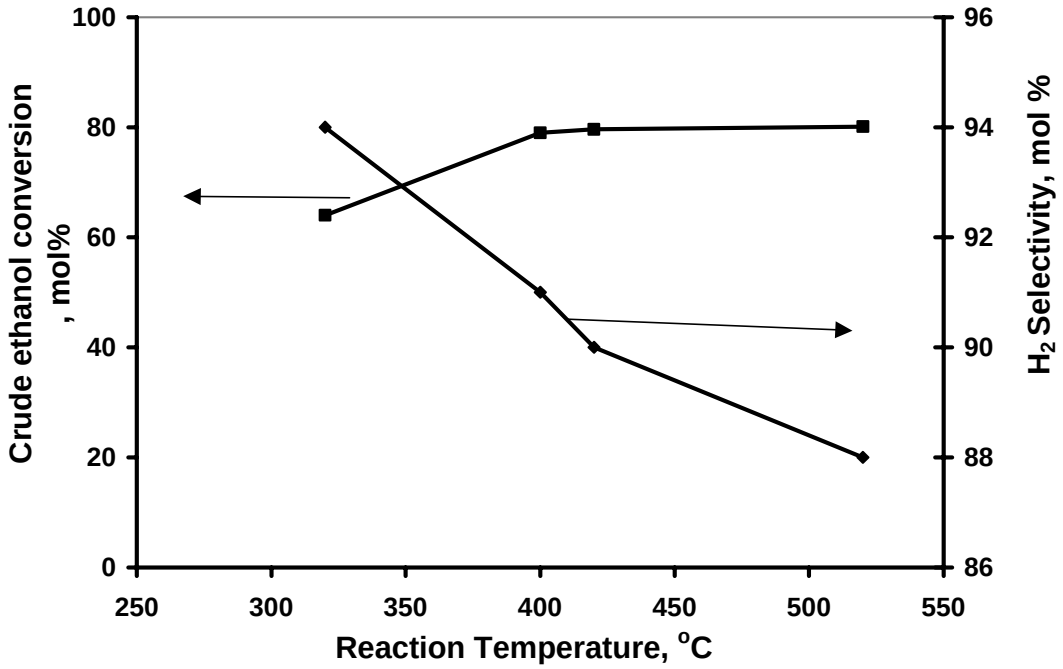

Figure 4.16: Variation of crude ethanol conversion and hydrogen selectivity as functions of temperature for CP15 at WHSV=1.68h^{-1}

4.24.2 Effect of W/F$_{crude\text{-}ethanol}$ on Crude Ethanol Conversion, Hydrogen Selectivity and Yield

Experiments were also performed to study the effect of W/F$_{crude\text{-}ethanol}$ ratio in the range 0.22 to 0.59 h (i.e. WHSV in the range 1.68-4.62h^{-1}) on crude ethanol conversion and hydrogen selectivity and yield using CP15 at a reaction temperature of 420^{o}C. The results are given in Figure 4.17, which shows that the conversion of crude ethanol increased from 35.6 mol% for W/F$_{crude\text{-}ethanol}$ ratio of 0.22 h to 79.8 mol% for W/F$_{crude\text{-}ethanol}$ ratio of 0.59 h. This behavior was expected as the reactant had a longer residence time for reaction inside the reactor. The effect of W/F$_{crude\text{-}ethanol}$ ratio on hydrogen yield was similar to that for crude-ethanol conversion as also shown in Figure 4.17. The hydrogen

yield increased from 1.95 to 4.33 (moles H_2/mole crude ethanol fed) with an increase in $W/F_{crude\text{-}ethanol}$ ratio from 0.22 to 0.59 h. The hydrogen selectivity also increased with $W/F_{crude\text{-}ethanol}$ ratio. The result was attributed to the excess water that is present in crude ethanol.

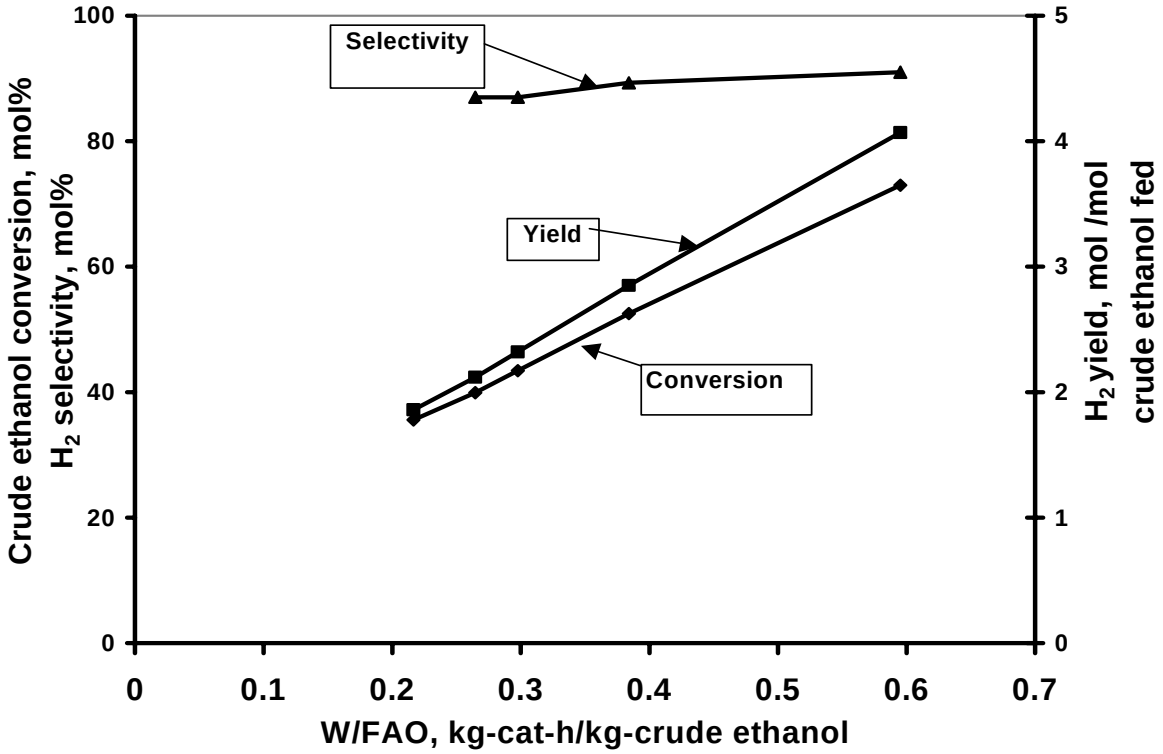

Figure 4.17: Conversion of crude ethanol and H_2 selectivity and yield as a function of $W/F_{crude\text{-}ethanol}$ for CP15 at T = 420°C

4.2.5 Catalyst Activity versus Time-on-Stream (TOS) Studies

Catalyst activity was evaluated as a function of time-on-stream. This was conducted on the CP15 operating at a WHSV of 1.68h^{-1}, reduction temperature of 600°C and a reaction temperature of 400°C. Figure 4.18 shows the crude ethanol conversion as a function of time-on-stream for 11 h of experimental run. The figure shows an initial high activity, which dropped from 80 mol% to 70 mol % within the

first 3 h of run and then stabilized for the remaining 8 h. In order to determine whether the drop in activity was due to the conditioning of the catalyst in the reaction environment or due to coke formation, it was decided to perform a temperature programmed oxidation (TPO) analysis of the spent sample obtained from the TOS studies. The results obtained for TG/DTA carried out under oxidative atmosphere are given in Figure 4.19. The figure shows a weight loss resulting from burning off of the coke deposited during the TOS run.

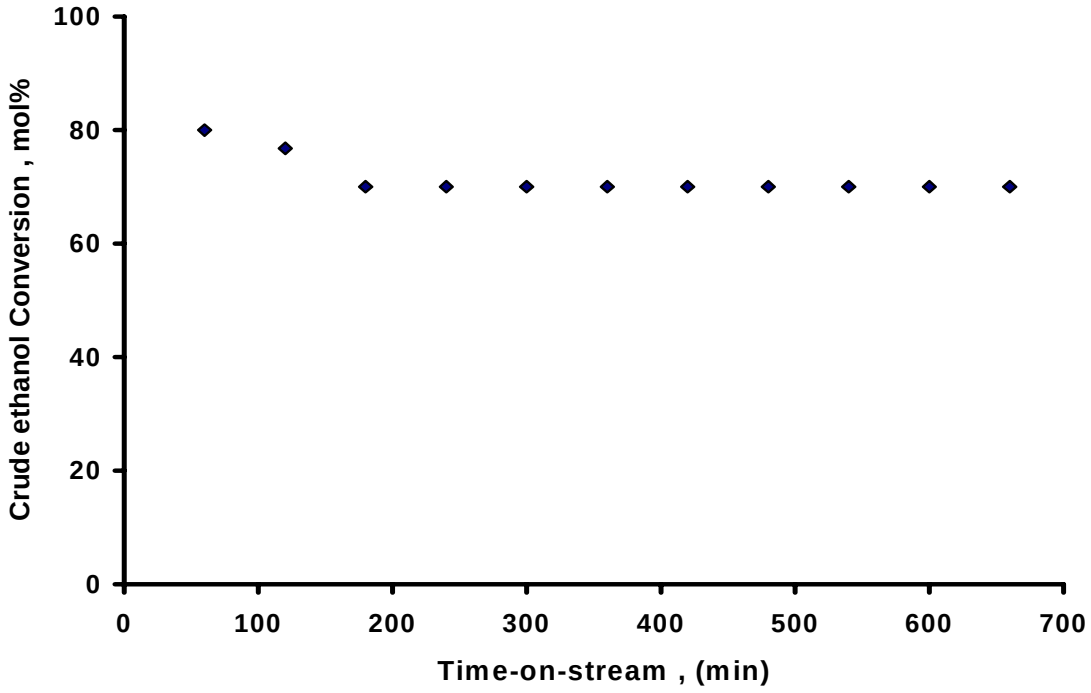

Figure 4.18: Conversion of crude-ethanol as a function of time-on-stream (min) for CP15 at T = 400^{o}C and WHSV=1.68h^{-1}

This shows that coke deposition was the problem but appeared to have stabilized after 3 h. In the TG/DTA profile itself, the initial step of weight reduction occurred over the temperature range of 100-200^{o}C. This was ascribed to the removal of easily oxidizable carbonaceous species as reported by Das, (2003) and Jianjun et al. (2004). The oxidation of coke (carbon deposit) to CO and CO_2 occurred mainly at 360^{o}C. After 3

months of runs there was problem of reactor plugging. This was attributed to blockage due to the presence of minerals in the fermentation broth.

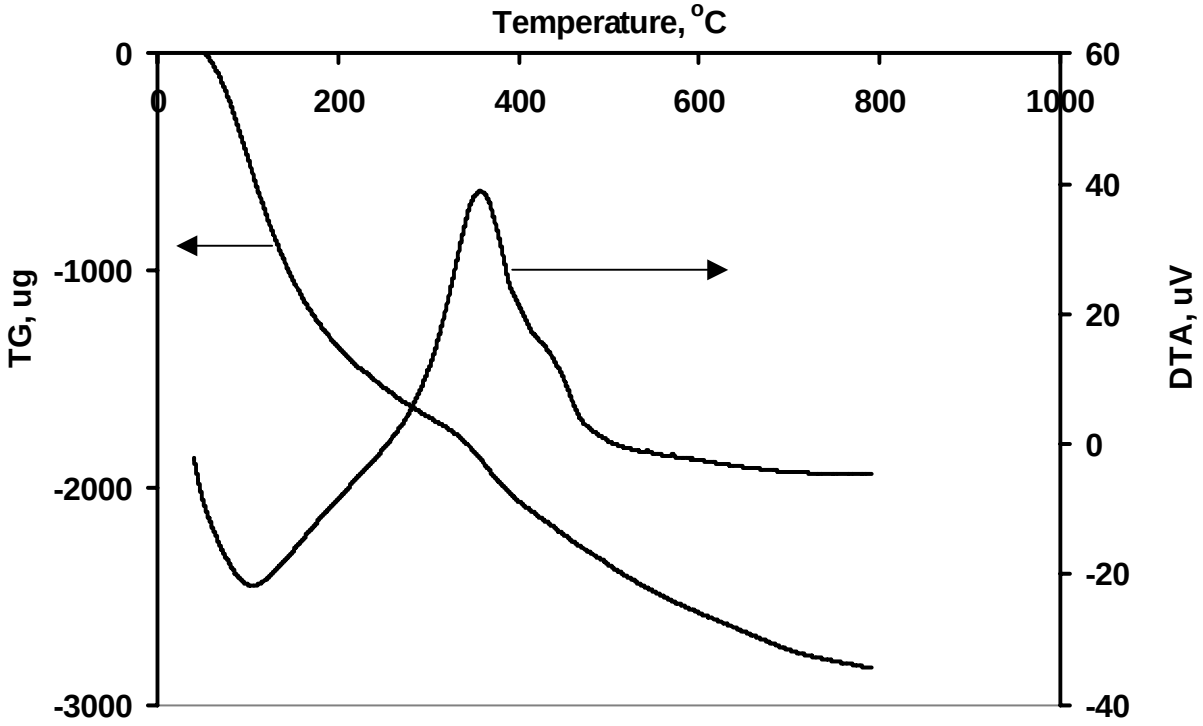

Figure 4.19: The TG/DTA profile of spent CP15 after 11 hours time-on-stream

4.3 Kinetic Studies

Kinetic studies and development of a kinetic model for the crude ethanol reforming process was necessary in order to accurately design the crude ethanol reformer. The objective of this study was to obtain a rate equation using method of experimentation and analysis based on fundamental kinetic studies. This was done to obtain a rate equation that could readily be combined with generalized equations for rates of physical transport process to produce a reactor model capable of extrapolation over a wide range of reactor operating conditions. The derivation of this rate equation was based on a mechanistic description of the crude ethanol reforming process together

with extensive kinetic measurements. Kinetic data were obtained in a kinetic regime under isothermal conditions in which the flow was close to plug flow. The experimental data were also fitted to a power law type rate model. Results of these derivations, measurements and analyses are discussed in the following sections.

4.3.1 Kinetic Data

The experiments to collect kinetic data were conducted in a catalyst bed in which fluids channeling was absent. This condition was achieved by employing catalyst in the appropriate average size range, as well as other conditions necessary and required for plug flow and isothermal behavior in the reactor (as stated in section 3.4.2). The choice of catalyst particle size was based on the report of Idem and Bakhshi (1996).

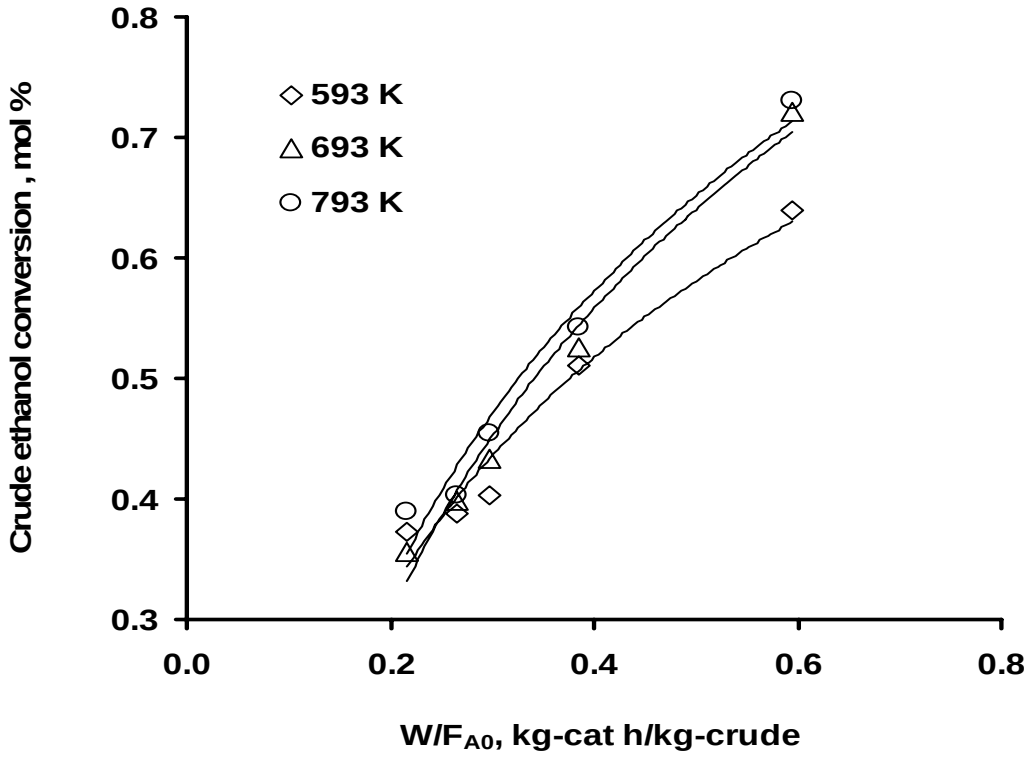

Figure 4.20: Variation of crude-ethanol conversion with space-time at 593, 693 and 793 K.

The kinetic data were obtained after 3 hours time-on-stream when the catalyst activity was stable with time. Results for the variation of crude ethanol conversion (X) with ratio of weight of catalyst to crude ethanol flow rate ratio (W/F_{AO}) at reaction temperatures of 593, 693, and 793 K are presented in Figure 4.20. These results show that the crude ethanol conversion initially increased rapidly with an increase in W/F_{AO}. Further increase in W/F_{AO} resulted in a slowing down of the corresponding increase of (X) for the three temperatures. These results are typical of the trend for most catalytic reactions where conversion depends on the amount of feed present.

4.3.1.1 Derivation of Kinetic Models

Rate expressions for crude ethanol reforming are not available in the literature. However since the stoichiometry is more familiar, the pure ethanol steam reforming reaction shown in Equation 4.6 was used to develop the kinetic models. There was no loss of accuracy by doing this since the atomic ratios indicated in Equation 4.6 were used just as illustrations of the presence of carbon, hydrogen and oxygen atoms in the organic fraction of the feed but not for any calculations.

$$C_2H_6O + 3H_2O \longrightarrow 2CO_2 + 6H_2 \tag{4.6}$$

A micro reactor was used to gather the experimental data and the design equation for the plug flow reactor was therefore applicable for data analysis. This was used in the differential form:

$$\frac{dX}{d(W/F_{AO})} = r_A \tag{4.7}$$

Slopes (i.e. $\frac{dX}{d(W/F_{AO})}$) were taken at various points of the X vs. W/F_{Ao} curves within the range of the operating conditions to obtain kinetic data for the three temperatures in order to determine experimental rates described in Equation 4.7. The kinetics experimental data for catalytic reforming of crude ethanol are shown in appendix D, Table D-1.

4.3.1.2 Rate Equation Based on Eley-Rideal Mechanism

After eliminating the influence of film and pore diffusion, three basic steps based on Eley Rideal mechanism were used in the derivation of the mechanistic type rate equations. Step one is the adsorption of crude ethanol on the catalyst surface, step two is the interaction of the adsorbed crude ethanol with an adjacent vacant site while step three involves two surface reactions. Four rate expressions, representing four possible rate controlling steps assumed, were derived. These are given in Equations 4.8, 4.9, 4.10 and 4.11 for mechanism in which the rate determining steps (RDS) were assumed to be adsorption of crude ethanol (model # 1), the dissociation of adsorbed crude ethanol (model # 2), surface reaction of adsorbed oxygenated hydrocarbon fraction with non-adsorbed water vapor (model # 3), and surface reaction of adsorbed hydrocarbon fraction with non-adsorbed water vapor (model # 4) respectively.

$$r_A = \frac{k_O e^{-E/RT}\left[C_A - \frac{C_C{}^2 C_D{}^6}{K_P C_B{}^3}\right]}{\left[1 + \frac{K_F C_C C_D{}^3}{C_B} + \frac{K_G C_C C_D{}^3}{C_B{}^2} + \frac{K_E C_C{}^2 C_D{}^6}{C_B{}^3}\right]} \qquad (4.8)$$

$$r_A = \frac{k_O e^{-E/RT}\left(C_A - \frac{C_C{}^2 C_D{}^6}{K_P C_B{}^3}\right)}{\left[1 + K_A C_A + \frac{K_F C_C C_D{}^3}{C_B} + \frac{K_G C_C C_D{}^3}{C_B{}^2}\right]^2} \tag{4.9}$$

$$r_A = \frac{k_O e^{-E/RT}\left(\frac{C_A C_B{}^3}{C_C C_D{}^3} - \frac{C_C C_D{}^3}{K_P}\right)}{\left(1 + K_A C_A + \frac{K_Q C_A C_B{}^2}{C_C C_D{}^3} + \frac{K_G C_C C_D{}^3}{C_B{}^2}\right)} \tag{4.10}$$

$$r_A = \frac{k_O e^{-E/RT}\left(\frac{C_A C_B{}^3}{C_C C_D{}^3} - \frac{C_C C_D{}^3}{K_P}\right)}{\left(1 + K_A C_A + \frac{K_F C_C C_D{}^3}{C_B} + \frac{K_H C_A C_B}{C_C C_D{}^3}\right)} \tag{4.11}$$

where r_A is the rate of crude-ethanol conversion (kmol-crude/kg-cat s), k_o is the collision frequency (kg-cat s)$^{-1}$, E is the activation energy (kJ/kmol), T is the absolute temperature (K), R is the Universal gas constant (kJ/kmol-K), K_p is the thermodynamic equilibrium constant, $C_2H_6O = A$, $CH_4O^* = A^*$, $H_2O = B$, $CH_2{}^* = S^*$, $CO_2 = C$ and $H_2 = D$, K_i = coefficient of term i in the denominator. Details concerning these derivations are given in Appendix E.

4.3.1.3 Power Law Model

The power law model was also used to fit the experimental data. The model is of the form given in Equation 4.12.

$$r_A = k_o e^{-E/RT} C_A{}^n \tag{4.12}$$

where *n*, is the order of reaction with respect to crude-ethanol. This form of the power law model (i.e. no terms involving the concentrations of H_2O and the products, H_2 and

CO_2) was adopted because H_2O was present in a large excess as compared to the combined concentration of the organic components of the crude, C_A, and because the reaction was more or less irreversible within the temperature range used in the kinetic studies.

4.3.1.4: Estimation of the parameters of rate models

The values of the parameters of the mechanism based rate models (Equations 4.8, 4.9, 4.10 and 4.11) as well as the model based on power-law (Equation 4.12) were estimated by using a nonlinear regression procedure according to the modified Levenberg-Marquardt algorithm, which is documented in IMSL MATH/library (1994). These rate equations were rewritten in terms of molar rates, N_i, in kmol/s as in Equations 4.13 to 4.17.

$$r_A = \frac{k_0 e^{-E/RT}[N_A - \frac{N_C^2 N_D^6}{K_P N_B^3}]}{[1 + \frac{K_F N_C N_D^3}{N_B} + \frac{K_G N_C N_D^3}{N_B^2} + \frac{K_E N_C^2 N_D^6}{N_B^3}]} \tag{4.13}$$

$$r_A = \frac{k_0 e^{-E/RT}(N_A - \frac{N_C^2 N_D^6}{K_P N_B^3})}{[1 + K_A N_A + \frac{K_F N_C N_D^3}{N_B} + \frac{K_G N_C N_D^3}{N_B^2}]^2} \tag{4.14}$$

$$r_A = \frac{k_0 e^{-E/RT}(\frac{N_A N_B^3}{N_C N_D^3} - \frac{N_C N_D^3}{K_P})}{(1 + K_A N_A + \frac{K_Q N_A N_B^2}{N_C N_D^3} + \frac{K_G N_C N_D^3}{N_B^2})} \tag{4.15}$$

$$r_A = \frac{k_0 e^{-E/RT}\left(\frac{N_A N_B^3}{N_C N_D^3} - \frac{N_C N_D^3}{K_P}\right)}{\left(1 + K_A N_A + \frac{K_F N_C N_D^3}{N_B} + \frac{K_H N_A N_B}{N_C N_D^3}\right)} \tag{4.16}$$

$$r_A = k_o e^{-E/RT} N_A^n \tag{4.17}$$

The subroutine called DBCLSF documented in the IMSL MATH/library (1994) was used to obtain the optimum fitting parameters, because this algorithm was proven to be very efficient in estimating the mass transfer parameters, as reported elsewhere Ji et al. (1999). The values obtained for the kinetics parameters are presented in Table 4.5.

Table 4.5. Fitted values of kinetics parameters

Parameter	Model # 1	Model # 2	Model # 3	Model # 4	Power Law
k_0	8.91×10^2	2.08×10^3	1.31×10^{14}	2.75×10^{-2}	3.12×10^{-2}
E	4.03×10^3	4.43×10^3	3.55×10^3	7.56×10^3	4.41×10^3
K_A	-	3.83×10^7	1.00×10^{20}	2.27×10^{14}	-
K_E	0.0	-	-	-	-
K_F	0.0	0.0	-	1.00×10^{20}	-
K_G	0.0	0.0	0.0		-
K_H	-	-	-	0.0	-
K_Q	-	-	3.66×10^{12}	-	-
n	-	-	-	-	0.43

4.3.2 Determination of the most realistic rate model

Figure 4.21 represents the comparison of measured rates and predicted rates using rate models of Equations 4.13 to 4.17. A close look at this parity chart shows that models 1 and 4 did not yield satisfactory results (with average absolute deviation, AAD%, greater than 20%) whereas models 2 and 3 as well as the power law model produced satisfactory results (AAD $\leq$ 11%). In fact, model 2 in particular yielded

excellent results with AAD% equal to 6%. Results of close inspection of both the parity rates chart (Figure 4.21) and the estimates of the values of the parameters (Table 4.5) in order to elucidate the circumstances behind the behavior of each model in fitting the kinetic data were discussed below.

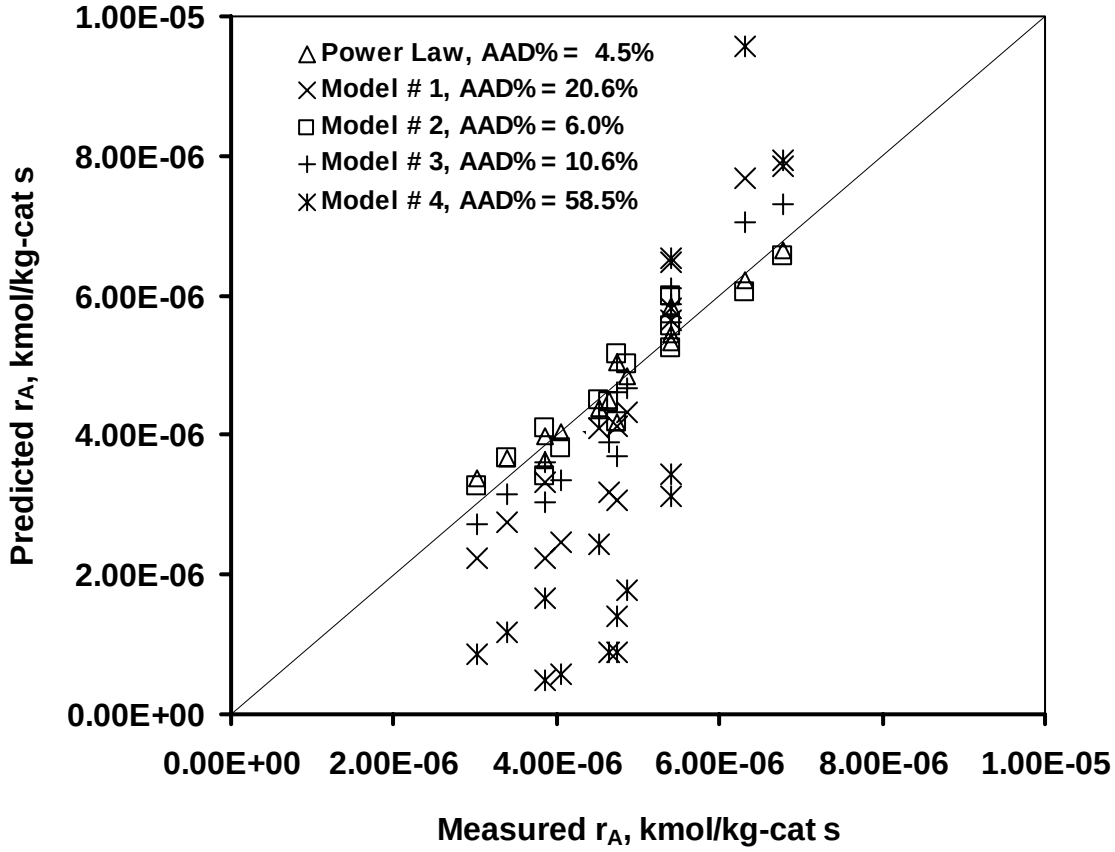

Figure 4.21. A comparison of measured and predicted rates within the temperature range 593 to 793 K.

4.3.2.1. Assumption of adsorption of crude ethanol on an active site as the rate-determining step (RDS)

Considering the estimated values of the parameters as well as the values of the thermodynamic equilibrium constant, the rate model based on the assumption of adsorption of crude ethanol on an active site as the rate-determining step reduces to:

$$r_A = k_0 e^{-E/RT}[N_A] \quad (4.18)$$

Equation 4.18 is very similar to the Power Law model except that the former has an order of reaction of unity whereas the Power law model has an order of reaction of 0.43. Even though they both have about the same activation energies, the Power law with an ADD% of 4.5% provides a better correlation of the kinetic data as compared with model # 1 represented in Equation 4.8, 4.13 or 4.18 as shown in Figure 4.21. This shows that the rate dependence of the concentration of crude ethanol was not accurately described by Equation 4.18 this led to rejection of the assumption of the adsorption of crude ethanol on an active site as the rate determining mechanism for the reforming of crude ethanol.

4.3.2.2. Assumption of dissociation of adsorbed crude ethanol as the RDS

By considering the estimated values of the parameters as well as the values of the thermodynamic equilibrium constant, the rate model based on the assumption of dissociation of adsorbed crude ethanol on an active site as the rate-determining step reduces to:

$$r_A = \frac{k_0 e^{-E/RT} N_A}{[1 + K_A N_A]^2} \quad (4.19)$$

This model has an ADD% of 6.0%, which is very close to that provided by the Power law model. Also, the activation energy derived from this model is almost identical to that obtained from the Power law model. These indicate that the assumption of dissociation of adsorbed crude ethanol as the RDS may be justified. If this is the case,

it is because the constraint of requiring two active sites to be available before the reaction can proceed as imposed in this assumption is more stringent as compared with the previous assumption of the adsorption of crude ethanol on an active site. This results in the dissociation of adsorbed crude ethanol taking a much longer time frame as compared with the adsorption of crude ethanol on an active site. However, before it can be concluded that this step is indeed the true rate determining mechanism, there is need to evaluate and then reject the models that are based on assuming the last two surface reaction steps as the RDS.

4.3.2.3. Assumption of reaction of adsorbed oxygenated hydrocarbon fraction with non-absorbed steam as RDS

By imposing the values of the constants from Table 4.5, the model based on assumption of the surface reaction between adsorbed oxygenated hydrocarbon fraction with non-absorbed steam as RDS reduces to Equation 4.20.

$$r_A = \frac{k_0 e^{-E/RT}\left(\frac{N_A N_B^{\,3}}{N_C N_D^{\,3}}\right)}{\left(1 + K_A N_A + \frac{K_Q N_A N_B^{\,2}}{N_C N_D^{\,3}}\right)} \qquad (4.20)$$

This model has an ADD% of 11%, which makes it reasonable to be included as one of the mechanistic based models. However, a comparison of the activation energies between the Power law model and this model shows a significant difference. Based on this large difference, it can be conclude that the model based on Equation 4.20 deviates from the mechanism that is illustrated in the Power law model whereas the model based on Equation 4.19 provides a more realistic mechanism for the reforming of crude ethanol than that base on Equation 4.20.

4.3.2.4. Assumption of reaction of adsorbed hydrocarbon fraction with non-absorbed steam as the RDS

In this case, a consideration of the values of the estimated parameters as given in Table 4.5 reduces the model to Equation 4.21.

$$r_A = \frac{k_0 e^{-E/RT}\left(\frac{N_A N_B^{\,3}}{N_C N_D^{\,3}}\right)}{\left(1 + K_A N_A + \frac{K_F N_C N_D^{\,3}}{N_B}\right)} \tag{4.21}$$

This model produced a very large ADD and the activation energy obtained is by far much different compare with one obtained for the Power law model. Thus, this model can be readily rejected as it does not represent a realistic mechanism for the reforming of crude ethanol. Consequently, Equation 4.19 appears to be the only model that represents the most realistic mechanism for the reforming of crude ethanol.

4.4 Reactor Modeling

The reactor modeling was carried out as part of this research by developing system of partial differential equations to describe the reactor system. The model was based on the coupling of mass and energy equation as well as the kinetic model developed for this process. The model was used to verify the assumption of plug flow behavior of the process and also to accurately predict the concentration profiles of all chemical species and temperature profiles of the fluid in both the axial and radial directions.

The model is based on the steady state mass and energy balances (Equations 4.22 and 4.23, respectively) around the reactor as reported by Bird et al. (2002). The

geometry of the packed bed tubular (PBTR) depicted in Figure 4.22, represents a schematic diagram of the catalytic packed bed tubular reactor used in the experimental work, the model equations can be presented in cylindrical coordinates for z components as in Equations 4.22 and 4.23.

$$v_Z \frac{\partial C_i}{\partial z} = D_r \left(\frac{\partial^2 C_i}{\partial r^2} + \frac{1}{r} \frac{\partial C_i}{\partial r} \right) + D_z \frac{\partial^2 C_i}{\partial z^2} + \rho_B r_j \tag{4.22}$$

$$\rho_g C_P v_Z \frac{\partial T}{\partial z} = \lambda_r \left(\frac{\partial^2 T}{\partial r^2} + \frac{1}{r} \frac{\partial T}{\partial r} \right) + \lambda_z \frac{\partial^2 T}{\partial z^2} + \rho_B \left[\sum -\Delta H_j r_j \right] \tag{4.23}$$

where D_z and D_r respectively denote the effective diffusivity in axial and radial directions, λ_z and λ_r respectively denote effective thermal conductivity in axial and radial directions, v denotes velocity, C_i denotes concentration of each chemical species, ρ_B denotes the catalyst bulk density, r_j denotes reaction rate (noting that if the diffusant is being consumed by the reaction, r_j is negative in these equations otherwise it is positive), ρ_g denotes gas density, C_p denotes heat capacity, T denotes temperature, and ΔH denotes heat of reaction. The initial and boundary conditions for the steady state mass and energy balance equations (Equations 4.22 and 4.23) in the case of using the packed bed tubular reactor (PBTR) that shown in figure 4.22 are as follows:

$C_i(r,0) = C_i^0$ $\quad$ $T(r,0) = T^0$ $\quad$ at z = 0 and $0 \le r \le r_1$

$\frac{\partial C_i}{\partial r}(0,z) = 0$ $\quad$ $\frac{\partial T}{\partial r}(0,z) = 0$ $\quad$ at r = 0 and $0 \le z \le L$

$\frac{\partial C_i}{\partial r}(r_1,z) = 0$ $\quad$ $-\lambda_r \frac{\partial T}{\partial r}(r_1,z) = U_{TW}(T_1 - T_2)$ $\quad$ at r = r_1 and $0 \le z \le L$

where U_{TW} denotes overall heat transfer coefficient across the tube wall and the superscript *0* denotes the inlet conditions.

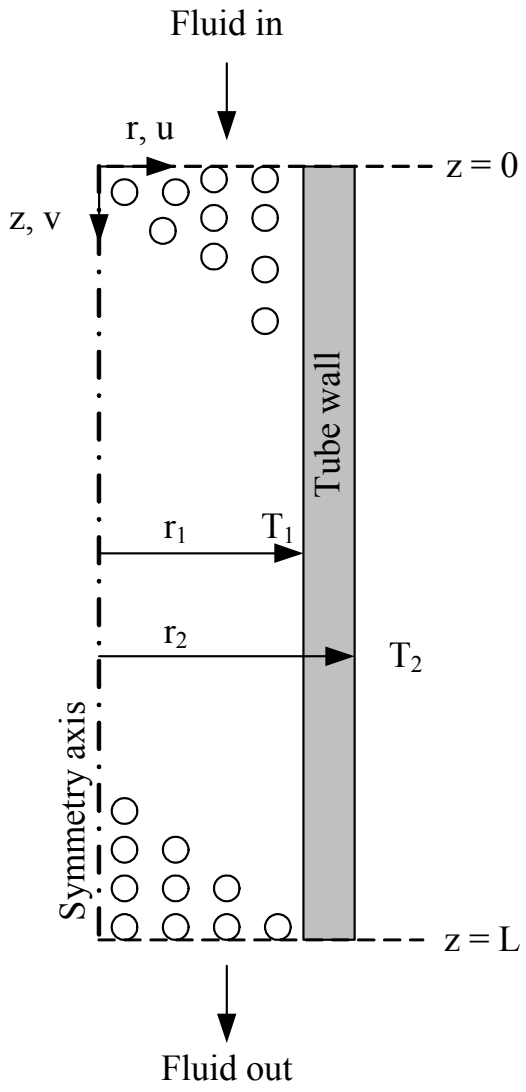

Figure 4.22. A schematic diagram of the packed bed tubular reactor (PBTR).

Regarding the boundary conditions at the outlet of the reactor (at $z = L$ and $0 \le r \le r_1$), it can be assumed that the convective part of the mass and heat transport vector dominates. The finite element method was used to solve the partial differential equations (Equations 4.22 and 4.23) subject to these initial and boundary conditions. It is important to note that these numerical model equations were solved without any

simplifying assumptions such as eliminating the axial dispersion term or the cylindrical coordinates.

4.4.1. Numerical Model Predictive Performance

The simulation and experimental results are given in the parity chart of Figure 4.23, which compares the experimental conversions of crude ethanol with those predicted by solving the partial differential equations 4.22 and 4.23 subject to the initial and boundary conditions and using the rate model given in Equation 4.14.

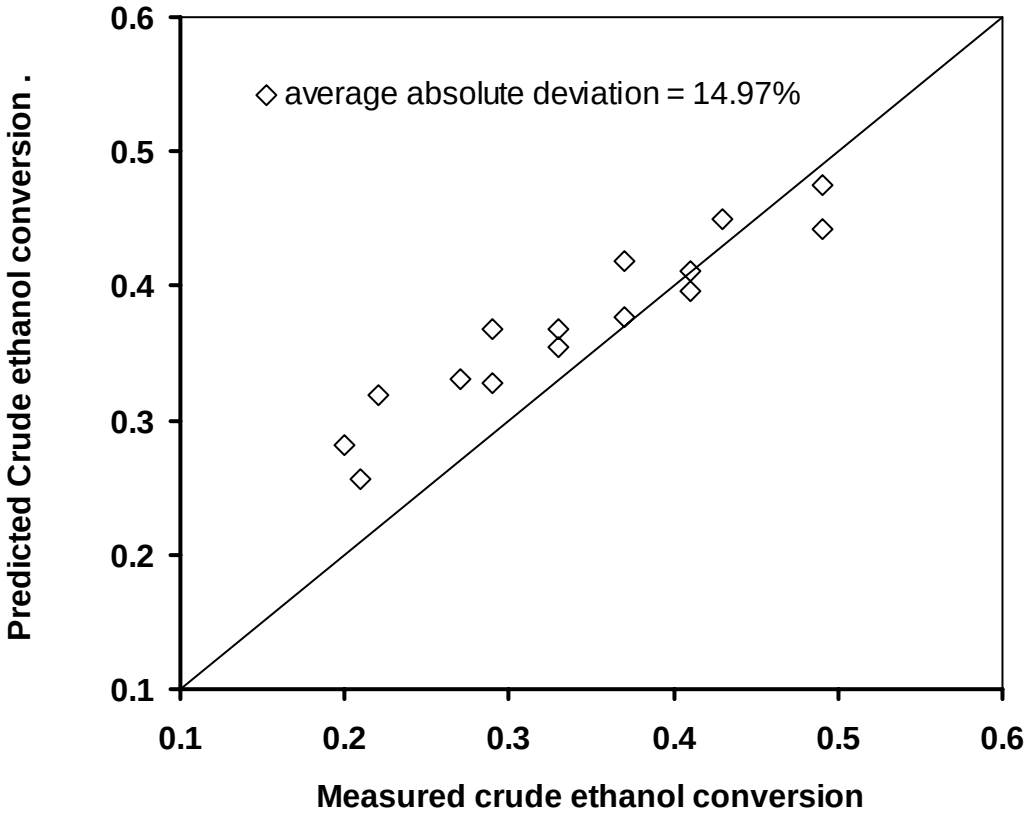

Figure 4.23: Comparison of measured and predicted crude ethanol conversion within the temperature range from 593 to 793 K and WHSV range from 1.68h^{-1} to 4.62h^{-1}

This figure shows very good predictive ability of the numerical model (Equations 4.22 and 4.23) with an average absolute deviation from the experimental data of 15%. It is important to note that the numerical solutions were arrived at without any simplifying assumptions, unlike what is obtained in some literature where the axial dispersion term is eliminated in order to simplify the solution of the partial differential equations.

4.4.2 Verification of Plug Flow Behavior

In performing the experiments to obtain kinetic data, the assumption was made that plug flow behavior was attained under the operating conditions.

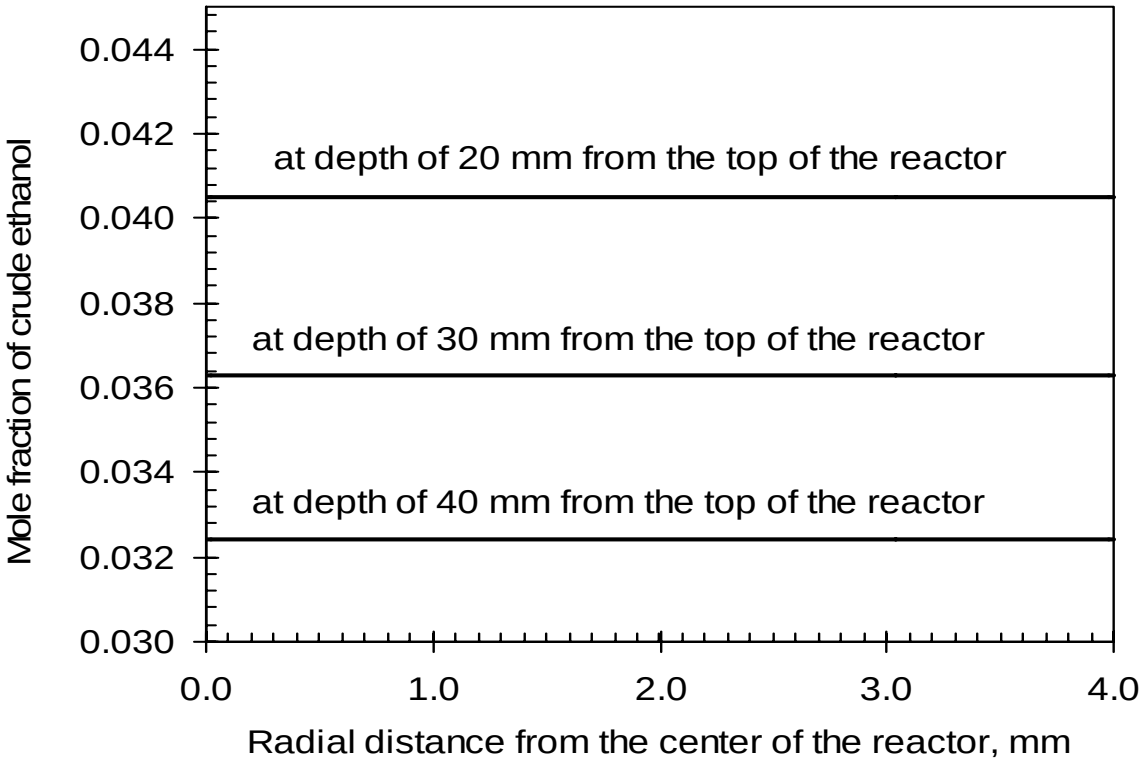

Figure 4.24: Radial mole fraction profiles of crude ethanol at various catalyst bed depths in the tubular reactor at inlet temperature of 593 K and W/F_{A0} of 2016 kg-cat s/kg-crude

With plug flow behavior, isothermalilty as well as flat concentration profiles for all the species were assumed. The model was used to examine whether this assumption was justified with particular reference to reactor bed height and internal diameter. Typical results for the concentration and temperature profiles in the radial direction within the range of conditions used for obtaining kinetic data are shown in Figures 4.24 and 4.25, respectively at different depths of the catalyst bed. As seen in the figures, somewhat isothermal behavior and plug flow behavior were attained.

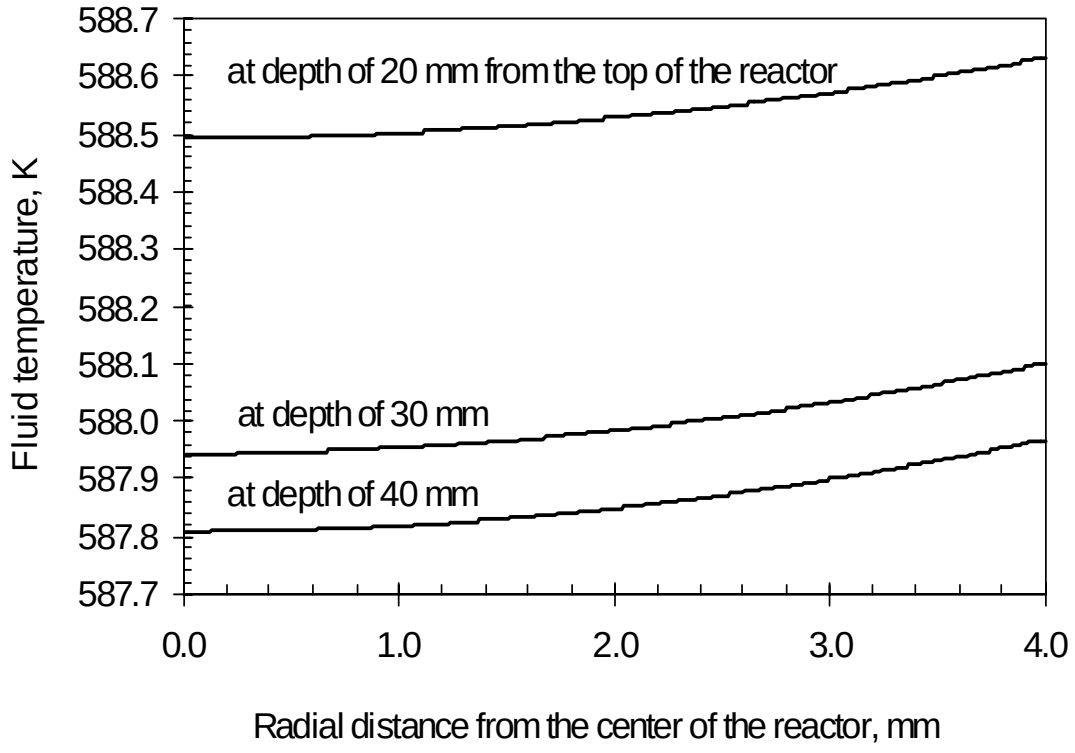

Figure 4.25: Radial temperature profiles of fluid at various catalyst bed depths in the tubular reactor at W/F_{A0} of 2016 kg-cat s/kg-crude.

4.4.3: Simulation of Concentration Profiles of Chemical Species along the Reactor Length

The concentration profiles of all the species along the reactor were also simulated using the solution of the numerical model subject to the initial and boundary conditions in conjunction with the kinetic model. Typical profiles for crude ethanol feed temperature of 593 K and W/F_{A0} of 2016 kg-cat s/kg-crude ethanol is shown in Figure 4.26. The exit concentrations based on the solution of the numerical model for the production of hydrogen from the reforming of crude ethanol for all the species for this run were compared with the corresponding concentrations obtained experimentally by GC and HPLC analyses. The results are given in Table 4.6. There is excellent agreement between the predicted and experimental results with an average absolute deviation (AAD%) of 6.2%.

Table 4.6: Outlet concentration profiles of the reactor at feed temperature of 593 K and W/F_{A0} of 2016 kg-cat s/kg-crude

Fluid	Measured mole fraction	Predicted mole fraction	AAD%
Crude ethanol	0.029	0.028	3.45
Water	0.805	0.822	2.11
CO_2, CO, CH_4, etc.	0.043	0.039	9.30
Hydrogen	0.123	0.111	9.76
		AAD%	6.15

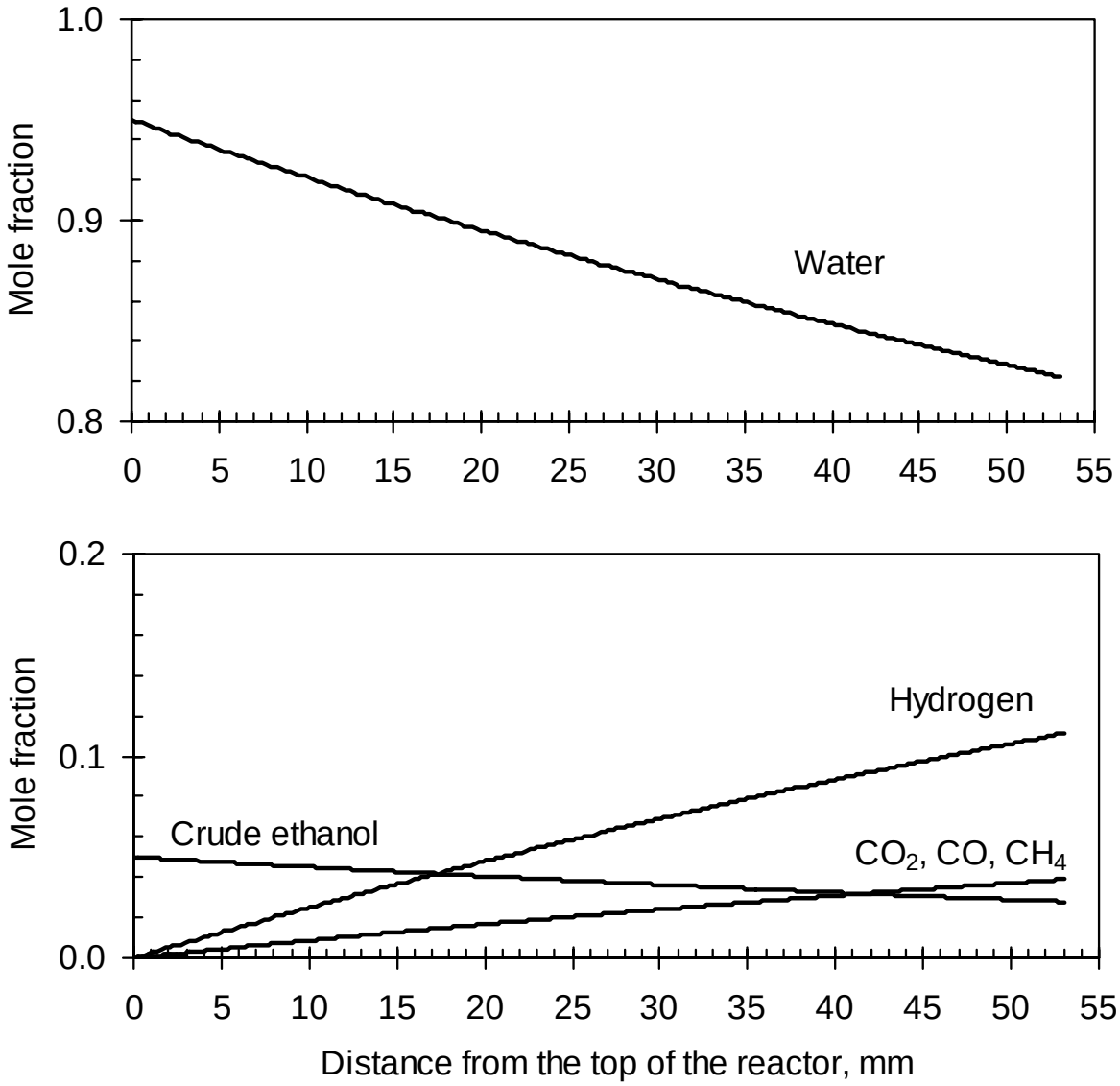

Figure 4.26: Concentration profiles along the reactor at a feed temperature of 593 K and W/F_{A0} of 2016 kg-cat s/kg-crude

4.4.4. Effect of the Axial Dispersion Term

The numerical model was used to determine the possible effects of neglecting axial dispersion as well as the conditions in which it is not appropriate to assume plug flow behavior. The simulated results in the case of neglecting or not neglecting axial dispersion are shown in Figures 4.27 and 4.28 in terms of the radial conversion profile

of crude ethanol and the radial temperature profile of the fluid in the reactor, respectively. The results exhibit more or less plug flow and isothermal behaviors. However, the results show that by neglecting the axial dispersion term, the crude ethanol conversion is under predicted (Figure 4.27), and the extent of under prediction

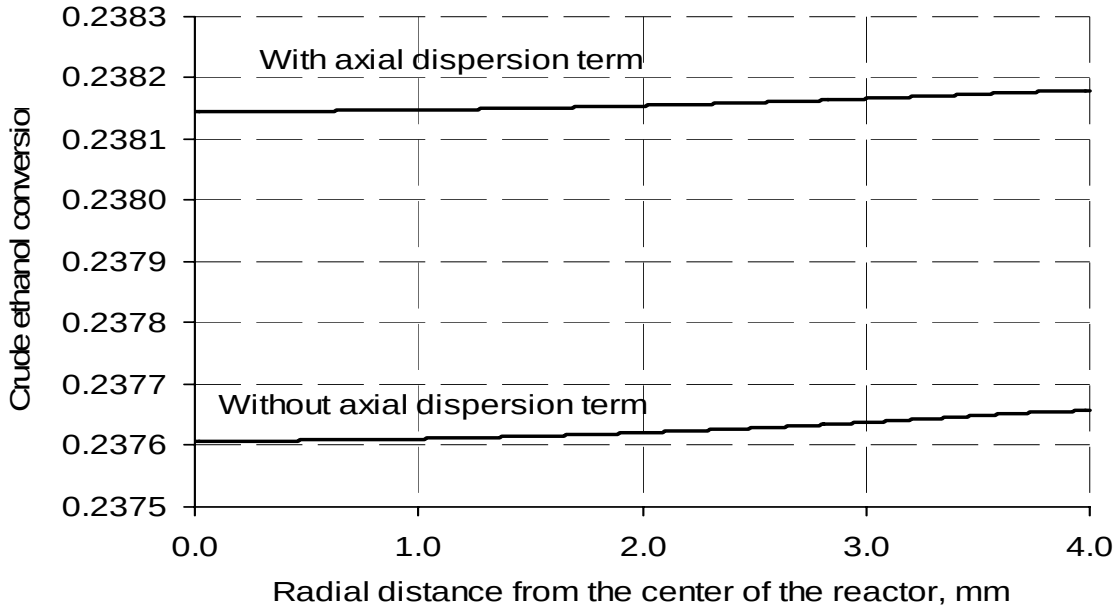

Figure 4.27. Effect of axial dispersion term on the crude ethanol conversion profile at a depth of 30 mm from the top of the catalyst bed at a feed temperature of 593 K and W/F_{A0} of 2016 kg-cat s/kg-crude

depends on the ratio of the velocity to the diffusivity (v_z/D_z) with a lower v_z/D_z ratio resulting in a lower prediction. Similar behavior and discussion is applied to the reaction temperature shown in Figure 4.28. The slightly lower temperature shown in the center of the reactor is due to the endothermic nature of the reaction.

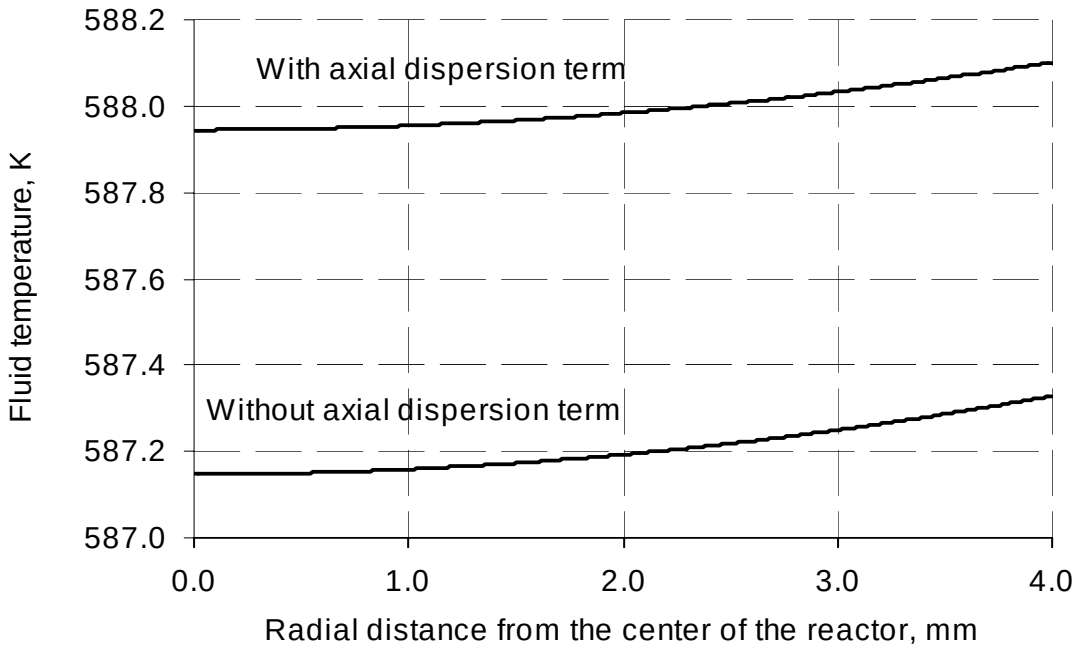

Figure 4.28. Effect of axial dispersion term on the temperature profile at a depth of 30 mm from the top of the catalyst bed at a feed temperature of 593 K and W/F_{A0} of 2016 kg-cat s/kg-crude

4.4.5: Simulation of Effect of Reactor Length and W/F_{A0}

In some instances, the objective of a process may be to enhance the performance of the reactor in a given process. Such an enhancement may be achieved by an increase in the length of the catalyst bed or increase in W/F_{A0} ratio both of which result in an increase in the residence time of the feed in the reactor. The first effect was simulated by increasing the catalyst bed length from 0.05 m to 0.2 m at temperatures in the range of 373-873 K.

The results are shown in Figure 4.29 for a fixed W/F_{A0} ratio of 2000 s for this range of temperatures. These results show that even though there are some benefits to be derived by increasing the length of the catalyst bed, these benefits however diminish as the reaction temperature increases. In fact, at the highest temperatures used, the

benefit is so insignificant that the reaction is more or less completed after a catalyst bed length of about 0.15 m so that the extra length of catalyst bed beyond 0.15 m is not utilized. At the lower temperature (373 K), there is no additional conversion beyond 0.2 m. This is attributed to the higher degree of reversibility of the reaction at this temperature. Thus, irrespective of the temperature, the benefit of an increase in length is limited

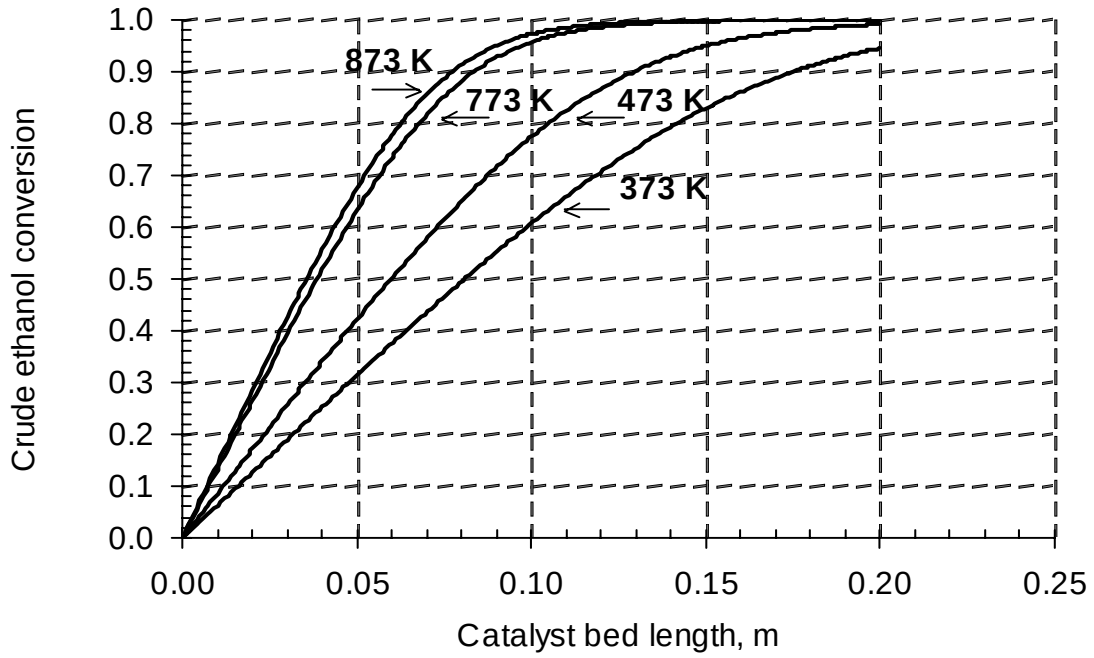

Figure 4.29: Effect of catalyst bed length on crude ethanol conversion at various feed temperatures and W/F_{A0} of 2000 s.

The corresponding axial temperature profile for a run conducted at W/F_{A0} = 2016 kg-cat s/kg-crude and inlet feed temperature of 593 K is shown in Figure 4.30. This figure shows a rapid drop in temperature at the top of the catalyst bed, which become slower after 20 mm depth as the feed progressed towards the bottom of the catalyst bed. This is

a reflection of a slowing down of the reaction (crude ethanol conversion) as shown in Figure 4.29, and consequently, a lesser endothermic demand for heat supply as the reaction mixture progresses towards the bottom of the catalyst bed.

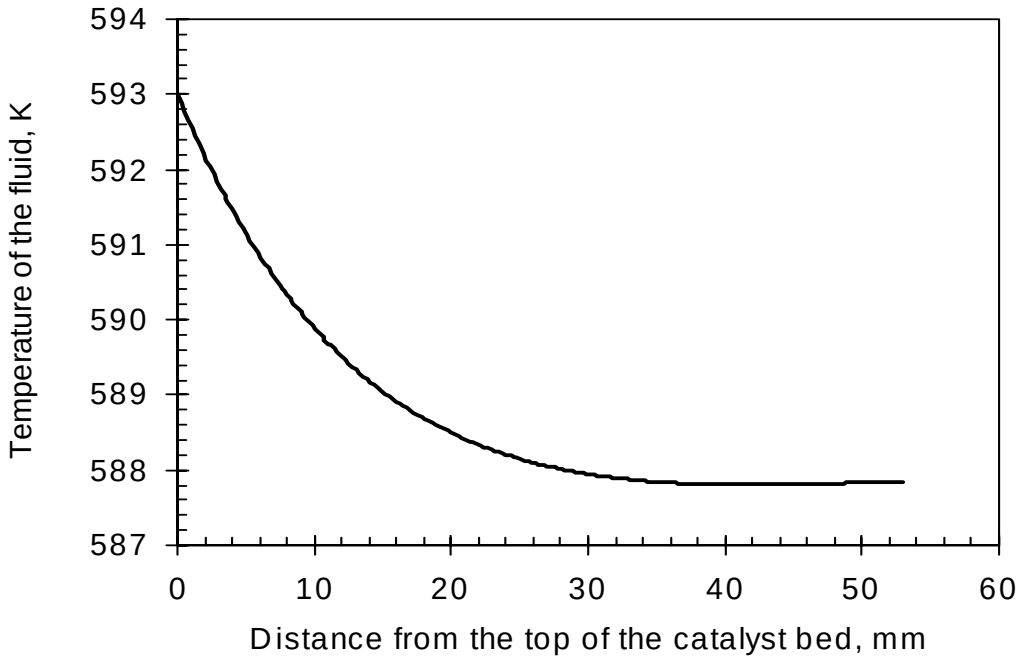

Figure 4.30: Axial temperature profile of the fluid along the center of the tubular reactor. at W/F_{A0} of 2016 kg-cat s/kg-crude and inlet feed temperature of 593 K

In the case of a change in W/F_{A0} ratio, the results are given in Figure 4.31 for a fixed catalyst bed length of 0.53 m and temperature of 693 K for W/F_{A0} in the range of 1000 to 16000 s. The results show that the benefit is huge (i.e. linear increase in the conversion of crude ethanol with W/F_{A0}) for the lower W/F_{A0} values. However, as the W/F_{A0} values increase (i.e. extremely low flow rates), the beneficial effects start to diminish. The effects of both the increase in catalyst bed length and the W/F_{A0} ratio on crude ethanol conversion demonstrate that there are limits as to how much

enhancements could be achieved without modifying the activity of the catalyst to provide for higher activity. However, it points to the region where we can maximize the gains by optimizing the relevant parameters for increasing the production of hydrogen by the reforming of crude ethanol.

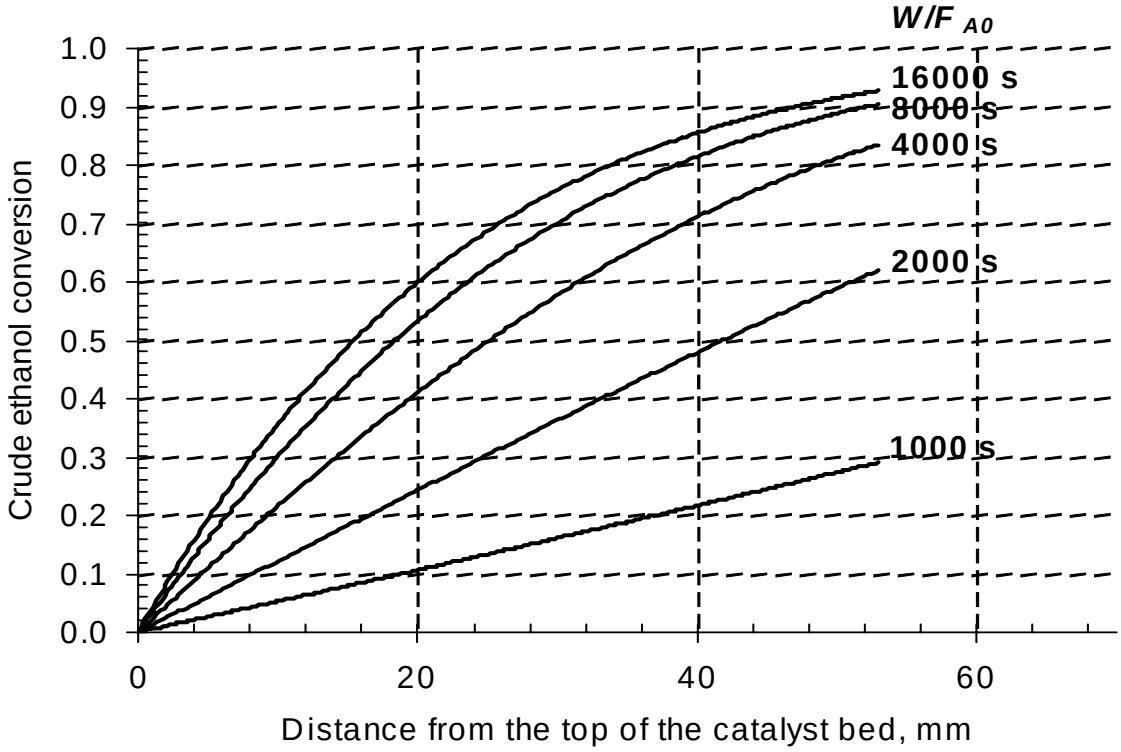

Figure 4.31: Effect of W/F_{A0} on crude ethanol conversion in the axial direction at 693 K

5.0 CONCLUSIONS AND RECOMMENDATIONS

5.1 Conclusions

1 As a result of the type of species generated by the preparation method, the PT catalysts were more reducible than the CP and IM catalysts.

2 Catalysts prepared by precipitation generally exhibited lower crystallite sizes of NiO species than the corresponding catalysts prepared by coprecipitation. The catalysts prepared by impregnation had the largest crystallite sizes except IM10 which had the smallest crystallite size.

3 A combination of small crystallite size and higher reducibility for PT catalysts resulted in higher crude ethanol conversions for the PT catalysts. These conversions were followed by those of the CP catalysts, which had slightly bigger crystallite sizes but lower reducibility. The IM catalysts exhibited the lowest crude ethanol conversions because of larger crystallite sizes and lower reducibility.

4 Catalysts with 15% Ni loading gave the best crude ethanol conversions for each method of synthesis with PT15 (catalyst with 15% Ni loading prepared by precipitation) giving the best overall crude ethanol conversion of 85mol%. This was attributed to small crystallite size and high reducibility of PT15 as compared to CP15 and IM15.

5 The precipitation method resulted in NiO as the dominant species in the catalysts whereas $NiAl_2O_4$ was a major species in catalysts prepared by the coprecipitation and impregnation methods.

6 In terms of H_2 yield, CP15 gave the highest yield as compared to corresponding catalysts prepared by precipitation and impregnation.

7 Coking was observed at the onset of the reaction but stabilized after 180 min time-on-stream.

8 A new kinetic model was developed to describe the experimental kinetics data. This was an Eley-Rideal type rate model based on the assumption of dissociative adsorption of crude ethanol on active sites as the rate-determining step. The average absolute deviation from the experimental rate was 6%

9 The kinetics model compared well with an empirical power-law rate model, which had an average absolute deviation of 4.5% from the experimental rate

10 A comprehensive model for the design and simulation of packed bed tubular reactors was developed.

5.2 Recommendation

1 The effects of higher reduction temperatures on crude ethanol conversion should be studied on catalyst CP15.

2 Modification of catalyst support by using CeO_2-ZrO_2 mixed oxides should be investigated, this is because CeO_2-ZrO_2 limits carbon deposition due to its redox properties and also promotes metal activity.

3 Effect of addition of oxygen to the reaction mixture in order to minimize coke formation should be investigated.

4 Quantitative and qualitative analysis of coke formation to evaluate the amount and type of coke formed by the catalyst should be done.

6.0 REFERENCES

Athanasios, N.F.and D.I. Kondaridesm, "Production of hydrogen for fuel cells by reformation of biomass-derived ethanol", Catalysis Today, 75, 145-155 (2002).

Athanasio, N.F. and X.E Verykios, "Reaction network of steam reforming of ethanol over Ni-based catalysts", Journal of Catalysis 225 439-452 (2004).

Ahuja, V. and R. Green, "Carbon dioxide removal from air for alkaline fuel cells operating with liquid hydrogen – A synergistic advantage", Int. J. Hydrogen Energy, 23 (2), 131-137 (1998).

Aupretre, F., C. Descorme and D. Duprez, "Bio-ethanol catalytic steam reforming over supported metal catalyst", Catalysis Communication 3, 263-267 (2002).

Austin, L. G., "Fuel Cells", Energy in Our Society, 3, 188-194 (1959).

Bird, R.B., W. E. Stewart and E.N. Lightfoot, "Transport Phenomena", 2nd Edition, JohnWiley & Sones, Inc., (2002).

Breen, J.P., R. Burch and H. M. Coleman, "Metal-catalyzed steam reforming of ethanol in the production of hydrogen for fuel cell applications", Applied catalysis B: Environmental, 39, 65-74 (2002).

Cavallaro, S. and S. Freni, "Ethanol steam reforming in a molten carbonate fuel cell. A preliminary kinetic investigation", Int. J. Hydrogen Energy, 21, 6, 465-469, (1996).

Cavallaro, S., V. Chiodo, S. Freni, N. Mondello and F. Frusteri, "Performance of Rh/Al_2O_3 catalyst in the steam reforming of ethanol: H_2 production for MCFC", Applied catalysis A: General 249, 119-128 (2003).

Cortright, R. D., R. R. Davda and J.A. Dumesic, "Hydrogen from catalytic reforming of biomass-derived hydrocarbon in liquid water", Letters to nature, 418, 964-967, (2002).

Creveling, H. F., "Proton Exchange Membrane (PEM) Fuel Cell System R & D for Transportation Applications", Proc. Annual Automotive Technology Development Contractors' Coordination Meeting, Society of Automotive Engineers, pp 485-492, Oct. 19-21, (1992).

Das , N., "Low temperature steam reforming of ethanol", Masters thesis Department of Chemical Engineering, University of Saskatchewan, (2003).

Freni, S., "Rh based catalysts for indirect internal reforming ethanol applications in molten carbonate fuel cells", Journal of Power Sources, 94, 14-19 (2001).

Freni, S., S. Cavallaro, N. Mondello and L. Spadaro and F. Frusteri "Steam reforming of ethanol on Ni/MgO catalyst: H_2 production for MCFC", Journal of power sources, 108, 53-57, (2002).

Freni, S., G. Maggio, and S.Cavallaro, "Ethanol steam reforming in a molten carbonate fuel cell: A thermodynamic approach ". Journal of Power Sources, 62, 67-73, (1996).

Froment, G. F. and K. B. Bischoff, "Chemical Reactor Analysis and Design" 2nd Edition. John Wiley & Sones, Inc., (1990).

Garcia, L., R. French, S.Czernik, and E. Chornet, "Catalytic Steam Reforming of Bio-Oils for the production of Hydrogen: Effects of Catalyst Composition", Appl. Catal., 201, 225-239, (2000).

Gary, J.H., G.E. Handwerk, "Petroleum Refining Technology and Economics", 3rd Edition, Marcel Dekker, Inc., New York, (1994).

Galvita, A.A., G.L. Semin, V.D. Belyaev, V.A. Semikolenov, P.Tsiakaras and V.A. Sobyanin, "Synthesis gas production by steam reforming of ethanol", Applied catalysis A: General 220, 123-127(2001).

Garcia, E. Y. and M. A. Laborde, "Hydrogen Production by the Steam Reforming of Ethanol: Thermodynamic Analysis", Int. J. Hydrogen Energy, 16 (5), 307-312 (1991).

Geankoplis, C. J. "Transport Processes and Separation Process Principles", Pearson Education Inc (2000).

Gulzow, E. "Alkaline fuel cells: a critical view", Journal of Power Sources, 61, 99 – 104 (1996).

Hsu, M., D. Nathanson and E. Hoag, "ZTEK Advanced Planner SOFC for Atmospheric and Pressurised Operation", AIAA 29th Intersoc. Energy Convers. Eng. Conf., Monterey, CA. 847-851 (1994).

Haga, F., T. Nakajima, K.Yamashita, and S. Mishima, "Effect of crystallite size on the catalysis of Alumina-supported cobalt catalyst for steam reforming of ethanol", Reaction kinectic.catalysis letter, 63, 2, 253-259. (1997)

Idem, R. O., "Production of hydrogen from the low-temperature steam reforming of methanol", PhD thesis Department of Chemical Engineering, University of Saskatchewan, (1995).

Idem, R. O. and N.N. Bakhshi, "Kinetic modeling of the production of hydrogen from the methanol-steam reforming process over Mn-promoted coprecipitated Cu-Al catalyst" Chemical Engineering Science, 51, 14 , 3697-3708 (1996).

Idem, R. O. and N.N. Bakhshi, "Production of Hydrogen from Methanol 1. Characterization Studies" Ind. Eng. Chem. Res.(33), 2047-2055 (1994a).

Idem, R. O. and N.N. Bakhshi, "Production of Hydrogen from Methanol 2. Experimental Studies", Ind. Eng. Chem Res.(33), 2056-2065 (1994b).

Idem, R.O., S.P.R. Katikaneni, R. Sethuraman, and N.N. Bakhshi, "Production of C_4 hydrocarbons from modified fischer-tropsch synthesis over Co-Ni-ZrO_2/sulphated-ZrO_2 hybrid Catalysts" Energy and fuel 14 1072-1082 (2000).

IMSL MATH/LIBRARY: FORTRAN Subroutines for Mathematical Applications. Visual Numerics Inc.Texas, (1994).

Jae-Hee L., J. Eun-Gu, J. Oh-shim, J. Kwang-Deog "Stabilization of Ni/Al_2O_3 catalyst by Cu addition for CO_2 reforming of methane", Applied catalysis A: General 269 1-6, (2004).

Jianjun G., H. Lou, H. Zhao, D. Chai and X. Zheng, " Dry reforming of methane over nickel catalyst supported on magnesium aluminate spinels", Applied catalysis A: General (2004, in press)

Ji, X., W. Kritpiphat, A. Aboudheir, P.Tontiwachwuthikul, "Mass Transfer Parameter Estimation using Optimization Technique: Case Study in CO_2 Absorption with Chemical Reaction", Can. J. Chem. Eng. 77, 69-73, (1999).

Jordi, L. and P. Ramirez, "Direct production of hydrogen from ethanol aqueous solutions over oxide catalysts", The royal society of chemistry. Chem. commun. 641-642 (2001).

Jordi, L., N. Homs, J. Sales and P. Ramirez de la Piscina, " Efficient Production Of Hydrogen over supported Cobalt Catalysts from Ethanol Reforming" Journal of catalysis, 209,306-317 (2002).

Jose, C., F. Marino, M. Laborde and N. Amadeo, "Bio-ethanol steam reforming on Ni/Al_2O_3 catalyst", Chemical Engineering Journal, (Accepted 2003, in press).

Juan-Juan, J., M.C. Roman-Martinez and M.J. Illan-Gomez, "Catalytic activity and characterization of Ni/Al_2O_3 and Ni/Al_2O_3 catalysts for CO_2 methane reforming", Applied catalysis A: General 264, 169-174 (2004) .

Klouz, V., V.Fierro, P.Denton, H. Katz, J.P. Lisse, S. Bouvot-mauduit and C.Mirodatos, "Ethanol reforming for hydrogen production in a hybrid electric vehicle: process optimization", Journal of Power Source 105, 26-34 (2002).

Leclerc, S., R.F. Mann and B.A. Peppley, "Evaluation of the catalytic ethanol-steam reforming process as a source of hydrogen-rich gas for fuel cells", Prepared for the CANMET Energy Technology Centre (CETC), (1998).

Luengo, C.A., G. Ciampi, M.O. Cencig, C. Steckelberg and M.A Larbode, "A novel catalyst system for ethanol gasification", International Journal of Hydrogen Energy, 17, 9, 667-681, (1992).

Marino, F., E. Cerrella, S. Duhalde, M. Jobbagy and M. Laborde, "Hydrogen from steam reforming of ethanol. Characterization and performance of copper-nickel supported catalysts", International Journal of Hydrogen Energy, 23, 1095-1101, (1998).

Ming-Tseh, T., F. Chang, "Characterisation of rice husk ash-supported nickel catalysts prepared by ion exchange", Applied Catalysis A: General 203, 15-22 (2002).

Parathasarathi, B., M. Rajamathi, M.S. Hegde, and P.V Kamath, "Thermal behaviour of hydroxides, hydroxysalts and hydrotalcites", Bull. Mater.Sci, 23, 2 141-145 (2000).

Rase, H.F., "Chemical Reactor Design for Process Plants". Wiley New York, (1987).

Richardson, J.T., "Principles of catalyst development" Plenum Press, New York, (1989)

Simanzhenkov, V. and R.O. Idem, "Crude oil chemistry", Marcel Dekker, New York, (2003).

Smith, J.M., H. C. Vanness and M.M. Abbott, "Introduction to Chemical Engineering Thermodynamics", 5th Edition, Mcgraw-hill, (1996).

Sorcha, C., "Faversham House Group Ltd"(2003) www.edie.net/news/Arhive/8065.cfm (found on October, 2004).

Theophilos, I. "Thermodynamic analysis of ethanol processors for fuel cell applications", Journal of Power Sources, 92, 17-25, (2001).

Vasudeva, K., N. Mitra, P. Umasankar, and S. C. Dhingra, "Steam Reforming of Ethanol for Hydrogen Production: Thermodynamic Analysis", International Journal of Hydrogen Energy, 21 (1), 13-18 (1996).

Velu, S., N. Satoh, and S.C. Gopinath, "Oxidative reforming of bio-ethanol over CuNiZnAl, mixed oxides catalysts for hydrogen production". Catalysis letters, 82, 145-151 (2002).

Whitaker, F. L., "The Phosphoric Acid PC25™ Fuel Cell Power Plant – and beyond",AIAA 29th Intersoc. Energy Convers. Eng. Conf., Monterey, CA., 1258 – 1259 (1994).

7.0 APPENDICES

Appendix-A: Energy Efficiency

The thermodynamics studies of Garcia and Laborde (1991), Vasudeva et al. (1996) and Freni et al. (1996) showed that high temperatures (above 300^{o}C) favored the production of hydrogen in a steam reforming reaction. Also, it is well documented in the literature as shown in section 2.5 that steam reforming reactions have been carried out at temperatures $\geq 300^{o}$C. In some cases temperatures as high as 700^{o}C have been used. Thus, irrespective of the type of feed material used, a relatively high temperature is required for the reaction. However the unique advantage of this process in terms of energy savings is that it eliminates the energy intensive distillation process involved during production of pure ethanol.

Evaluating the energy efficiency of this process involves a comparison of the amount of useful energy obtained when a fixed amount of crude ethanol is used to produce hydrogen for fuel cell to run an automobile, with the amount of useful energy obtained when pure ethanol is used as direct combustion fuel in an automobile.

Calculation of chemical energies of ethanol and hydrogen

The chemical energy store in ethanol and hydrogen is regarded as the enthalpy of combustion; this can be calculated as follows:

Combustion of ethanol: $C_2H_5OH + 3O_2 \longrightarrow 2CO_2 + 3H_2O$ A-1

Enthalpy of combustion $(\Delta H_R) = \sum (H_f, \text{product} - H_f, \text{reactant})$ A-2

Table A-1: Heat of formation of gases

	H_f (kJ/mol)
H_2	0
O_2	0
CO_2	-393.5
H_2O	-241.83
C_2H_5OH	-235.31

Density of hydrogen = 8.5×10^{-5} g/mL

From Equation A-2,

Enthalpy of combustion of ethanol $(\Delta H_R) = (2 \times H_f{}^c + 3 H_f{}^w) - (1 \times H_f{}^e)$ A-3

$= ((2 \times -393.5) + (3 \times -241.83)) - (1 \times -235.31)$

= -1277.18 kJ/mol of ethanol

$= (\Delta H_R) =$ 1277.18 kJ/mol of ethanol

Or = -27.76kJ/g of ethanol

Where superscript c, w, and e indicate carbon dioxide, water and ethanol respectively.

Similarly,

Combustion of hydrogen $H_2 + 1/2O_2 \longrightarrow H_2O$ A-4

Enthalpy of combustion $(\Delta H_R) = (H_f{}^w) - (0)$

$= -241.83$ kJ/mol H_2 = -10.28 kJ/LH_2

$= (\Delta H_R)$ = -10.28 kJ/LH_2

Heat conversion efficiency

If 1 litre of pure ethanol is used directly as a fuel (heat engine) in a car, only about 20% of the chemical energy stored in ethanol can be converted to useful mechanical work. If the same amount of ethanol is converted to hydrogen to run a fuel cell, about 60% of the stored chemical energy in hydrogen can be converted to electrical energy (Sorcha, 2003).

Mechanical work output by heat engine

Basis: 1 litre (1000mL) of ethanol

$$\text{Chemical/Heat energy available } (\Delta H) = 1000\text{mL} \times \frac{0.791\text{g}}{\text{mL}} \times \frac{-27.76\text{kJ}}{\text{g}}$$

$$= -21916.94\text{kJ}$$

with only about 20% efficiency, the useful work output

$$= 0.2 \times -21916.94\text{kJ} = -4392.39\text{kJ} \qquad \text{A-5}$$

Electrical work output by fuel cell

Pure ethanol as source of hydrogen

$$\text{Number of moles of 1 litre ethanol} = 1000\text{mL} \times \frac{0.791\text{g}}{\text{mL}} \times \frac{1\text{mole}}{46\text{g}}$$

$$= 17.2\text{mol}$$

Theoretical number of moles of H_2 that can be produced from 1 litre of ethanol

$$= 6 \times 17.2 = 103.17 \text{ mol}$$

Assuming 90% H_2 yield by steam reforming reaction

$$= 103.17\text{mol} \times 0.9 = 92.85 \text{ moles of } H_2$$

The volume of H_2 produced at ideal state $= 92.85\text{mol} \times \frac{22.4\text{L}}{\text{mol}}$

$= 2079.84$ L

The energy available $\Delta H = 2079.84\,\text{L} \times \frac{-10.28\text{kJ}}{\text{L}}$

$= -21380.86$ kJ

with only 60% efficiency, the useful electrical work output;

$= 0.6 \times -21380.86 = -12828.52$ kJ A-6

Crude ethanol as source of hydrogen

Fermentation broth (from feedstock analysis) contains 12%v/v ethanol.

Amount of fermentation broth that will provide 1 liter of ethanol = 1/0.12=8.333Liter of feedstock.

From reforming experiments (Run # 12)

$13.2*10^{-3}$ L (fermentation broth feedstock) produced 0.149moles H_2

8.33 L (fermentation broth feedstock) will produce

$$\frac{8.33}{13.2*10^{-3}} * 0.149 = 94.028 \text{ moles of } H_2$$

The volume of H_2 (assume ideal state) produced is therefore;

$= 94.028$ moles $\times$ 22.4Liter/mole

$= 2106.23$L

Heat energy available = $-10.28\ \text{kJ/L}_{H2} \times 2106.23\text{L}_{H2}$

$= -21652.04$ kJ

with about 60% efficiency, the useful electrical work output

$= 0.6 \times -21652.04$ kJ

$= -12991.22$ kJ (A-7)

A close look at Equations A-5, A-6 and A-7 show that effective energy output is much greater in fuel cell system when used as source of energy than the heat engine, due to the higher energy conversion advantage of the fuel cell. This implies that when equal amounts of ethanol are used as a direct fuel for automobile or reformed to produce H_2 for fuel cells to run automobile, the overall energy is enhanced in the latter than the former.

Appendix-B: Calculations of Equilibrium Conversion

The basic steam reforming reaction of ethanol will be used to evaluate the equilibrium conversion of this process.

The reaction is:

$$C_2H_5OH + 3H_2O = 6H_2 + 2CO_2 \quad \text{(B-1)}$$

at 673K

Thermodynamic data, Smith et al. (1996)

	A	B	C	D	H_f (kJ / mol)	G_f (kJ / mol)
H_2	3.249	4.22E-04	0.00E+00	8.30E+03	0.00E+00	0.00E+00
CO2	5.457	1.05E-03	0.00E+00	-1.16E+05	-3.94E+02	-3.94E+02
H2O	3.47	1.45E-03	0.00E+00	1.21E+04	-2.86E+05	-2.37E+02
C_2H_5OH	3.518	2.00E-02	-6.00E-06	0.00E+00	-2.35E+05	-1.68E+02

Where $\Delta = 6 * (H_2) + 2 * (CO_2) - (C_2H_5OH) - 3 * (H_2O)$

	ΔA	ΔB	ΔC	ΔD	ΔH^0 (kJ/ /mol)	ΔG^0 (kJ / mol)
H_2 CO_2 H_2O C_2H_5OH	16.48	-1.973E-02	6.002E-06	2.179E+05	305.572	91.159

Step 1: Calculation of thermodynamic equilibrium constant Kp

Kp, the thermodynamic equilibrium constant is a function of temperature and can be obtained from the Gibb's free energy as follows,

$$-\ln(Kp) = \Delta G / RT, \quad \text{(B-2)}$$

this can also be expressed as

$$-\ln(K_P) = \Delta G^0/RT = (\Delta G_0^0 - \Delta H_0^0)/RT_0 + \Delta H_0^0/RT + 1/T \int_{To}^{T} \Delta C^0{}_p / R \, dT -$$

$$\int_{To}^{T} \Delta C^0 p / RT \, dT \qquad \text{(Smith, 1996)} \qquad \text{(B-3)}$$

Where, ΔH^0 and ΔG^0 are enthalpy and Gibbs energy of formation respectively in kJ/mol.

$Cp / R = A + BT + CT^2 - DT^{-2}$ T in Kelvin from T =298 to T_{max}

So, $\Delta Cp / R = \Delta A + \Delta BT + \Delta CT^2 - \Delta DT^{-2}$

Now,

$$\int_{To}^{T} \Delta C^0{}_p / R \, dT = \int_{298}^{673} \Delta C^0{}_p / R \, dT = \int_{298}^{673} [16.48 - 1.973E\text{-}02\ T + 6.002E\text{-}06\ T^2 - 2.179E{+}05\ T^{-2}]\, dT$$

$$= 2587.9 \qquad \text{(B-4)}$$

and

$$\int_{298}^{673} \Delta C^0 p / RT \, dT = \int_{298}^{673} [16.48 - 1.973E\text{-}02\ T + 6.002E\text{-}06\ T^2 - 2.179E{+}05\ T^{-2}]/T \, dT$$

$$= 6.03 \qquad \text{(B-5)}$$

Solving equation (B-3), we get

$Kp = 6.52 * 10^{14}$

Step 2: Calculations of mole fraction in the product mixture

The equilibrium expression is as given in equation B-6,

$$\prod_i (y_i \varphi_i)^{v_i} = (P / P^O)^{-v} K_P \qquad \text{(B-6)}$$

$$\frac{[y_{H2}]^6 * [\varphi_{H2}]^6 * [y_{CO2}]^2 * [\varphi_{CO2}]^2}{[y_{C2H5OH}] * [\varphi_{C2H5OH}] * [y_{H2O}]^3 * [\varphi_{H2O}]^3} = (P / P^O)^{-v} K_P \qquad \text{(B-7)}$$

Where,

φ_i = activity coefficient of species i

y_i = mole fraction of species i

$\varphi = \exp [P_r / T_r (\beta_0 + \omega\beta_1)]$

$\beta_0 = 0.083 - 0.422 / (T_r)^{1.6}$
and
$\beta_1 = 0.139 - 0.172 / (T_r)^{4.2}$

$\nu = \nu_{H2} + \nu_{CO2} - \nu_{C2H5OH} - \nu_{H2O} = 6 + 2 - 1 - 3 = 4$

Thermodynamic data**,** Smith et al.(1996)

	ω	**T_c (K)**	**P_c (bar)**	**Tr**	**Pr**	**β_o**	**β_1**	**φ**
H2	-2.16E-01	3.32E+01	1.31E+01	1.79E+01	8.38E-02	7.88E-02	1.39E-01	1.00E+00
CO2	2.24E-01	3.04E+02	7.38E+01	1.95E+00	1.49E-02	-6.20E-02	1.29E-01	1.00E+00
H2O	3.45E-01	6.47E+02	2.21E+02	9.17E-01	4.99E-03	-4.02E-01	-1.09E-01	9.98E-01
C2H5OH	6.45E-01	5.14E+02	6.15E+01	1.15E+00	1.79E-02	-2.52E-01	4.48E-02	9.97E-01

P = Operating pressure, 1.00 bar

P^O = Standard-state pressure, 1.00 bar

T = 673.0 K

Solving equation (B-6):

$$\frac{[y_{H2}]^6 [y_{CO2}]^2}{[y_{C2H5OH}][y_{H2O}]^3} = (.9886) * K \qquad \text{(B-8)}$$

Let the equilibrium reaction coefficient be C_e
Total moles at any time = $1 + 3 + 0 + 0 - C_e - 3C_e + 6C_e + 2C_e = 4 + 4C_e$

$y_{H2} = 6C_e / (4 + 4C_e)$

$y_{CO2} = 2C_e / (4 + 4C_e)$

$y_{H2O} = (3 - 3C_e) / (4 + 4C_e)$

$y_{C2H5OH} = (1 - C_e) / (4 + 4C\varepsilon_e)$

Replacing these values in equation (B-7) and simplifying, we get:

$$\frac{27Ce^8}{(1+Ce)^4 (1-Ce)^4} = 0.9886 * Kp \qquad \text{(B-9)}$$

by further simplification we obtained

$$C_e^{\,8}(1-C_e)^{-4} * (1+C_e)^{-4} - 2.41*10^{13} = 0 \qquad \text{(B-10)}$$

Equation (B-10) could not be solved at high temperature (673K), however the solutions at lower temperatures 495K and 520K were as follows:

For T = 495 K, $C_e = 0.96$

For T = 520K, $C_e = 0.98$

The value of C_e increases with temperature as expected for an endothermic reaction, it can be concluded that C_e approaches unity as the reaction temperature increases up to 673 K.

Appendix C: HPLC Calibration Curves for the Feed Crude ethanol and Liquid Condensate

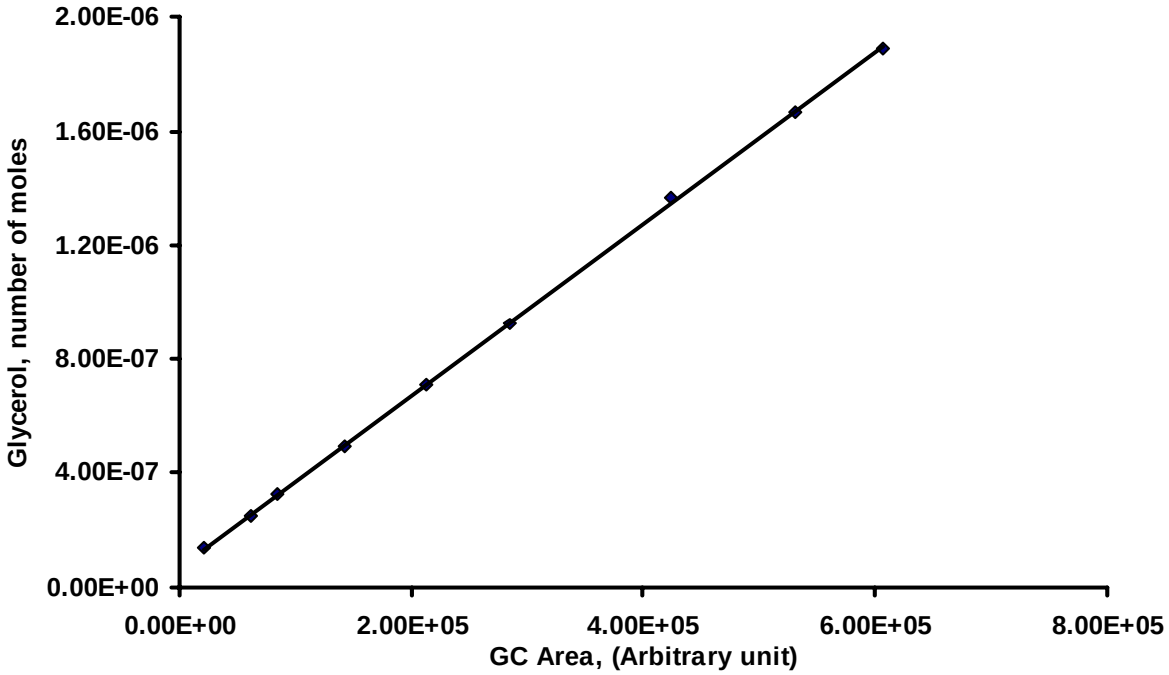

Figure C1: HPLC Calibration curve for glycerol

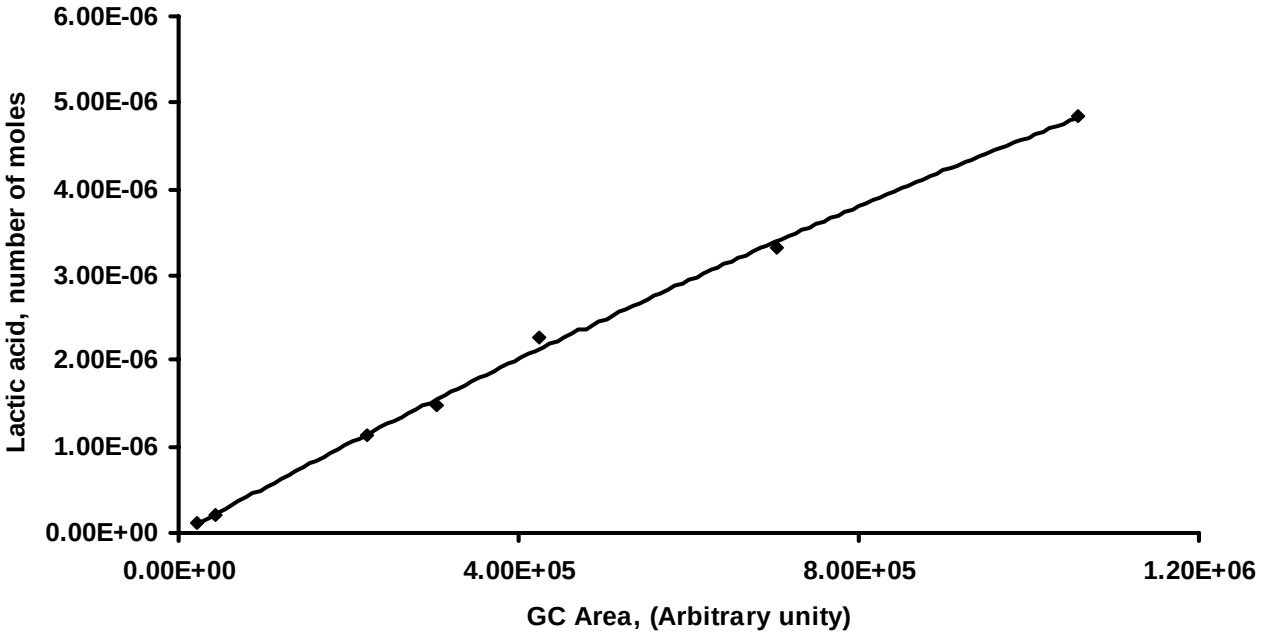

Figure C2: HPLC Calibration curve for lactic acid

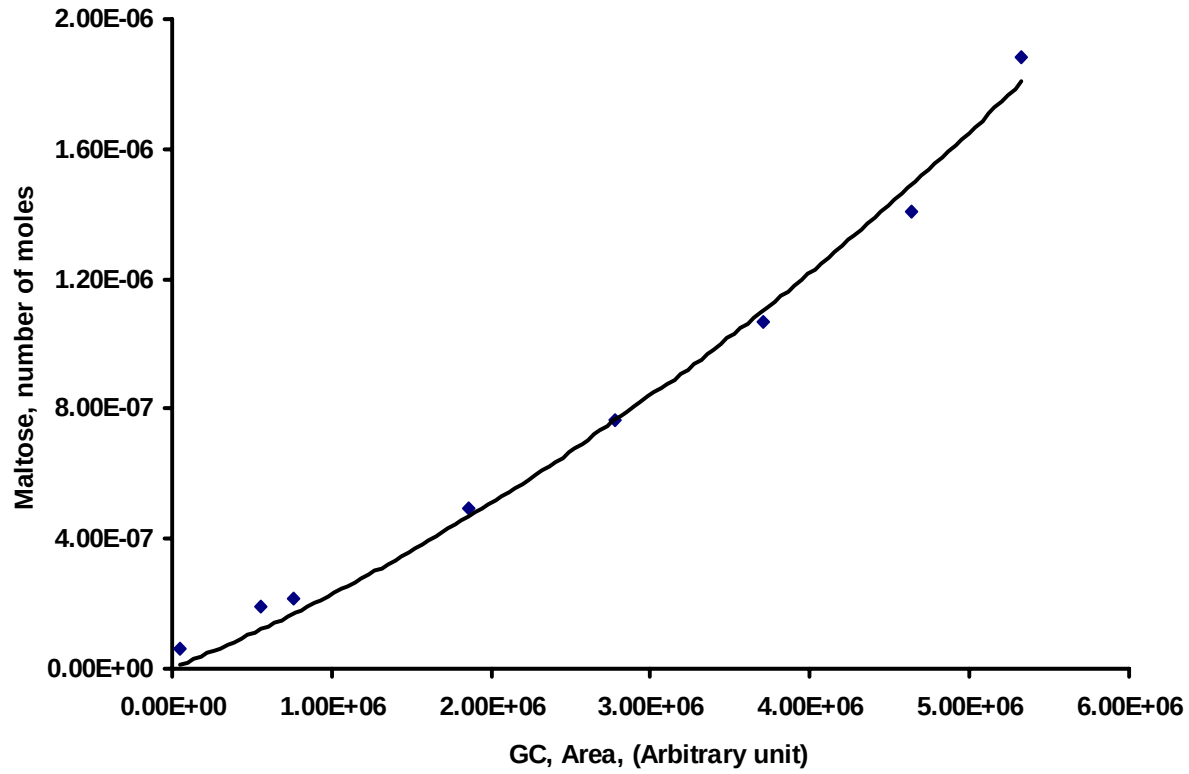

Figure C3: HPLC Calibration curve for maltose

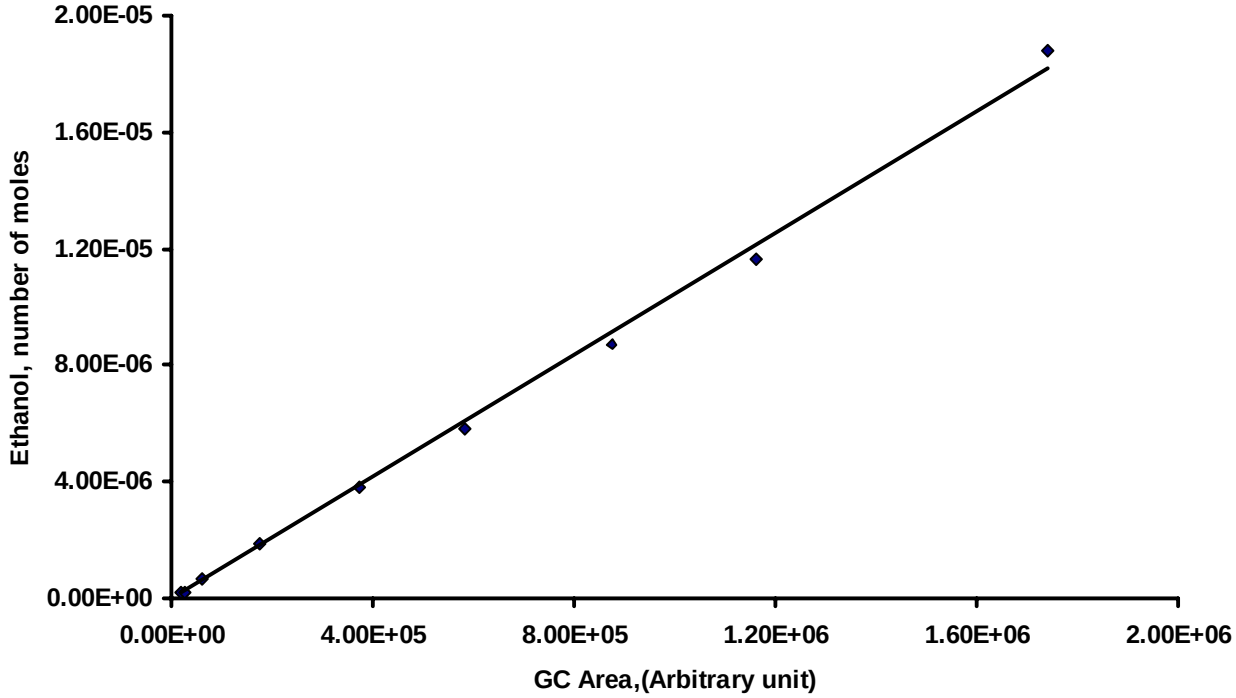

Figure C4: HPLC Calibration curve for ethanol

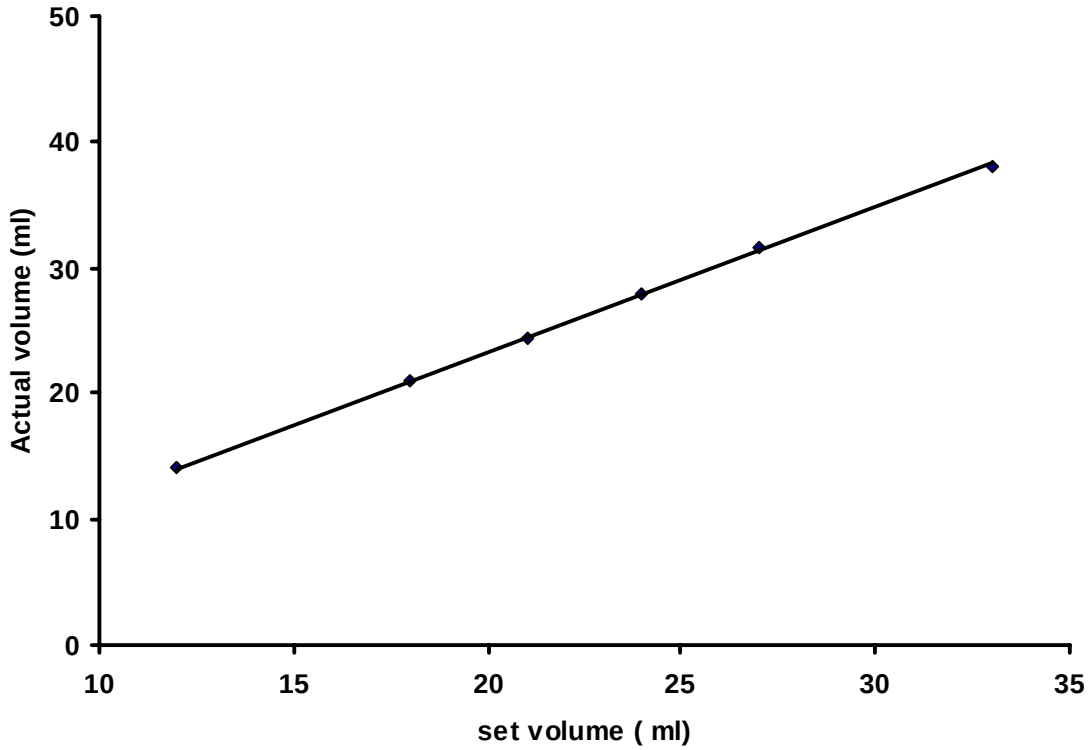

Figure C5: Feed pump calibration

Appendix D: kinetic Data

Table D-1. Kinetics experimental data.

T (K)	Rate of reaction (kmol-crude/kg-cat s)	N_A (kmole/s)	N_B (kmole/s)	N_C (kmole/s)	N_D (kmole/s)	K_P	Run #
593	3.03286E-06	5.70596E-09	1.57331E-07	8.40614E-09	2.40685E-08	2.45431E+11	1
593	3.38489E-06	6.96321E-09	1.81138E-07	8.66974E-09	2.48233E-08	2.45431E+11	2
593	3.8669E-06	8.43861E-09	2.0793E-07	8.81142E-09	2.52289E-08	2.45431E+11	3
593	4.51138E-06	1.03925E-08	2.4341E-07	8.99906E-09	2.57662E-08	2.45431E+11	4
593	5.41583E-06	1.64558E-08	3.51408E-07	9.27356E-09	2.65521E-08	2.45431E+11	5
693	3.8669E-06	5.02195E-09	1.57821E-07	1.0229E-08	2.92878E-08	3.36674E+15	6
693	4.73885E-06	6.94639E-09	1.91534E-07	1.02336E-08	2.93008E-08	3.36674E+15	7
693	4.87424E-06	9.80704E-09	2.41648E-07	1.02403E-08	2.93201E-08	3.36674E+15	8
693	5.41583E-06	1.27534E-08	2.91574E-07	1.00001E-08	2.86323E-08	3.36674E+15	9
693	6.31485E-06	1.73306E-08	3.66116E-07	9.18524E-09	2.62993E-08	3.36674E+15	10
793	4.06187E-06	5.11495E-09	1.60744E-07	1.04184E-08	2.98302E-08	4.45742E+18	11
793	4.64136E-06	6.56813E-09	1.86765E-07	1.05044E-08	3.00763E-08	4.45742E+18	12
793	4.73885E-06	8.52993E-09	2.21894E-07	1.06204E-08	3.04085E-08	4.45742E+18	13
793	5.41583E-06	1.20164E-08	2.81443E-07	1.04052E-08	2.97921E-08	4.45742E+18	14
793	6.76978E-06	1.62475E-08	3.50781E-07	9.71516E-09	2.78165E-08	4.45742E+18	15

Appendix E: Derivation of Eley-Rideal Rate Expressions for Crude Ethanol Reforming

Since the stoichiometry is more familiar, the pure ethanol steam reforming reaction shown in Equation E-1 was used to develop the kinetic models. There was no loss of accuracy by doing this since the atomic ratios indicated in Equation E-1 were used just as illustrations of the presence of carbon, hydrogen and oxygen atoms in the organic fraction of the feed but not for any calculations.

$$C_2H_6O + 3H_2O \longrightarrow 2CO_2 + 6H_2 \qquad \text{(E-1)}$$

Three basic steps based on Eley-Rideal mechanism were used in the derivation of the mechanistic type rate equations with the assumption that intrinsic data were collected, and as such, mass and heat transfer limitations were absent: step one is the adsorption of crude ethanol on the catalyst surface, step two is the interaction of the adsorbed crude-ethanol with an adjacent vacant site while step three involves two surface reactions. The mechanism is as given in Equations (E-2) to (E-5).

Adsorption of crude ethanol on an active site:

$$C_2H_6O + (a) \xleftrightarrow{k_{1,-1}} C_2H_6O(a) \qquad \text{(E-2)}$$

Dissociation of adsorbed crude ethanol into hydrocarbon and oxygenated hydrocarbon fractions:

$$C_2H_6O(a) + (a) \xleftrightarrow{k_{2,-2}} CH_4O^*(a) + CH_2{}^*(a) \qquad \text{(E-3)}$$

Surface reaction of adsorbed oxygenated hydrocarbon fraction with non-adsorbed water vapor:

$$CH_4O^*(a) + H_2O(g) \xleftrightarrow{k_{3,-3}} CO_2 + 3H_2 + (a) \quad \text{(E-4)}$$

Surface reaction of adsorbed hydrocarbon fraction with non-adsorbed water vapor:

$$CH_2{}^*(a) + 2H_2O(g) \xleftrightarrow{k_{4,-4}} CO_2 + 3H_2 + (a) \quad \text{(E-5)}$$

where (a) represents an active site, k_i represents the forward reaction rate constant for reaction *i*, and k_{-i} represents the backward reaction rate constant for reaction *i*.

Let $C_2H_6O = A$, $CH_4O^* = A^*$, $H_2O = B$, $CH_2{}^* = S^*$, $CO_2 = C$ and $H_2 = D$

Then the equilibrium relations for the above reaction can be given as in Equations E-6 to E-9.

$$K_1 = \frac{C_{A(a)}}{C_A C_{(a)}} \quad \text{(E-6)}$$

$$K_2 = \frac{C_{A^*(a)} C_{S^*(a)}}{C_{A(a)} C_{(a)}} \quad \text{(E-7)}$$

$$K_3 = \frac{C_C C_D{}^3 C_{(a)}}{C_{A^*(a)} C_B} \quad \text{(E-8)}$$

$$K_4 = \frac{C_C C_D{}^3 C_{(a)}}{C_{S^*(a)} C_B{}^2} \quad \text{(E-9)}$$

where $\frac{k_i}{k_{-i}} = K_i$ = equilibrium constant for reaction *i*.

Four cases of possible rate controlling mechanisms were evaluated. In the first case (i.e. formulation of model #1), adsorption of crude-ethanol (Equation E-2), is

assumed as the rate-determining step (RDS). The rate of reaction for this case can be written as Equation E-10.

$$r_A = k_1 C_A C_{(a)} - k_{-1} C_{A(a)} \qquad \text{(E-10)}$$

Using Equations E-7-E-9 to eliminate the unknown quantity, $C_{A(a)}$, and factorizing we obtain

$$r_A = k_1 C_{(a)} [C_A - \frac{C_C{}^2 C_D{}^6}{K_1 K_2 K_3 K_4 C_B{}^3}] \qquad \text{(E-11)}$$

where

$C_{A(a)}$ = Concentration of A on an active site

$C_{A^*(a)}$ = Concentration of intermediate A, adsorbed on an active site

$C_{(a)}$ = Concentration of unoccupied active sites,

C_{S^*} = Concentration of intermediate S, adsorbed on an active site

C_A, C_B, C_C, are concentrations of A, B and C, respectively in kmoles

$K_1 K_2 K_3 K_4 = K_P$, the thermodynamic equilibrium constant.

The only immeasurable quantity at this point is $C_{(a)}$. This can be eliminated as follows: If we let C_t be the total number of sites available on the catalyst whether occupied by adsorbed species or not, then

$$C_t = C_{(a)} + C_{A(a)} + C_{A^*(a)} + C_{S^*(a)} \qquad \text{(E-12)}$$

where,

$C_{(a)}$ = unoccupied sites

$C_{A(a)}$ = site occupied by A

$C_{A^*(a)}$ = site occupied by A^*

$C_{S^*(a)}$ = site occupied by S*

Using the equilibrium relations to eliminate the last three terms of Equation E-12 we obtain:

$$C_t = C_{(a)} + \frac{C_C C_D{}^3}{K_3 C_B} C_{(a)} + \frac{C_C C_D{}^3}{K_4 C_B{}^2} C_{(a)} + \frac{C_C{}^2 C_D{}^6}{K_2 K_3 K_4 C_B{}^3} C_{(a)} \qquad \text{(E13)}$$

$$C_{(a)} = \frac{C_t}{[1 + \frac{K_F C_C C_D{}^3}{C_B} + \frac{K_G C_C C_D{}^3}{C_B{}^2} + \frac{K_E C_C{}^2 C_D{}^6}{C_B{}^3}]} \qquad \text{(E-14)}$$

Let $K_A = K_1$, $K_F = 1/K_3$, $K_H = K_1 K_2 K_3$, $K_G = 1/K_4$, $K_Q = K_1 K_2 K_4$ and $K_E = 1/K_2 K_3 K_4$.

On substituting Equation E-14 into E-11, we obtain:

$$r_A = \frac{k_1 C_t [C_A - \frac{C_C{}^2 C_D{}^6}{K_P C_B{}^3}]}{[1 + \frac{K_F C_C C_D{}^3}{C_B} + \frac{K_G C_C C_D{}^3}{C_B{}^2} + \frac{K_E C_C{}^2 C_D{}^6}{C_B{}^3}]} \qquad \text{(E-15)}$$

Written in terms of the Arrhenius law, $k_1 C_t = k_o e^{-E/RT}$. Hence, the rate equation becomes

$$r_A = \frac{k_O e^{-E/RT}\left[C_A - \frac{C_C^{\,2} C_D^{\,6}}{K_P C_B^{\,3}}\right]}{\left[1 + \frac{K_F C_C C_D^{\,3}}{C_B} + \frac{K_G C_C C_D^{\,3}}{C_B^{\,2}} + \frac{K_E C_C^{\,2} C_D^{\,6}}{C_B^{\,3}}\right]} \qquad \text{(E-16)}$$

where r_A is the rate of crude-ethanol conversion (kmol-crude/kg-cat s), k_o is the collision frequency (kg-cat s)$^{-1}$, E is the activation energy (kJ/kmol), T is the absolute temperature (K), R is the Universal gas constant (kJ/kmol-K), K_p is the thermodynamic equilibrium constant. Equation E-16 is referred to as model # 1.

On the other hand, in the second case (formulation of model # 2), Equation E-3, the dissociation of adsorbed crude ethanol (which requires an additional active site) is assumed as the rate determining step. The rate of reaction can be written as:

$$r_A = k_2 C_{A(a)} C_{(a)} - k_{-2} C_{A^*(a)} C_{S^*(a)} \qquad \text{(E-17)}$$

Using equilibrium relations E-6, E-8 and E-9 to eliminate the immeasurable $C_{A(a)}$, $C_{A^*(a)}$ and $C_{S^*(a)}$, and factorizing, we obtain the rate as:

$$r_A = k_2 K_1 C_{(a)}^{\,2}\left[C_A - \frac{C_C^{\,2} C_D^{\,6}}{K_P C_B^{\,3}}\right] \qquad \text{(E-18)}$$

where $K_P = K_1 K_2 K_3 K_4$, the thermodynamic equilibrium constant

Also, the only immeasurable quantity at this point is $C_{(a)}$. This can be eliminated in the same manner as was done for the first model that resulted in Equation E-16. Thus, after all the eliminations and substitutions, we obtained a rate equation in the form of Equation E-19, which is referred to as model # 2.

$$r_A = \frac{k_O e^{-E/RT}\left(C_A - \frac{C_C^{\,2} C_D^{\,6}}{K_P C_B^{\,3}}\right)}{\left[1 + K_A C_A + \frac{K_F C_C C_D^{\,3}}{C_B} + \frac{K_G C_C C_D^{\,3}}{C_B^{\,2}}\right]^2} \qquad \text{(E-19)}$$

In the third case (for formulation of model # 3), surface reaction E-4 is assumed to be the rate-determining step. Then, the rate of reaction can be written in the form of Equation E-20.

$$r_A = k_3 C_{A^*(a)} C_B - k_{-3} C_C C_D^{\,3} C_{(a)} \qquad \text{(E-20)}$$

Using equilibrium relations E-6, E-7 and E-9 to eliminate the immeasurable $C_{A^*(a)}$ and factorizing, the rate equation becomes:

$$r_A = K_1 K_2 K_4 k_3 C_{(a)} \left(\frac{C_A C_B^{\,3}}{C_C C_D^{\,3}} - \frac{C_C C_D^{\,3}}{K_1 K_2 K_3 K_4}\right) \qquad \text{(E-21)}$$

Again, $C_{(a)}$ can be eliminated in the same manner as described for cases 1 and 2. Thus, after all the eliminations and substitutions, we obtained a rate equation in the form of Equation E-22, which is referred to as model # 3.

$$r_A = \frac{k_O e^{-E/RT}\left(\frac{C_A C_B^{\,3}}{C_C C_D^{\,3}} - \frac{C_C C_D^{\,3}}{K_P}\right)}{\left(1 + K_A C_A + \frac{K_Q C_A C_B^{\,2}}{C_C C_D^{\,3}} + \frac{K_G C_C C_D^{\,3}}{C_B^{\,2}}\right)} \qquad \text{(E-22)}$$

where $K_1 K_2 K_4 k_3 C_t = k_O e^{-E/RT}$

The fourth case (for formulation of model # 4) involved the assumption of surface reaction E-5 as the rate-determining step. The procedure used to derive the

kinetic model based on this rate determining step was similar to the ones used for previous three cases, and the final rate equation was of the form of Equation E-23, which is referred to as model # 4.

$$r_A = \frac{k_O e^{-E/RT}\left(\frac{C_A C_B^{\,3}}{C_C C_D^{\,3}} - \frac{C_C C_D^{\,3}}{K_P}\right)}{\left(1 + K_A C_A + \frac{K_F C_C C_D^{\,3}}{C_B} + \frac{K_H C_A C_B}{C_C C_D^{\,3}}\right)} \qquad \text{(E-23)}$$

Appendix-F: Material Balance Calculations

The calculations are based on data collected for experimental run number 12

Feed:

Crude ethanol = 0.0344 mol = 1.81 g

H_2O = 0.63 mol = 11.35 g

Total mass entering the system = 1.81+11.35 = 13.16g

Product:

From gas and liquid sample analyses:

H_2 = 0.1488mol = 0.2975 g

CO_2 = 0.0360mol = 1.5828 g

CO = 0.0092 mol = 0.2567g

CH_4 = 0.0056 mol = 0.0903 g

Acetic acid & others = 2.9E-9 mole

Total moles of products $\cong$ 0.1995 mol = 2.2273 g

Crude ethanol = 0.0072 mol = 0.3452 g

Water $\cong$ 0.5481 mol = 9.866 g

Crude Ethanol Conversion:

$$(X) = \frac{(\text{Moles Crude ethanol})\text{in} - (\text{Moles crude ethanol})\text{out}}{(\text{Moles crude ethanol})\text{in}} \times 100\%$$

$$\frac{(0.0344 - 0.0072)}{0.0344} \times 100\% \qquad \cong 78.98\ \%$$

Hydrogen Yield:

$$\text{Hydrogen yield (Y)} = \frac{(\text{Moles } H_2)\text{out}}{6.07 \times (\text{Moles crude ethanol})\text{in}} \times 100\%$$

$$\frac{0.1488}{0.0344 \times 6.07} \times 100\% = 71.3\%$$

or

71.3% of 6.07 = 4.33 mol H_2 / mol crude ethanol fed

Mass Recovery:

$$\text{Percentage mass recovery} = \frac{\text{Weight of outlet stream}}{\text{Weight of inlet stream}} \times 100\%$$

$$\frac{(0.2975 + 1.5828 + 0.0903 + 0.2567 + 10.1849 + 0.3452)}{(1.81 + 11.35)} \times 100\%$$

$$= 96.94\%$$

Product compositions:

$$H_2 = \frac{\text{Moles } H_2 \text{ produced}}{\text{Total moles product}} \text{ x } 100\ \% = (0.1488 / 0.1995) \text{ x } 100\ \% = 74.59\ \%$$

$$CO_2 = \frac{\text{Moles } CO_2 \text{ produced}}{\text{Total moles product}} \text{ x } 100\ \% = (0.0360 / 0.1995) \text{ x } 100\% = 18.05\ \%$$

$$CO = \frac{\text{Moles CO produced}}{\text{Total moles product}} \times 100\% = (0.0092 / 0.1995) \text{ x } 100\% = 4.61\%$$

$$CH_4 = \frac{\text{Moles } CH_4 \text{ produced}}{\text{Total moles product}} \times 100\% = (0.0056 / 0.1995) \text{ x } 100\% = 2.83\ \%$$

$$CH_3\text{-COOH and others} = \frac{\text{Moles } CH_3COOH \text{ and others out}}{\text{Total moles product}} \times 100\%$$

$$= (2.9E\text{-}9/0.1995)*100\%$$

$$= 0.00015\%$$

Appendix-G: Reproducibility Test

Reproducibility of stable crude-ethanol conversion (X)

Catalyst: CP15

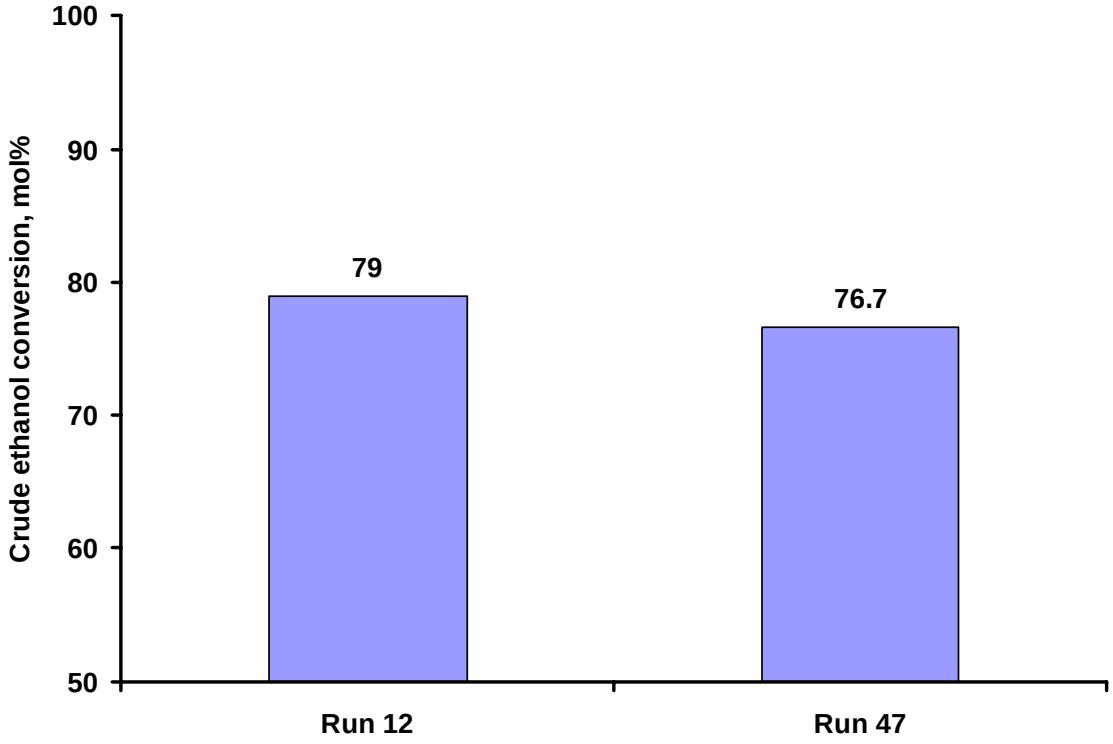

Sample calculations:

Run 12, X =79%

Run 47, X=76.7%

Deviation = (79-76.7)/79×100% = 2.9%

Catalyst: IM15

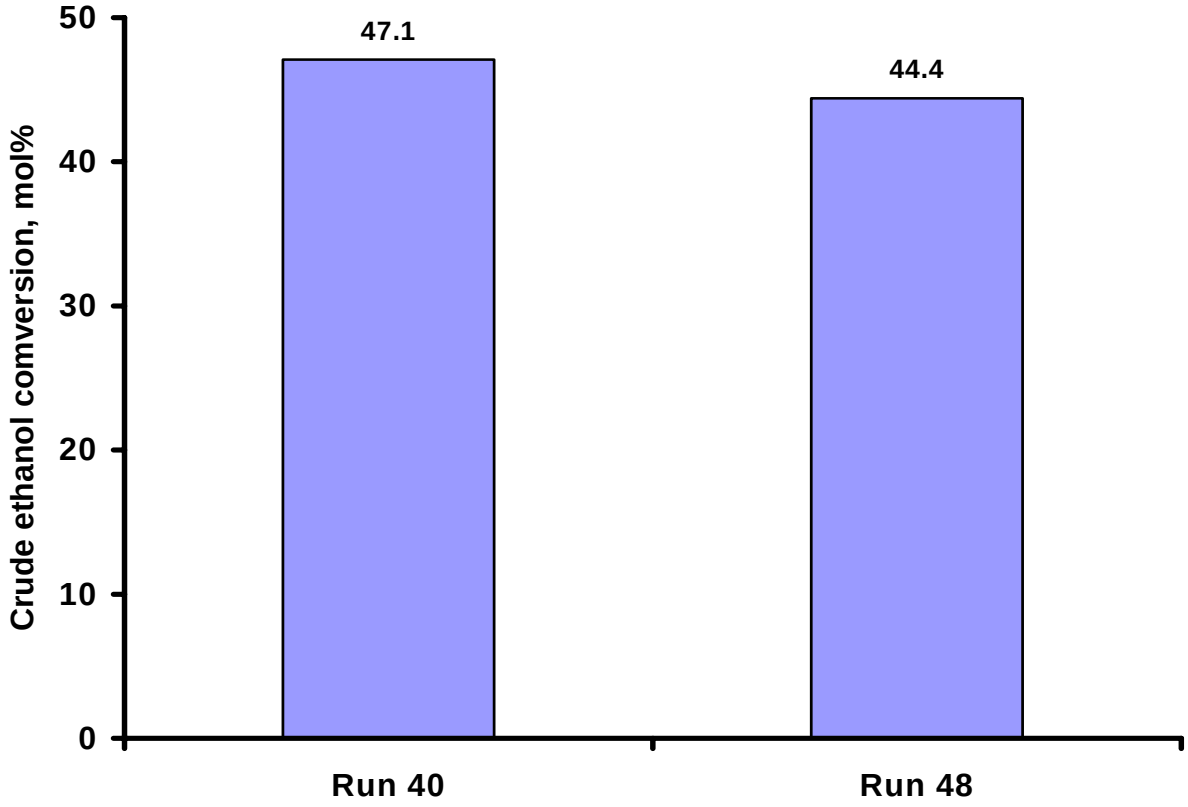

Sample calculations:

Run 40, X =47.1%

Run 48, X=44.4%

Deviation = (47.1-44.4)/47.1 × 100% = 5.7%

Catalyst: PT15

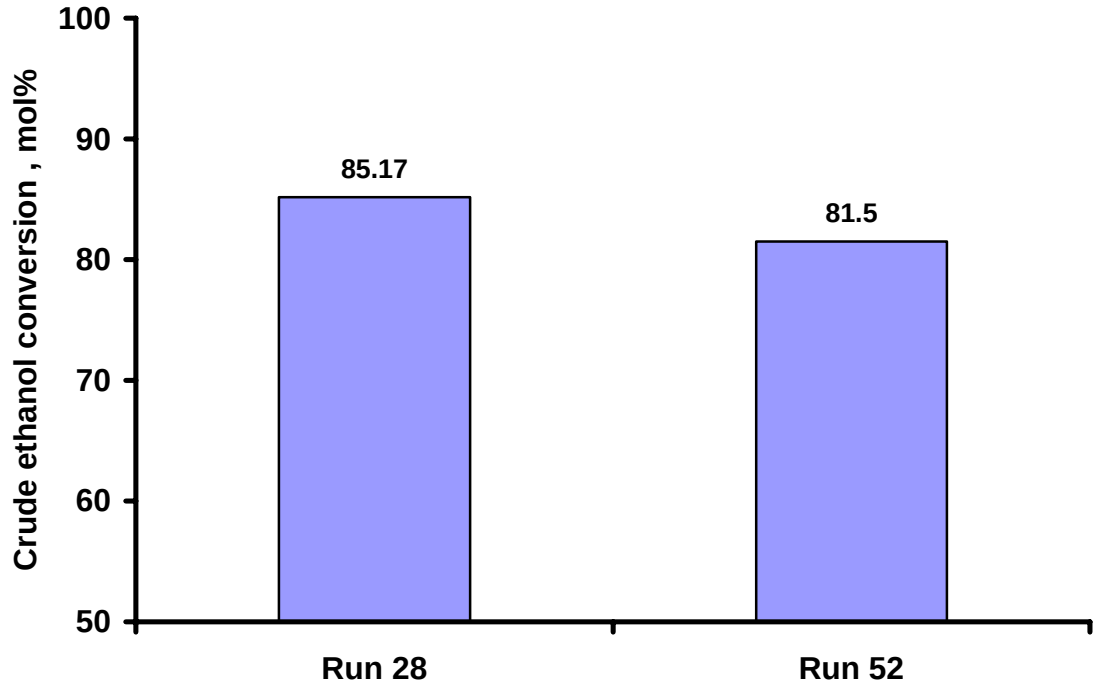

Sample calculations:

Run 28, X = 85.17%

Run 52, X = 81.5%

Deviation = (85.17-81.5)/85.17 × 100% = 4.3%

Appendix-H :
Experimental Results

	Run 5	Run 6	Run 7	Run 8
Catalyst used	CP10	CP10	CP10	CP10
Reduction temperature (^oC)	600.00	600.00	600.00	600.00
Time-on-stream (min)	60.00	120.00	180.00	240.00
Reaction temperature ^oC	400.00	400.00	400.00	400.00
Volume feed rate ml/min	0.20	0.20	0.20	0.20
Crude ethanol feed (moles)	3.44E-02	3.44E-02	3.44E-02	3.44E-02
$W/F_{crude\ ethanol}$ (h)	5.95E-01	5.95E-01	5.95E-01	5.95E-01
Crude ethanol conversion (mol%)	65.65	44.29	32.28	32.10
H_2 yield (mols H_2 / mol crude ethanol fed)	3.51	2.43	2.09	2.12
Product composition (mol%)				
H_2	7.23E+01	7.14E+01	7.01E+01	7.20E+01
CO_2	1.80E+01	1.95E+01	1.77E+01	1.77E+01
CH_4	4.56E+00	4.10E+00	7.06E+00	6.13E+00
CO	5.13E+00	5.03E+00	5.13E+00	4.15E+00
Acetic acid and others	2.00E-04	4.00E-04	5.00E-04	5.00E-04
Total product (mol)	1.67E-01	1.15E-01	1.01E-01	1.01E-01
Weight loss (% mass loss)	3.52	1.59	1.20	1.35

Appendix-H :
Experimental Results

	Run 9	Run 10	Run 11	Run 12
Catalyst used	CP15	CP15	CP15	CP15
Reduction temperature (^oC)	600.00	600.00	600.00	600.00
Time-on-stream (min)	60.00	120.00	180.00	240.00
Reaction temperature ^oC	400.00	400.00	400.00	400.00
Volume feed rate ml/min	0.20	0.20	0.20	0.20
Crude ethanol feed (moles)	3.44E-02	3.44E-02	3.44E-02	3.44E-02
$W/F_{crude\ ethanol}$ (h)	5.95E-01	5.95E-01	5.95E-01	5.95E-01
Crude ethanol conversion (mol%)	88.95	85.72	78.98	79.00
H_2 yield (mols H_2 / mol crude ethanol fed)	4.73	4.60	4.30	4.33
Product composition (mol%)				
H_2	7.27E+01	7.32E+01	7.41E+01	7.46E+01
CO_2	2.00E+01	1.84E+01	1.84E+01	1.80E+01
CH_4	3.73E+00	3.83E+00	2.83E+00	2.83E+00
CO	3.52E+00	4.59E+00	4.60E+00	4.59E+00
Acetic acid and others	7.00E-05	9.00E-05	1.50E-04	1.50E-04
Total product (mol)	2.24E-01	2.16E-01	2.00E-01	2.00E-01
Weight loss (% mass loss)	1.77	2.56	2.95	3.06

Appendix-H :
Experimental Results

	Run 13	Run 14	Run 15	Run 16
Catalyst used	CP20	CP20	CP20	CP20
Reduction temperature (^oC)	600.00	600.00	600.00	600.00
Time-on-stream (min)	60.00	120.00	180.00	240.00
Reaction temperature ^oC	400.00	400.00	400.00	400.00
Volume feed rate ml/min	0.20	0.20	0.20	0.20
Crude ethanol feed (moles)	3.44E-02	3.44E-02	3.44E-02	3.44E-02
$W/F_{crude\ ethanol}$ (h)	5.95E-01	5.95E-01	5.95E-01	5.95E-01
Crude ethanol conversion (mol%)	77.96	68.36	53.66	53.82
H_2 yield (mols H_2 / mol crude ethanol fed)	4.28	3.61	2.91	2.91
Product composition (mol%)				
H_2	7.47E+01	7.17E+01	7.26E+01	7.27E+01
CO_2	1.55E+01	1.31E+01	1.58E+01	1.50E+01
CH_4	5.01E+00	9.33E+00	7.56E+00	7.52E+00
CO	4.72E+00	5.95E+00	4.05E+00	4.74E+00
Acetic acid and others	1.00E-04	1.00E-04	3.00E-04	3.00E-04
Total product (mol)	1.97E-01	1.74E-01	1.38E-01	1.38E-01
Weight loss (% mass loss)	2.22	2.28	1.35	1.64

Appendix-H :
Experimental Results

	Run 17	Run 18	Run 19	Run 20
Catalyst used	CP25	CP25	CP25	CP25
Reduction temperature (^oC)	600.00	600.00	600.00	600.00
Time-on-stream (min)	60.00	120.00	180.00	240.00
Reaction temperature ^oC	400.00	400.00	400.00	400.00
Volume feed rate ml/min	0.20	0.20	0.20	0.20
Crude ethanol feed (moles)	3.44E-02	3.44E-02	3.44E-02	3.44E-02
$W/F_{crude\ ethanol}$ (h)	5.95E-01	5.95E-01	5.95E-01	5.95E-01
Crude ethanol conversion (mol%)	80.23	70.58	60.45	59.49
H_2 yield (mols H_2 / mol crude ethanol fed)	4.41	3.80	3.18	3.17
Product composition (mol%)				
H_2	7.48E+01	7.30E+01	7.10E+01	7.15E+01
CO_2	1.85E+01	1.80E+01	1.86E+01	1.80E+01
CH_4	3.13E+00	4.43E+00	4.83E+00	4.83E+00
CO	3.59E+00	4.59E+00	5.59E+00	5.59E+00
Acetic acid and others	1.60E-04	2.70E-04	4.20E-04	4.40E-04
Total product (mol)	2.03E-01	1.79E-01	1.54E-01	1.52E-01
Weight loss (% mass loss)	2.47	2.70	1.74	1.86

Appendix-H :
Experimental Results

	Run 21	Run 22	Run 23	Run 24
Catalyst used	PT10	PT10	PT10	PT10
Reduction temperature (^{o}C)	600.00	600.00	600.00	600.00
Time-on-stream (min)	60.00	120.00	180.00	240.00
Reaction temperature ^{o}C	400.00	400.00	400.00	400.00
Volume feed rate ml/min	0.20	0.20	0.20	0.20
Crude ethanol feed (moles)	3.44E-02	3.44E-02	3.44E-02	3.44E-02
$W/F_{crude\ ethanol}$ (h)	5.95E-01	5.95E-01	5.95E-01	5.95E-01
Crude ethanol conversion (mol%)	54.48	51.80	43.77	43.80
H_2 yield (mols H_2 / mol crude ethanol fed)	2.97	2.79	2.34	2.33
Product composition (mol%)				
H_2	7.36E+01	7.25E+01	7.15E+01	7.07E+01
CO_2	1.56E+01	1.57E+01	1.35E+01	1.35E+01
CH_4	5.35E+00	5.71E+00	7.72E+00	8.75E+00
CO	5.42E+00	6.11E+00	7.32E+00	7.01E+00
Acetic acid and others	1.70E-03	1.80E-03	2.50E-03	2.50E-03
Total product (mol)	1.39E-01	1.32E-01	1.13E-01	1.13E-01
Weight loss (% mass loss)	2.06	1.95	1.86	1.70

Appendix-H :
Experimental Results

	Run 25	Run 26	Run 27	Run 28
Catalyst used	PT15	PT15	PT15	PT15
Reduction temperature (^{o}C)	600.00	600.00	600.00	600.00
Time-on-stream (min)	60.00	120.00	180.00	240.00
Reaction temperature ^{o}C	400.00	400.00	400.00	400.00
Volume feed rate ml/min	0.20	0.20	0.20	0.20
Crude ethanol feed (moles)	3.44E-02	3.44E-02	3.44E-02	3.44E-02
$W/F_{crude\ ethanol}$ (h)	5.95E-01	5.95E-01	5.95E-01	5.95E-01
Crude ethanol conversion (mol%)	96.15	92.59	85.32	85.17
H_2 yield (mols H_2 / mol crude ethanol fed)	4.82	4.70	4.24	4.24
Product composition (mol%)				
H_2	6.93E+01	7.03E+01	7.13E+01	7.05E+01
CO_2	1.22E+01	1.12E+01	1.22E+01	1.22E+01
CH_4	1.05E+01	1.25E+01	1.05E+01	1.13E+01
CO	8.00E+00	6.00E+00	6.00E+00	6.00E+00
Acetic acid and others	1.30E-03	2.60E-03	5.60E-03	5.60E-03
Total product (mol)	2.39E-01	2.30E-01	2.11E-01	2.11E-01
Weight loss (% mass loss)	3.50	3.06	2.75	2.60

Appendix-H :
Experimental Results

	Run 29	Run 30	Run 31	Run 32
Catalyst used	PT20	PT20	PT20	PT20
Reduction temperature (^oC)	600.00	600.00	600.00	600.00
Time-on-stream (min)	60.00	120.00	180.00	240.00
Reaction temperature ^oC	400.00	400.00	400.00	400.00
Volume feed rate ml/min	0.20	0.20	0.20	0.20
Crude ethanol feed (moles)	3.44E-02	3.44E-02	3.44E-02	3.44E-02
$W/F_{crude\ ethanol}$ (h)	5.95E-01	5.95E-01	5.95E-01	5.95E-01
Crude ethanol conversion (mol%)	94.67	83.53	83.20	83.14
H_2 yield (mols H_2 / mol crude ethanol fed)	4.76	4.20	4.18	4.23
Product composition (mol%)				
H_2	7.23E+01	7.03E+01	6.92E+01	7.00E+01
CO_2	1.22E+01	1.22E+01	1.23E+01	1.17E+01
CH_4	9.53E+00	1.15E+01	1.25E+01	1.29E+01
CO	6.00E+00	6.00E+00	6.00E+00	5.40E+00
Acetic acid and others	8.00E-04	3.00E-03	3.00E-03	3.90E-03
Total product (mol)	2.37E-01	2.08E-01	2.07E-01	2.08E-01
Weight loss (% mass loss)	2.80	2.65	2.47	2.49

Appendix-H :
Experimental Results

	Run 33	Run 34	Run 35	Run 36
Catalyst used	IM10	IM10	IM10	IM10
Reduction temperature (^oC)	600.00	600.00	600.00	600.00
Time-on-stream (min)	60.00	120.00	180.00	240.00
Reaction temperature ^oC	400.00	400.00	400.00	400.00
Volume feed rate ml/min	0.20	0.20	0.20	0.20
Crude ethanol feed (moles)	3.44E-02	3.44E-02	3.44E-02	3.44E-02
$W/F_{crude\ ethanol}$ (h)	5.95E-01	5.95E-01	5.95E-01	5.95E-01
Crude ethanol conversion (mol%)	73.00	48.50	43.97	44.20
H_2 yield (mols H_2 / mol crude ethanol fed)	3.69	2.46	2.27	2.28
Product composition (mol%)				
H_2	6.89E+01	6.78E+01	6.85E+01	6.89E+01
CO_2	1.13E+01	1.20E+01	1.23E+01	1.13E+01
CH_4	4.88E+00	5.56E+00	5.06E+00	4.86E+00
CO	1.49E+01	1.46E+01	1.41E+01	1.49E+01
Acetic acid and others	2.10E-02	7.00E-03	7.00E-03	6.33E-03
Total product (mol)	1.84E-01	1.24E-01	1.14E-01	1.14E-01
Weight loss (% mass loss)	4.50	2.89	2.69	2.89

Appendix-H :
Experimental Results

	Run 37	Run 38	Run 39	Run 40
Catalyst used	IM15	IM15	IM15	IM15
Reduction temperature (^oC)	600.00	600.00	600.00	600.00
Time-on-stream (min)	60.00	120.00	180.00	240.00
Reaction temperature ^oC	400.00	400.00	400.00	400.00
Volume feed rate ml/min	0.20	0.20	0.20	0.20
Crude ethanol feed (moles)	3.44E-02	3.44E-02	3.44E-02	3.44E-02
$W/F_{crude\ ethanol}$ (h)	5.95E-01	5.95E-01	5.95E-01	5.95E-01
Crude ethanol conversion (mol%)	72.00	49.00	46.70	47.10
H_2 yield (mols H_2 / mol crude ethanol fed)	3.80	2.56	2.50	2.52
Product composition (mol%)				
H_2	7.22E+01	7.01E+01	7.16E+01	7.23E+01
CO_2	4.91E+00	8.51E+00	7.60E+00	1.09E+01
CH_4	7.78E+00	7.18E+00	7.70E+00	7.74E+00
CO	1.51E+01	1.42E+01	1.31E+01	9.08E+00
Acetic acid and others	8.00E-03	2.20E-02	2.00E-03	3.50E-03
Total product (mol)	1.81E-01	1.25E-01	1.20E-01	1.21E-01
Weight loss (% mass loss)	5.47	3.28	3.23	2.45

Appendix-H :
Experimental Results

	Run 41	Run 42	Run 43	Run 44
Catalyst used	IM20	IM20	IM20	IM20
Reduction temperature (^oC)	600.00	600.00	600.00	600.00
Time-on-stream (min)	60.00	120.00	180.00	240.00
Reaction temperature ^oC	400.00	400.00	400.00	400.00
Volume feed rate ml/min	0.20	0.20	0.20	0.20
Crude ethanol feed (moles)	3.44E-02	3.44E-02	3.44E-02	3.44E-02
$W/F_{crude\ ethanol}$ (h)	5.95E-01	5.95E-01	5.95E-01	5.95E-01
Crude ethanol conversion (mol%)	65.20	53.30	46.90	47.00
H_2 yield (mols H_2 / mol crude ethanol fed)	3.36	2.77	2.45	2.45
Product composition (mol%)				
H_2	7.02E+01	7.12E+01	7.02E+01	7.01E+01
CO_2	6.91E+00	8.71E+00	6.91E+00	7.10E+00
CH_4	7.78E+00	6.02E+00	7.78E+00	6.78E+00
CO	1.51E+01	1.41E+01	1.51E+01	1.60E+01
Acetic acid and others	1.40E-03	2.30E-03	2.80E-03	3.20E-03
Total product (mol)	1.64E-01	1.36E-01	1.20E-01	1.20E-01
Weight loss (% mass loss)	4.51	3.68	3.35	3.44

Appendix-H :
Experimental Results

	Run 45	Run 46	Run 47	Run 48
Catalyst used	CP15	CP15	CP15	IM15
Reduction temperature (^oC)	400.00	500.00	600.00	600
Time-on-stream (min)	240.00	240.00	240.00	240
Reaction temperature ^oC	400.00	400.00	400.00	400
Volume feed rate ml/min	0.20	0.20	0.20	0.2
Crude ethanol feed (moles)	3.44E-02	3.44E-02	3.44E-02	3.44E-02
$W/F_{crude\ ethanol}$ (h)	5.95E-01	5.95E-01	5.95E-01	5.95E-01
Crude ethanol conversion (mol%)	49.73	58.46	76.67	44.4
H_2 yield (mols H_2 / mol crude ethanol fed)	2.84	3.17	4.15	2.34
Product composition (mol%)				
H_2	7.55E+01	7.27E+01	7.36E+01	7.17E+01
CO_2	1.80E+01	1.80E+01	1.90E+01	5.00E+00
CH_4	1.83E+00	4.13E+00	2.80E+00	7.93E+00
CO	4.59E+00	5.09E+00	4.56E+00	1.54E+01
Acetic acid and others	1.90E-02	1.60E-02	2.00E-04	2.59E-03
Total product (mol)	1.29E-01	1.50E-01	1.94E-01	1.12E-01
Weight loss (% mass loss)	2.57	2.00	2.70	3.82

Appendix-H :
Experimental Results

	Run 49	Run 50	Run 51	Run 52
Catalyst used	CP15	CP15	CP15	PT15
Reduction temperature (^oC)	600.00	600.00	600.00	600.00
Time-on-stream (min)	240.00	240.00	240.00	240.00
Reaction temperature ^oC	320.00	420.00	520.00	400.00
Volume feed rate ml/min	0.20	0.20	0.20	0.20
Crude ethanol feed (moles)	3.44E-02	3.44E-02	3.44E-02	3.44E-02
$W/F_{crude\ ethanol}$ (h)	5.95E-01	5.95E-01	5.95E-01	5.95E-01
Crude ethanol conversion (mol%)	57.60	79.60	80.10	81.5
H_2 yield (mols H_2 / mol crude ethanol fed)	3.41	4.31	4.31	3.98
Product composition (mol%)				
H_2	6.27E+01	7.02E+01	7.21E+01	6.86E+01
CO_2	1.98E+01	2.03E+01	1.86E+01	1.27E+01
CH_4	8.38E+00	7.22E+00	6.29E+00	1.25E+01
CO	9.04E+00	2.26E+00	3.00E+00	6.15E+00
Acetic acid and others	2.60E-03	1.10E-03	1.10E-03	6.47E-03
Total product (mol)	1.52E-01	1.71E-01	2.05E-01	2.03E-01
Weight loss (% mass loss)	1.30	6.47	1.00	2.1